Radiation-MHD Models Of Photoionised Pillars

Jonathan Mackey & Andrew J. Lim
Dublin Institute for Advanced Studies, Ireland
Argelander Institute for Astronomy, Bonn, Germany

- Observational overview and motivation
- Introduction to code and methods
- Simulation initial conditions
- Results in weak and strong B-field limits
- Comparison to observations

Argelander-Institut für Astronomie

Unterstützt von / Supported by
Alexander von Humboldt Stiftung/Foundation

9th international conference on high energy density laboratory astrophysics,
Tallahassee, Florida, 4th May 2012

Ideal and Real HII regions around massive stars

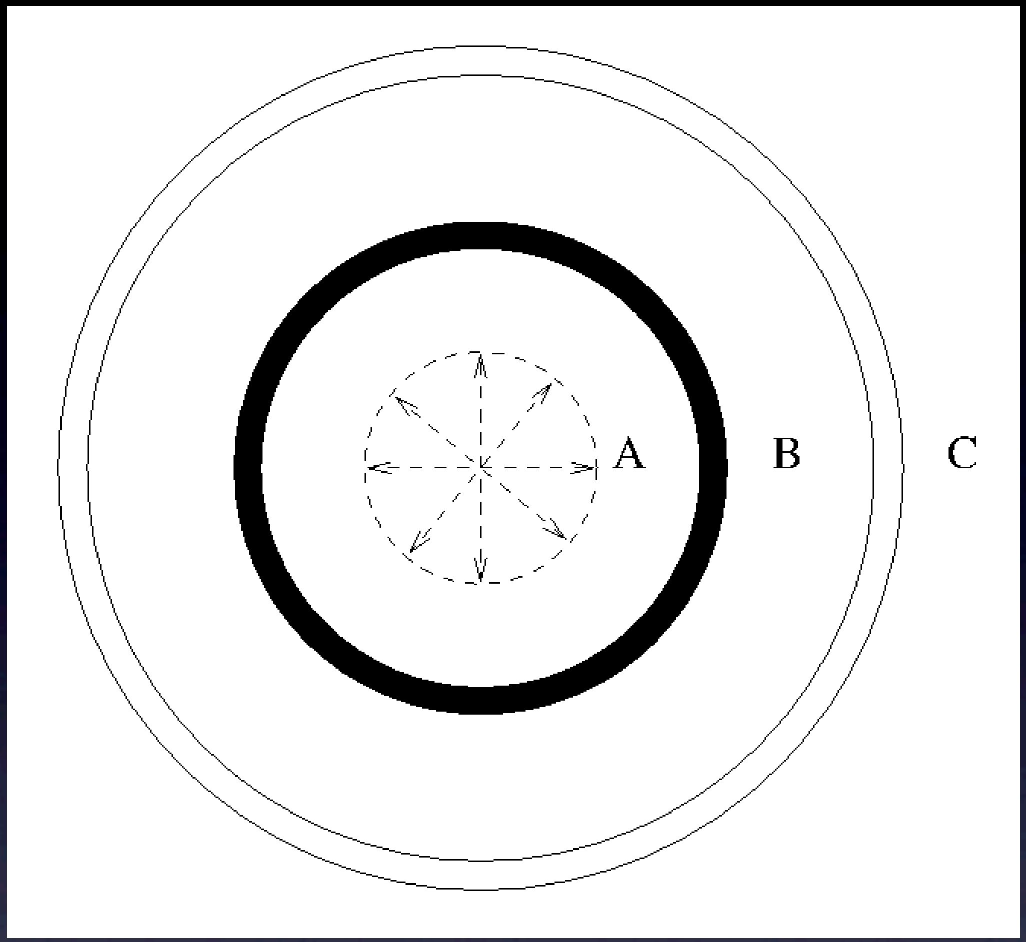

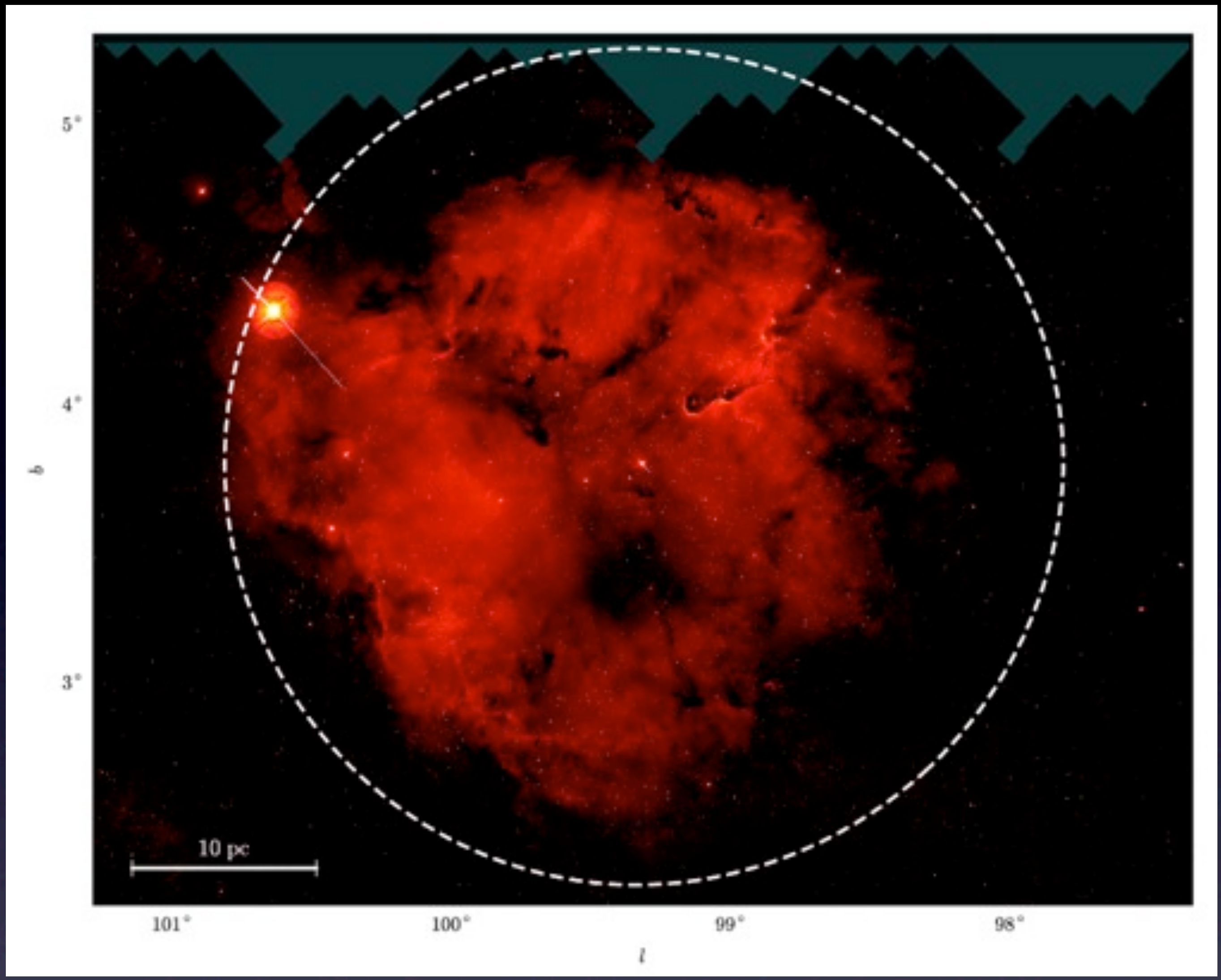

- From van Marle et al. (2004,RMxAC,22,136).
- Shows wind, hot bubble, HII region, ISM.
- Spherically symmetric...
- but contains 2 thin shells.

- IC 1396 in Hα (Barentsen+,2011)
- HII region boundary has pillars, clumps, substructure, including the "Elephant Trunk nebula". A broken shell.
- Wind-HII region interface not visible, so maybe no shell there.

IC 1396: size ~30pc, age~2-3Myr

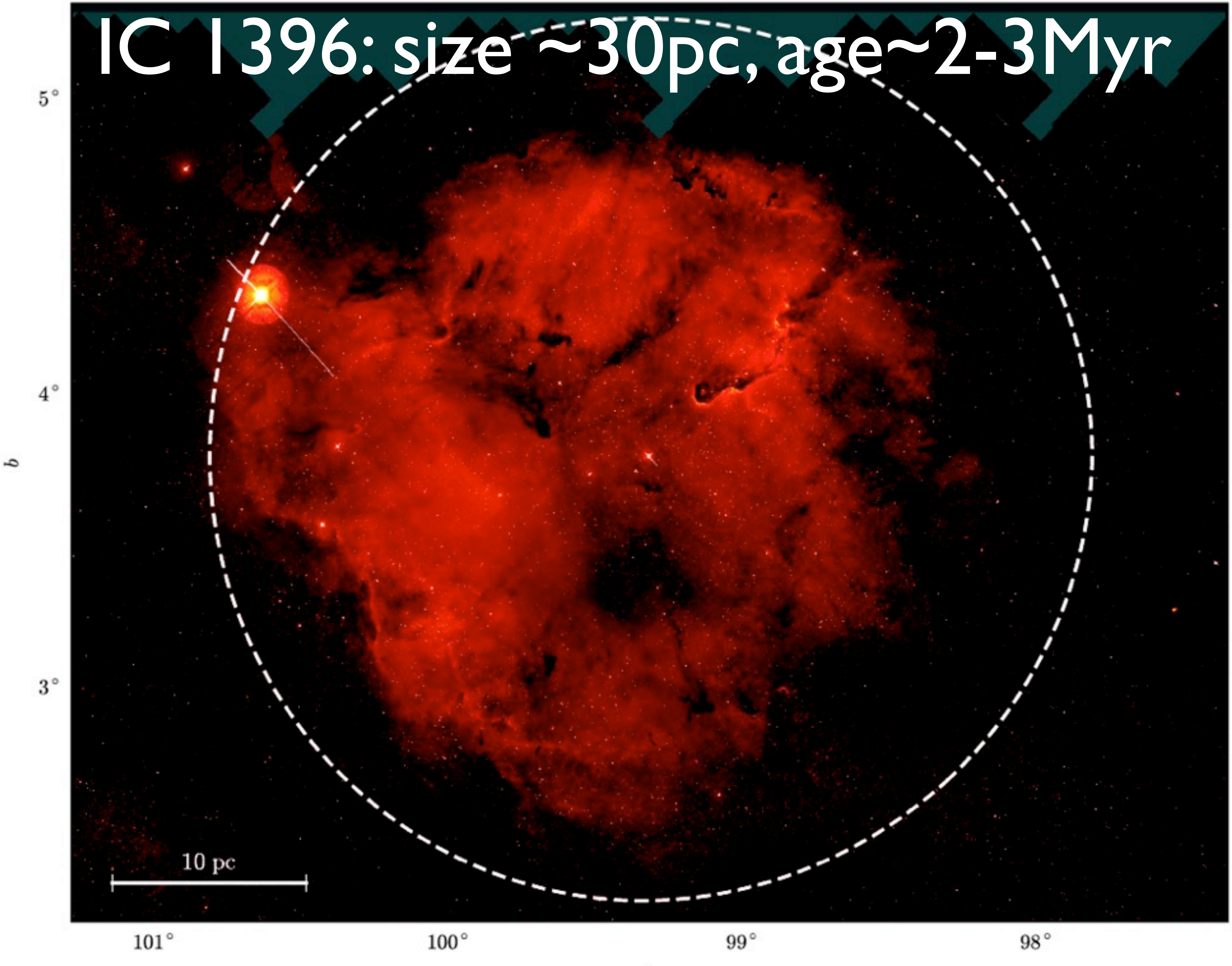

RCW 120: Younger, smaller HII Region

RCW 120: The Perfect Bubble

- Image from Deharveng+ (2009,A&A,496,177). Blue is Hα, green is Spitzer 8 μm and red 24 μm.
- 8 and 24μ figs shown separately below (V. Gvaramadze).
- ~3.5pc diameter.
- Age ~400 kyr (dynamical)
- Ionising star O9.5V
- Basically spherical, small-scale corrugations and pillars.
- Complex interaction between photoionisation, stellar winds, and possibly stellar motion.

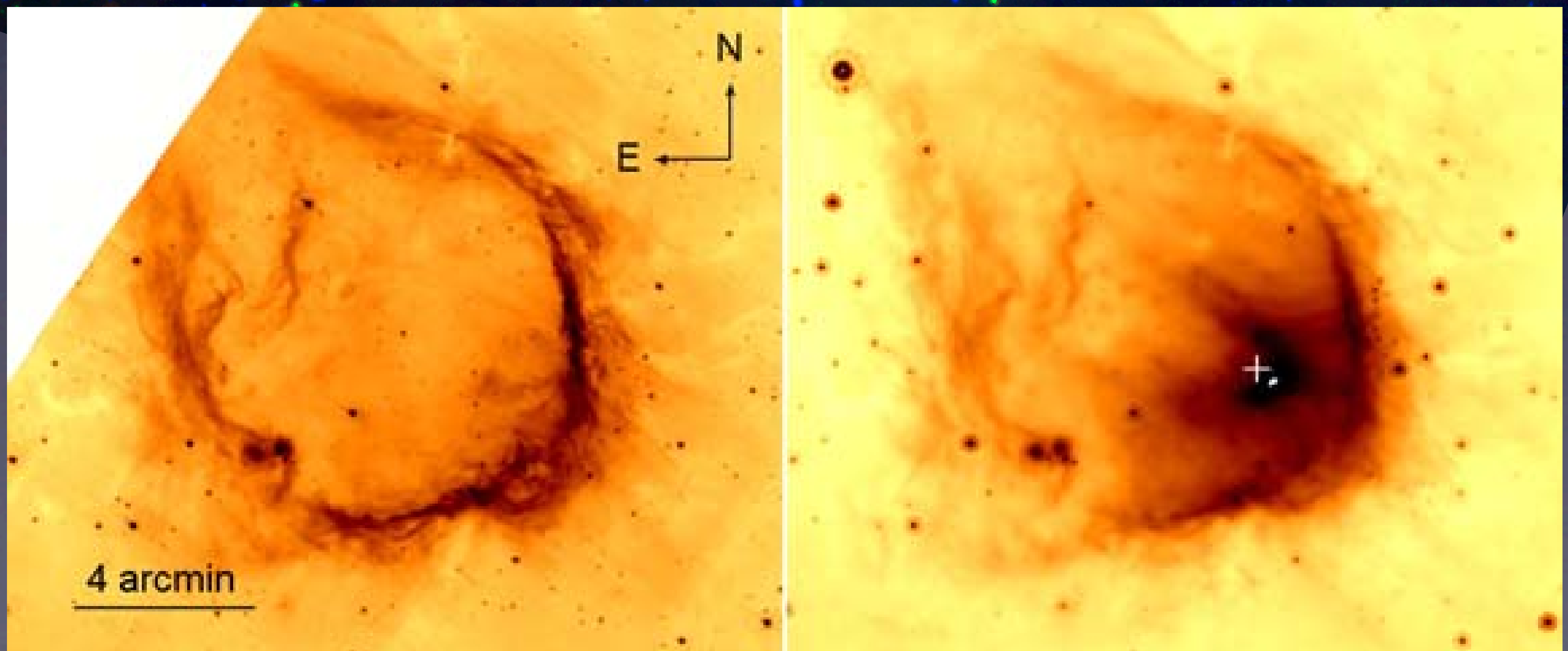

M16 and NGC 6611 (Eagle Nebula)

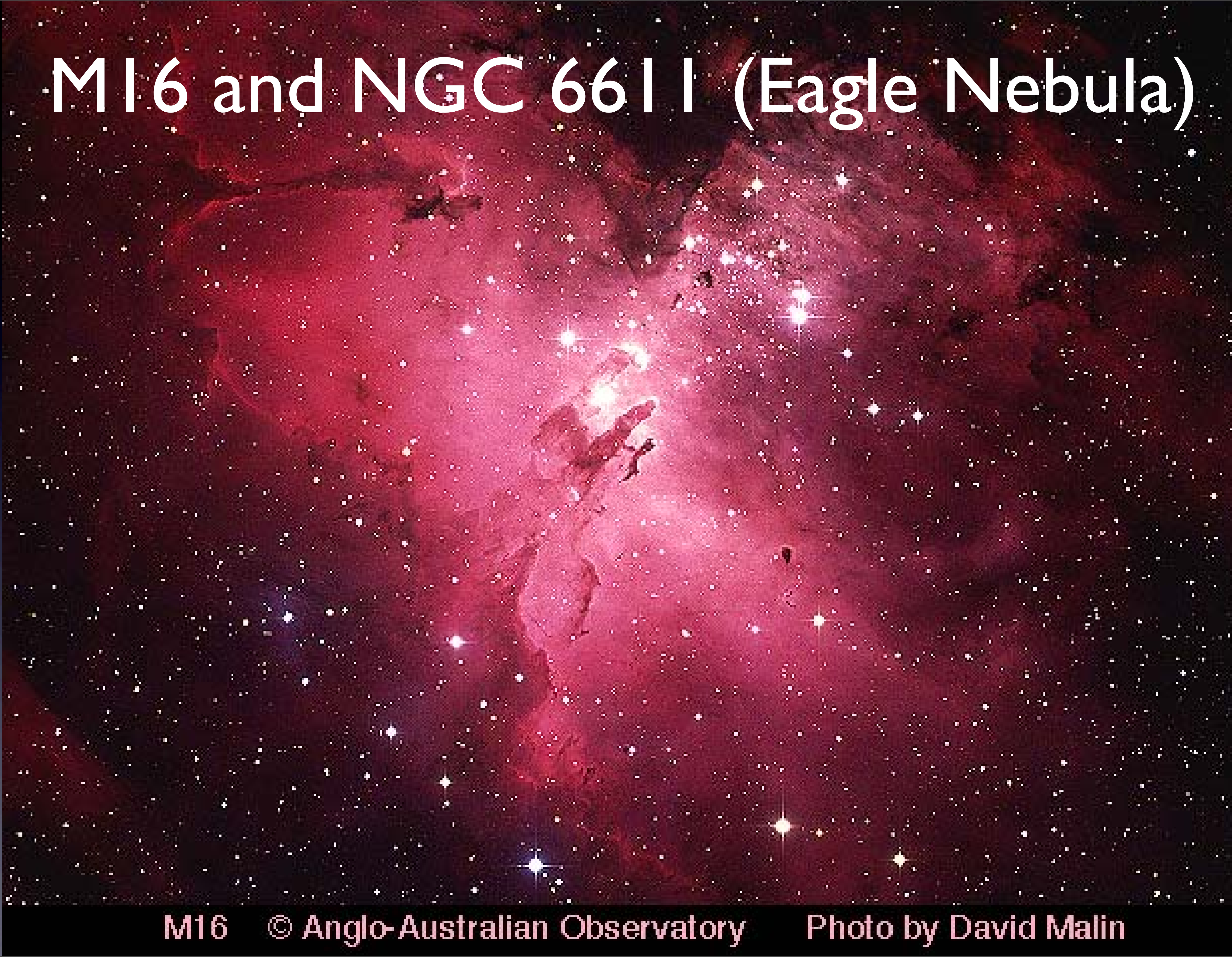

M16 and NGC 6611 (Eagle Nebula)

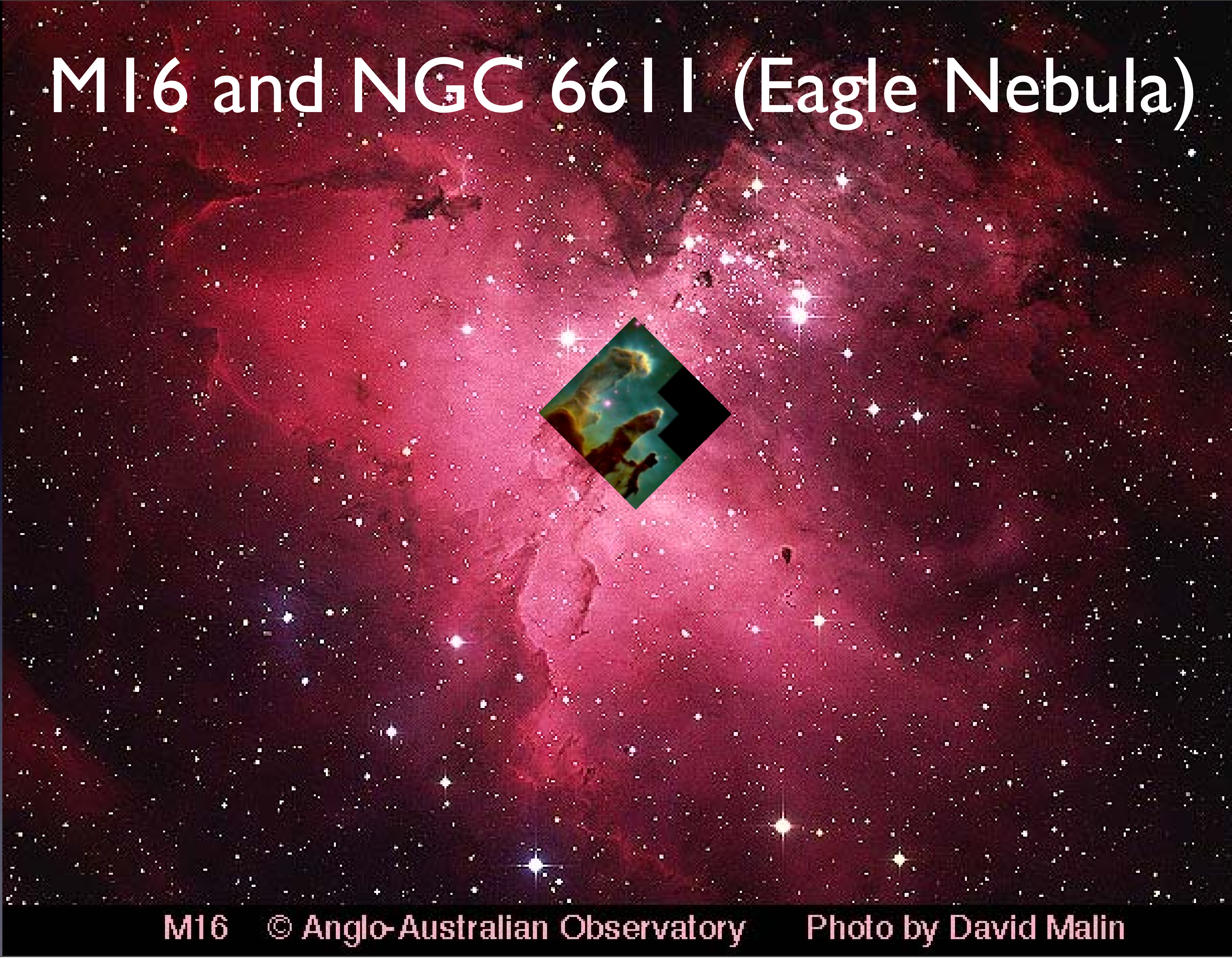

M16 and NGC 6611 (Eagle Nebula)

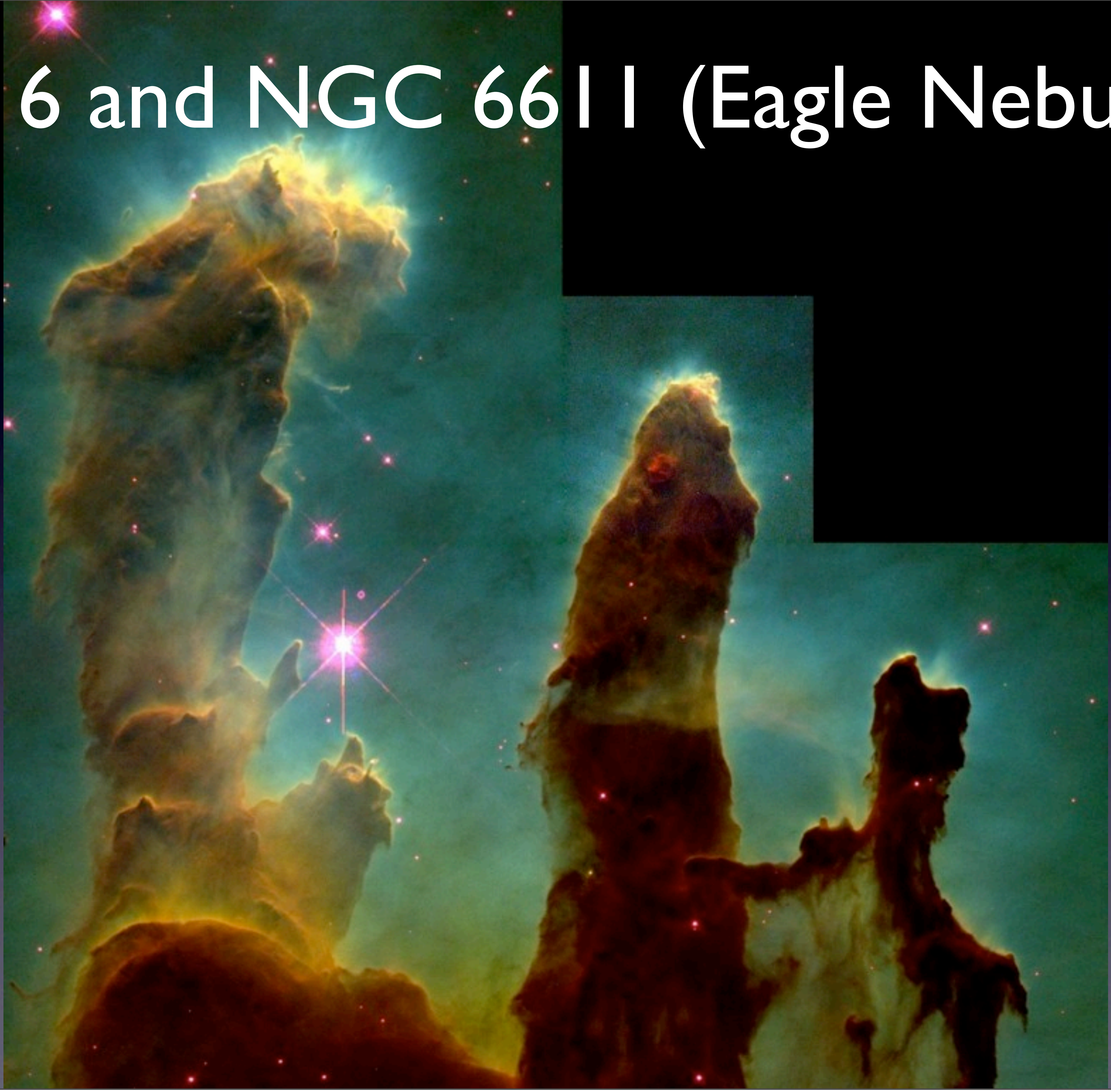

M16 and NGC 6611 (Eagle Nebula)

M16 and NGC 6611 (Eagle Nebula)

- - Hα image from AAT.
  - Main image from HST (Hester et al. 1996).
  - IR from VLT+ISAAC (McCaughrean+,2002, A&A)
- M16 is a young massive star-forming region
  - ~2 Myr old
  - ~10-20 pc diameter
- Much less spherically symmetric than RCW 120.
- Has large pillars/elephant trunks and other structures.
- Difference likely because M16 is larger and older.

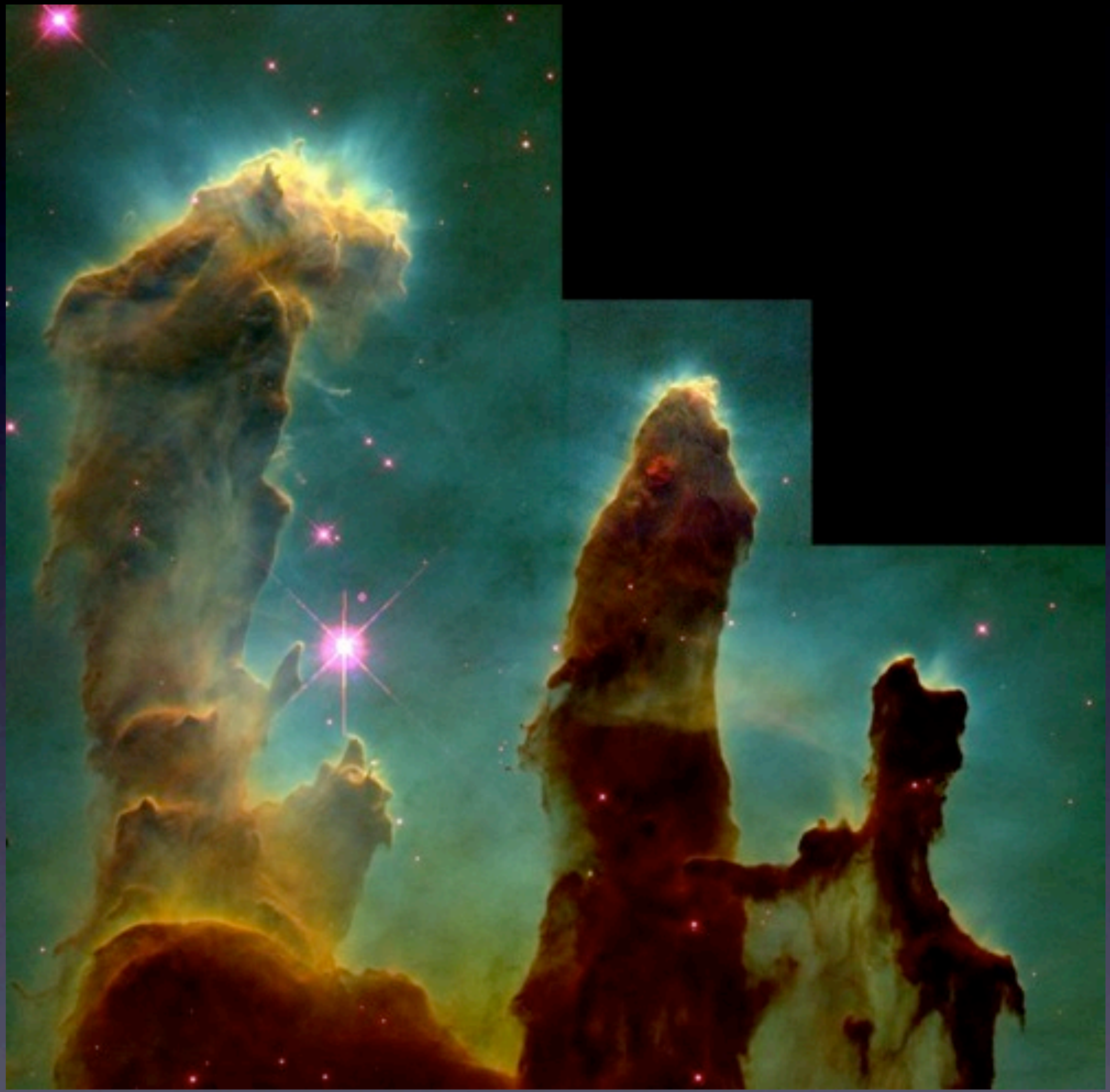

Elephant Trunks in H II regions

- Found in most HII regions.
- Multiple possible formation mechanisms (Williams+2001, Mizuta+2007, Kane +2005, Whalen+2008).
- Formation by...
    - I-front instabilities?
    - Collect and collapse?
    - Shadowing due to pre-existing structure?
    - All of the above?
- Magnetic fields dynamically important?
- Many pillars have embedded YSOs
    - Is star formation triggered?
- Do structures 'remember' formation mechanism?

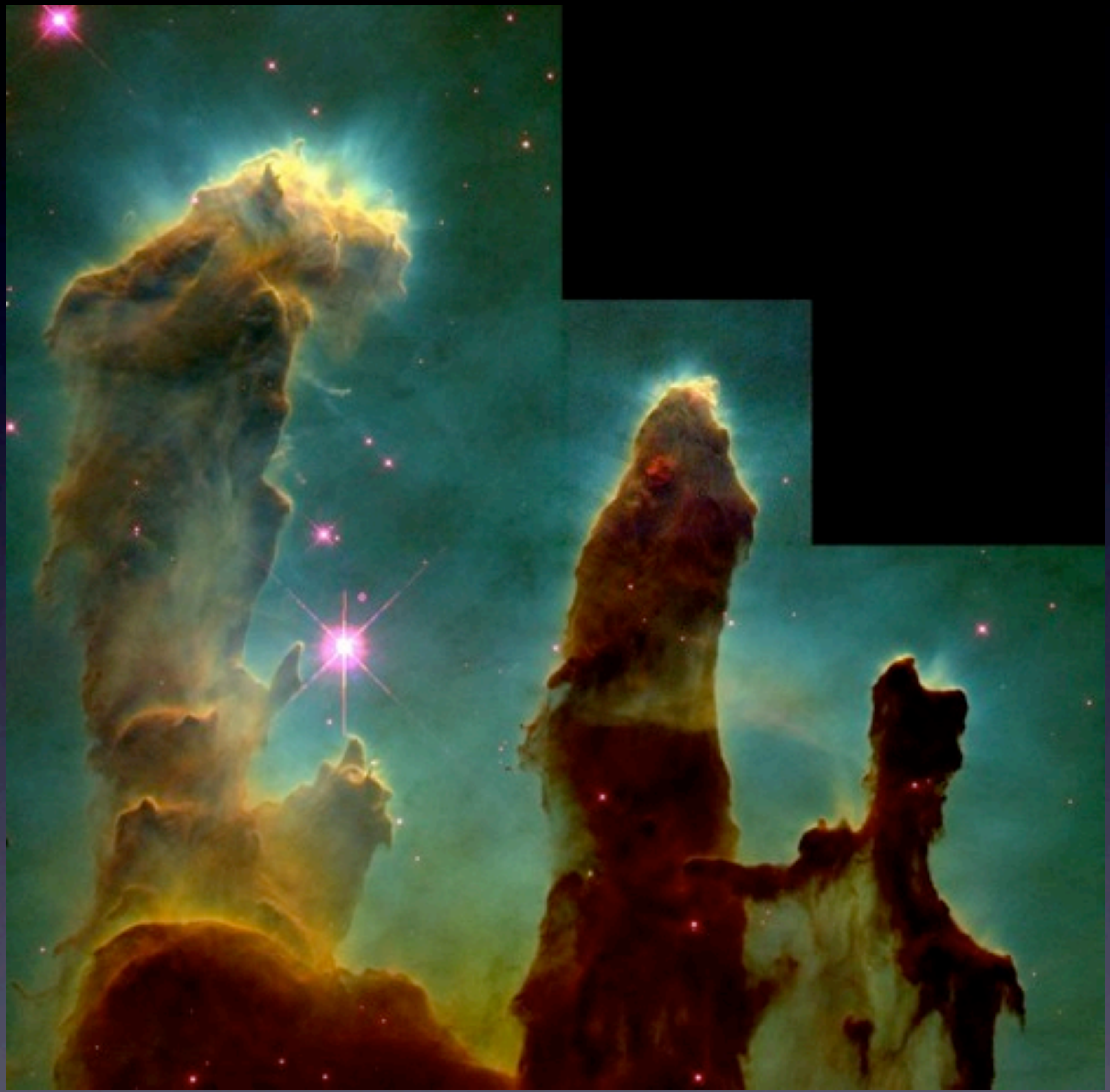

Magnetic Fields within in M16

- Dust grains are aligned by magnetic fields, resulting in polarised emission (far IR) and absorption (optical).
- Sugitani et al. (2007,PASJ) measured polarisation of background stars to study magnetic field in M16.
- Found large-scale coherent field (right).
- Field in pillars is aligned with pillar, misaligned with ambient field.
- Related to formation mechanism? Field strength?

Magnetic Fields within in M16

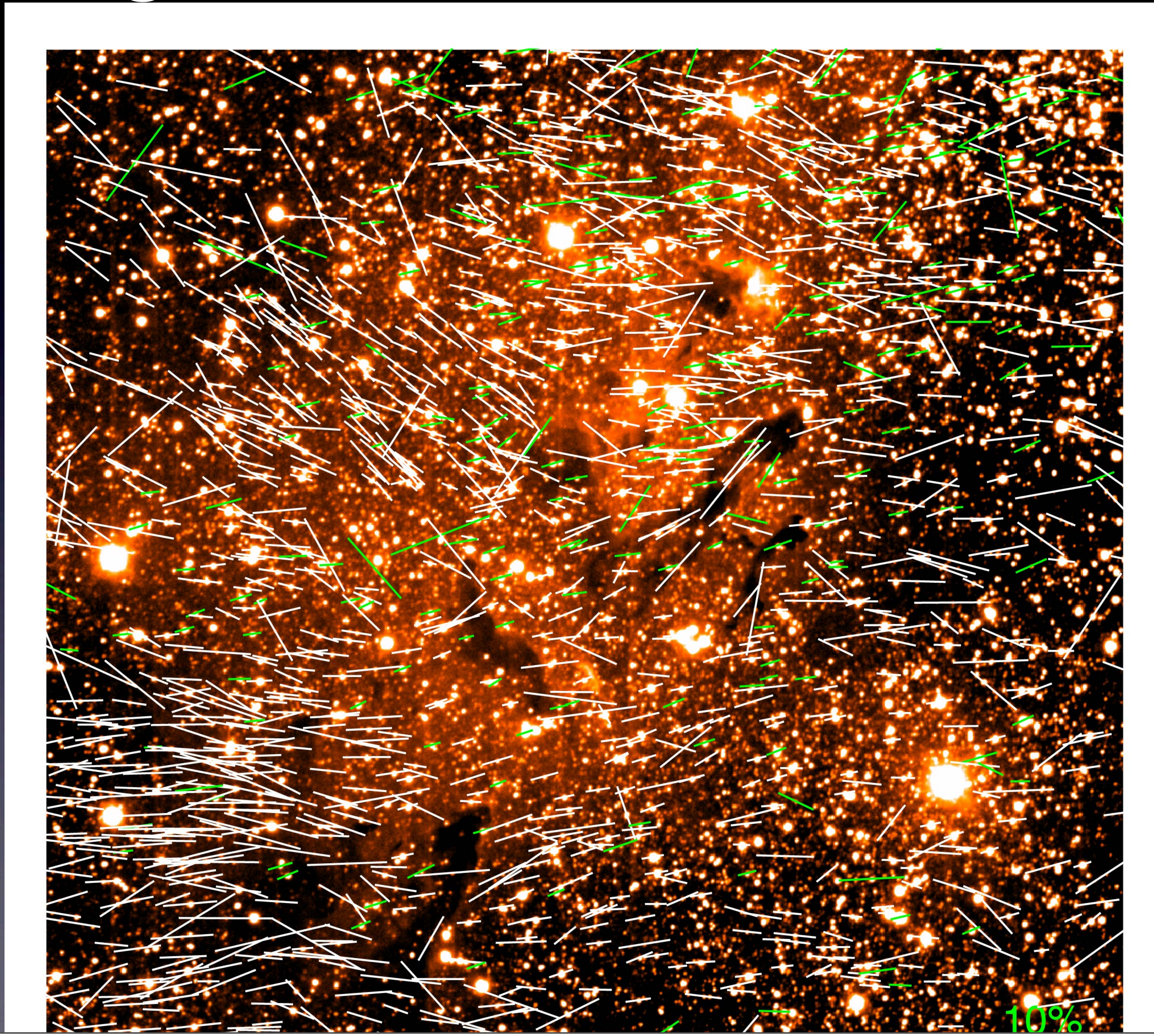

Magnetic Fields within in M16

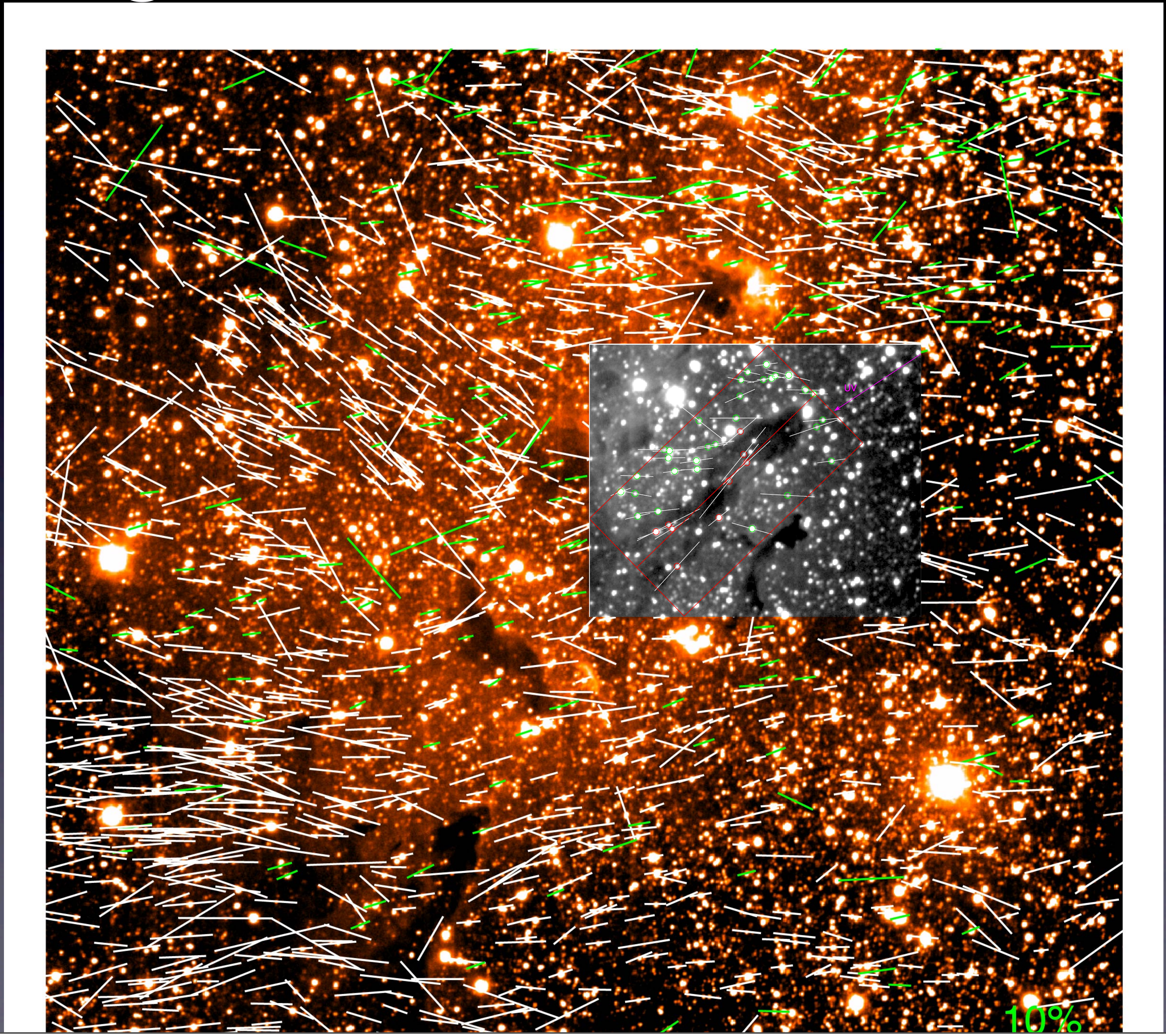

Magnetic Fields within in M16

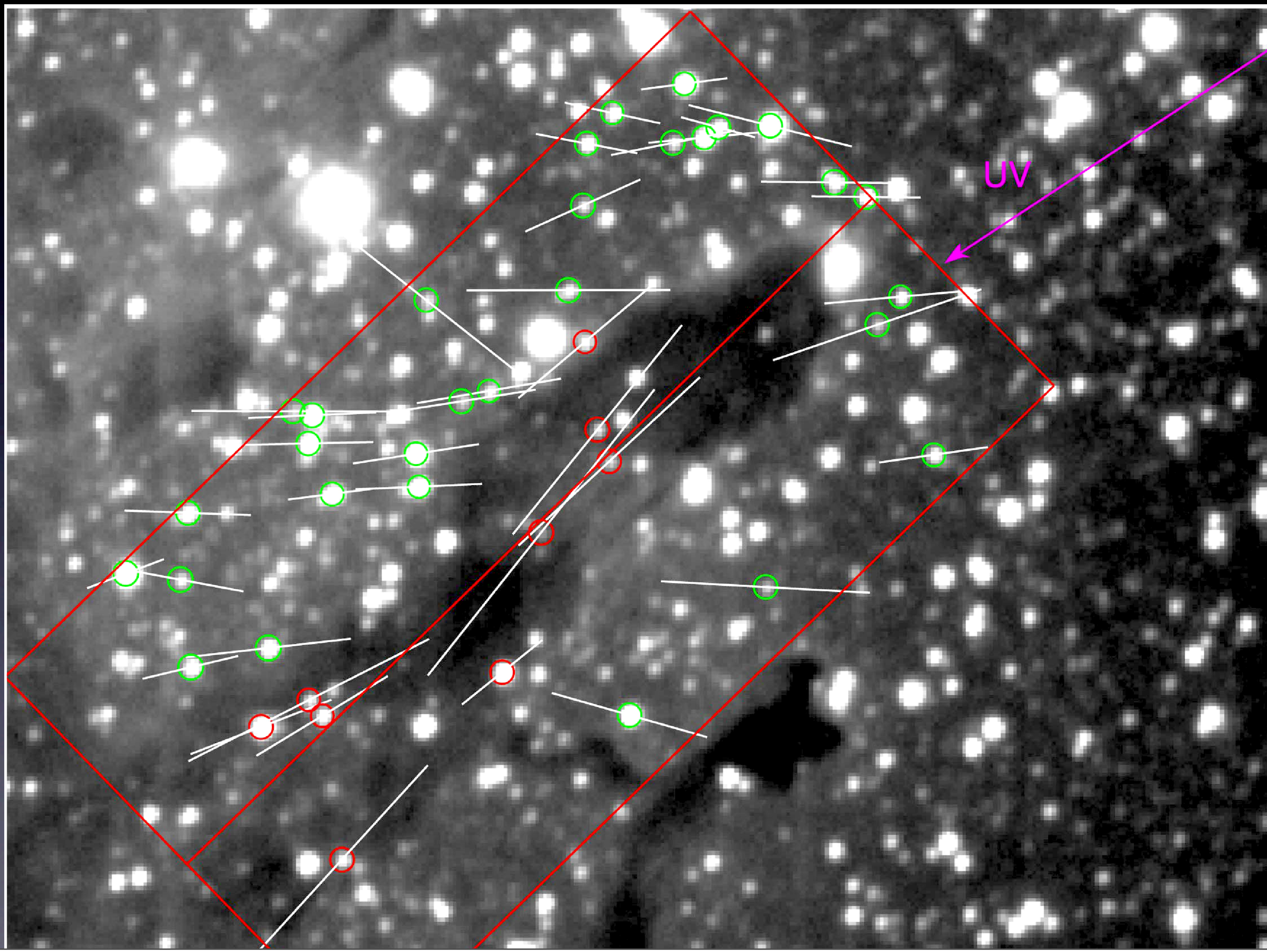

Questions addressed

- Effect of the ionisation-driven dynamics on the initial magnetic field?
- Effect of the B-field on the pillar morphologies?
- Effect of the B-field on photoevaporation flows?

RMHD - Computational Methods

- Grid-based code (Mackey & Lim, 2010,2011; Mackey,2012), based on Falle+(1998) 2nd order integration scheme for MHD.
- **Dynamics**: Solves the Euler or Ideal MHD equations on a uniform grid using a shock-capturing finite volume scheme with 2nd order spatial and temporal accuracy.
- Dedner+(2003) mixed-GLM divergence cleaning.
- **Ray-Tracing**: Track ionising radiation from discrete sources using the short characteristic tracer with the "On-the-Spot" approx.
- **Microphysics**: Within each cell we track non-equilibrium ionisation, heating and cooling by radiative and collisional processes (explicitly for Hydrogen, indirectly for others). Operator-split from dynamics.
- Methods are similar to those used in Lim & Mellema (2003), and the Mellema+(2006,NewA,11,374) C2-ray algorithm.
- Parallelised with MPI by domain splitting; rays cross domains causally, but still scales well to at least 512 cores.

Simulation Initial conditions

- Simulation box 6x3x3 pc (384x192x192).
- Star at [0,0,0] emits 10^{50} ionising photons /sec.
- Background density $n=200cm^{-3}$.
- 3 almost collinear clumps, mass 28 Msun, with overdensity 500x.
- Two field orientations: b ≃ [0, 0, 1], [1, 0, 0] ("perpendicular" and "parallel").
- Three strengths: |B| ≃ [18, 53, 160] μG,
- corresponding to [β ≫ 1, β~1, β ≪ 1] respectively.

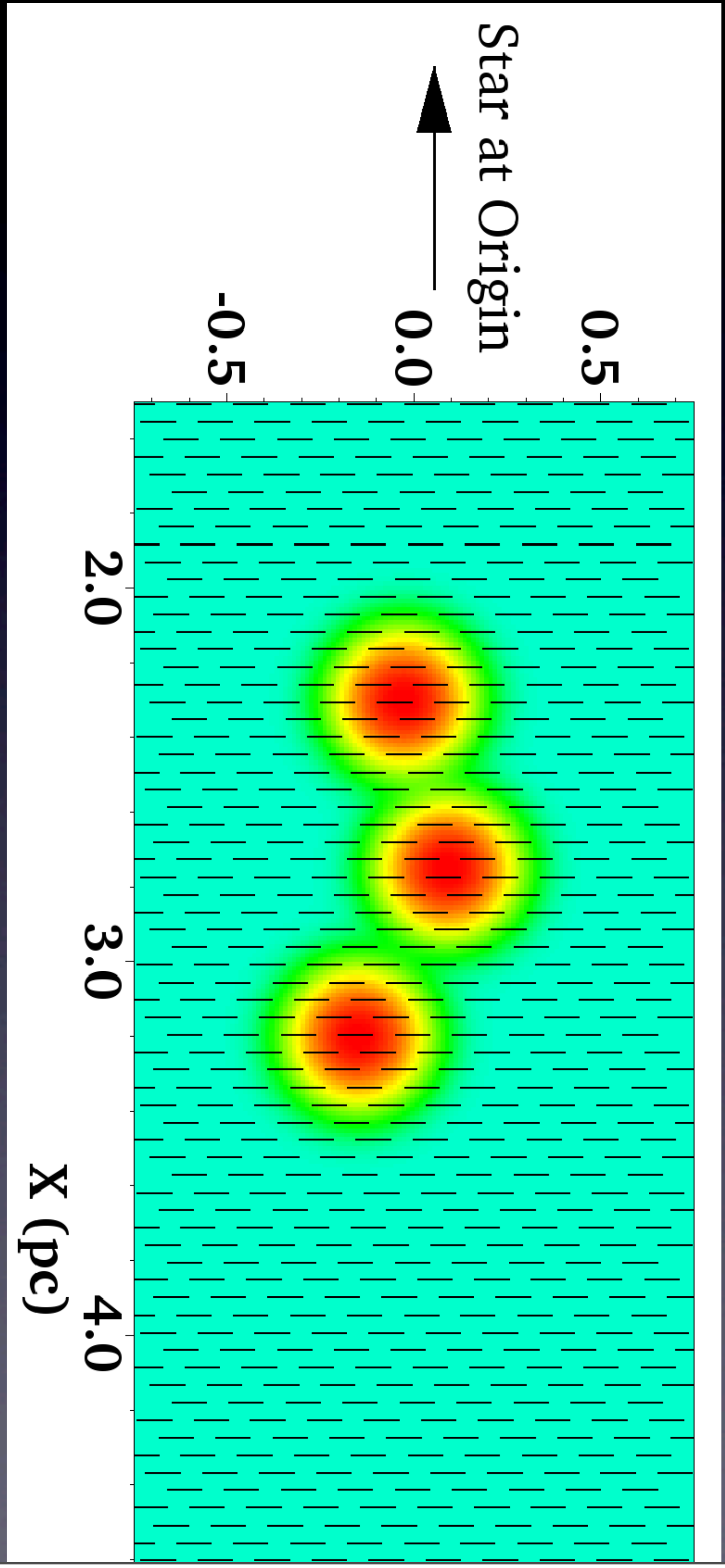

Weak, perpendicular B-field

Left: B-field along Line-of-Sight   Right: B-field perpendicular to LOS

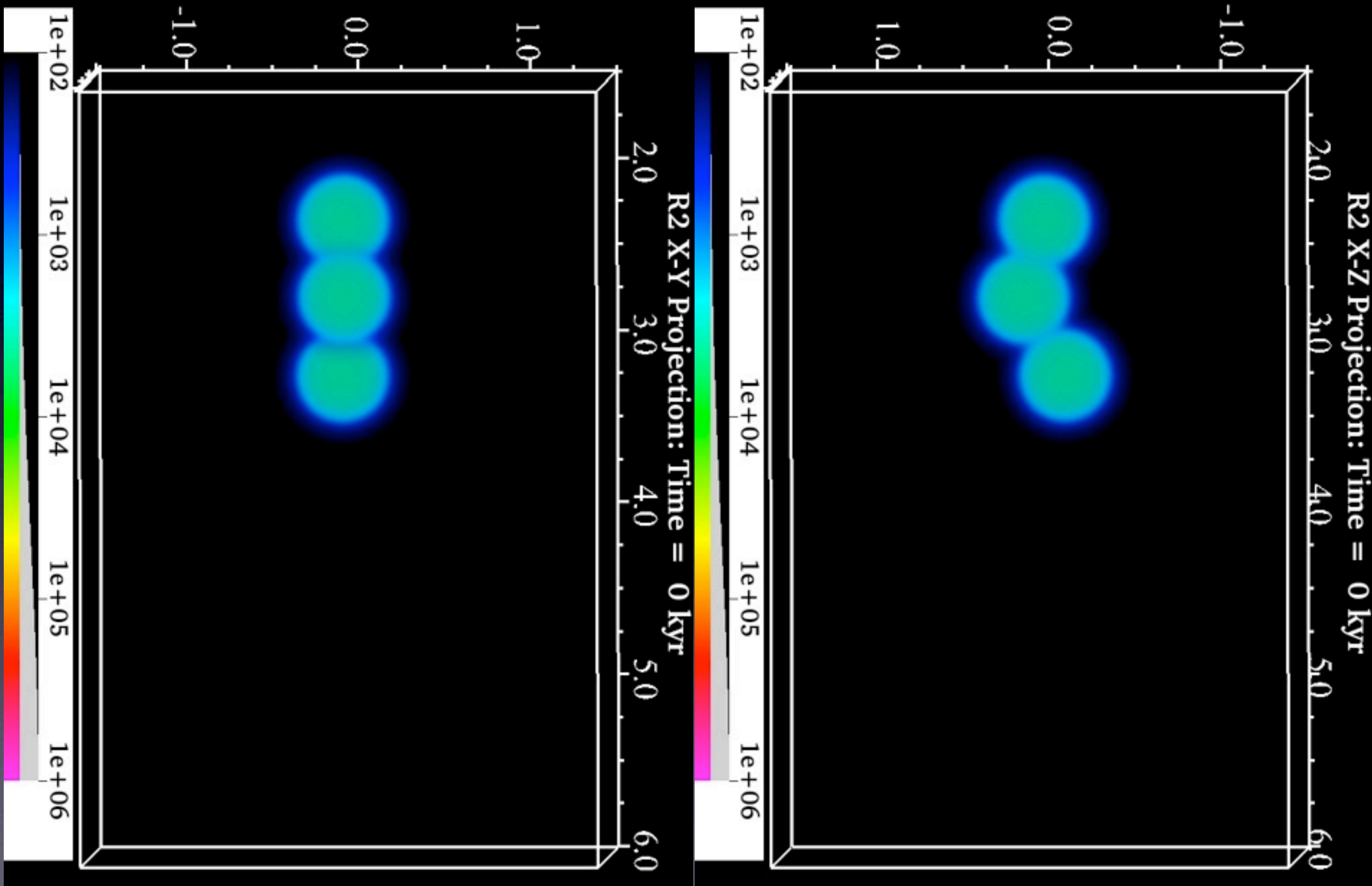

Weak, Perpendicular B-field - 25kyr

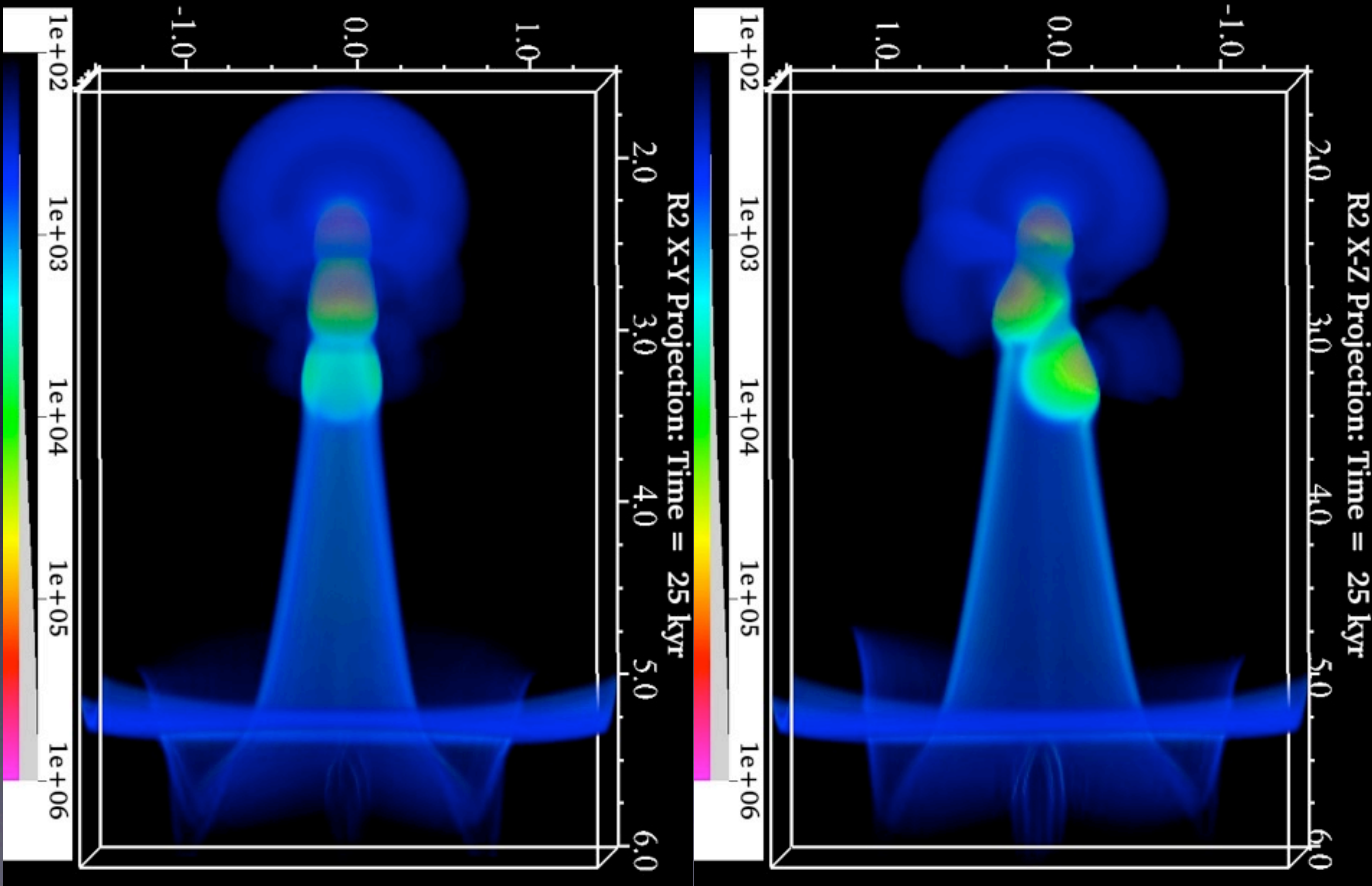

Weak, Perpendicular B-field - 50kyr

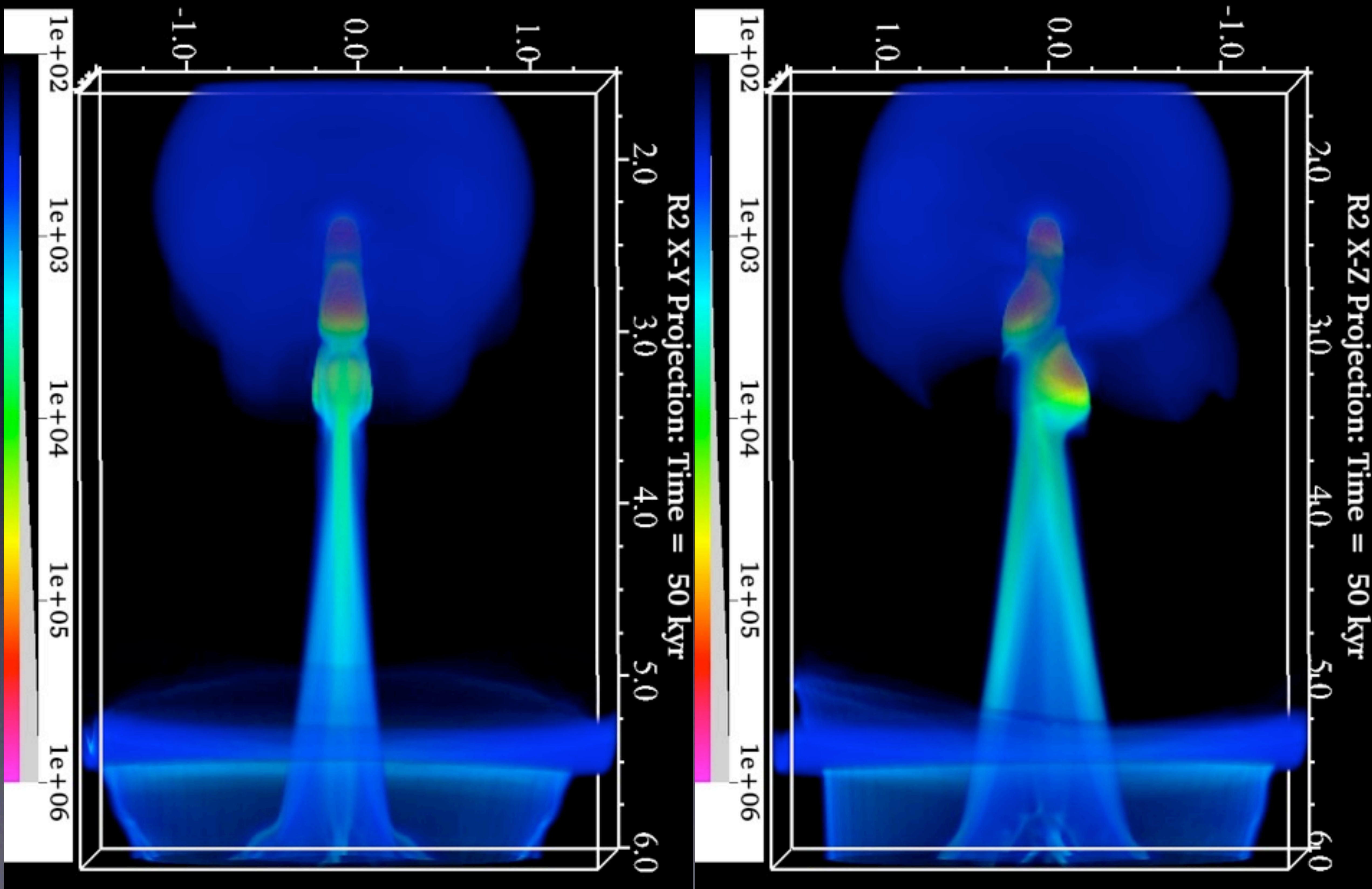

Weak, Perpendicular B-field - 100kyr

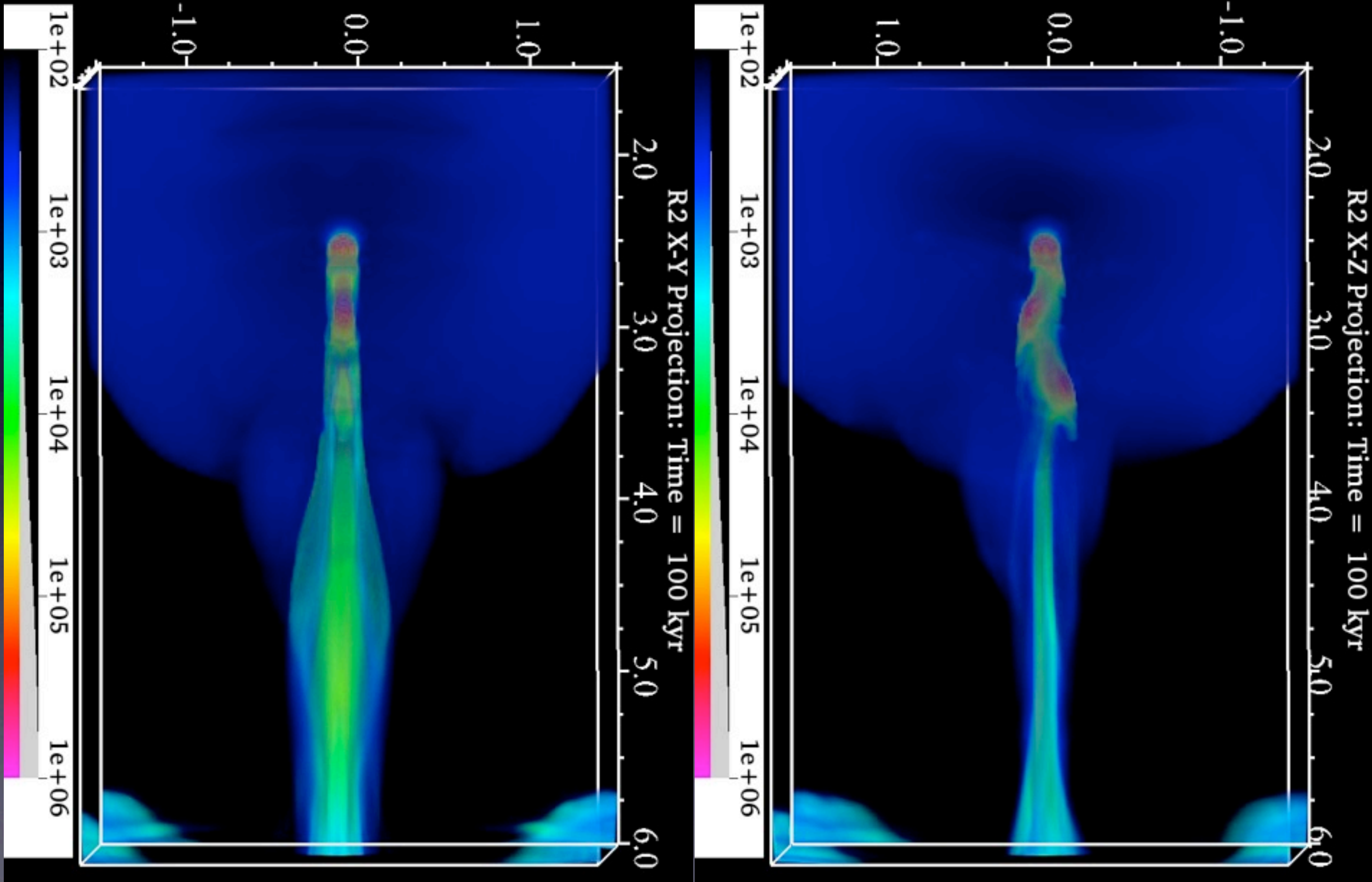

Weak, Perpendicular B-field - 150kyr

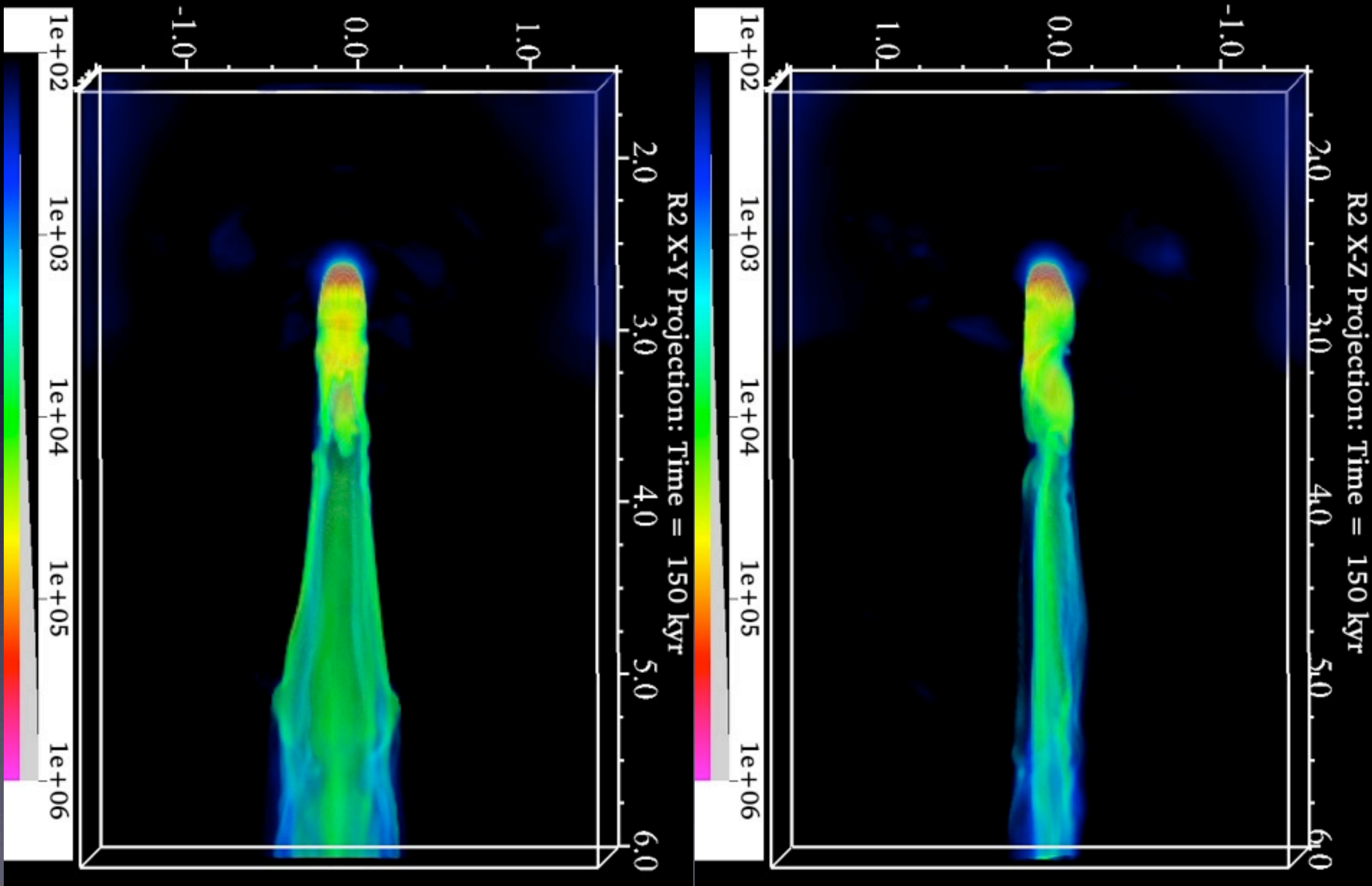

Weak, Perpendicular B-field - 200kyr

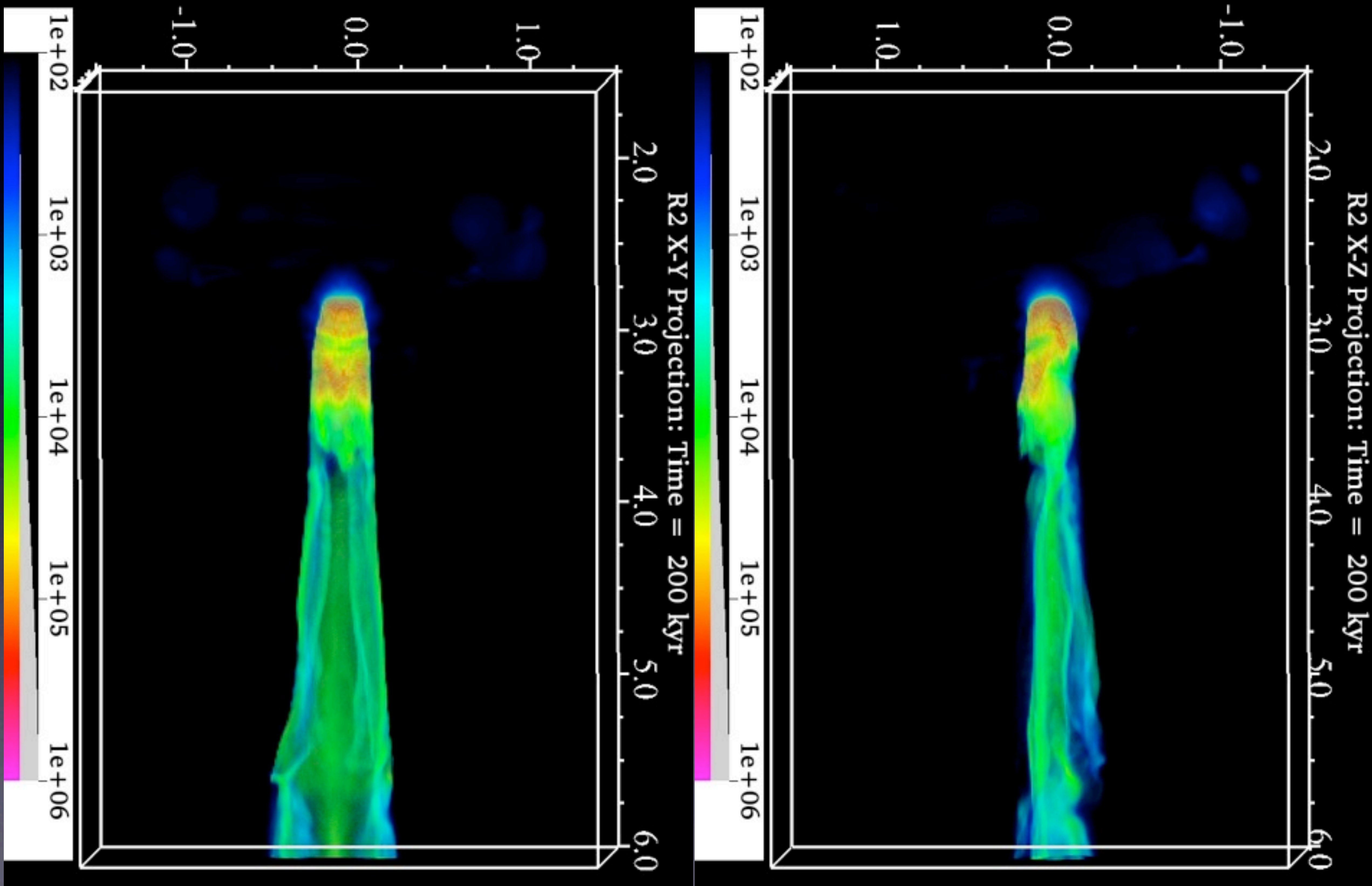

Weak, Perpendicular B-field - 250kyr

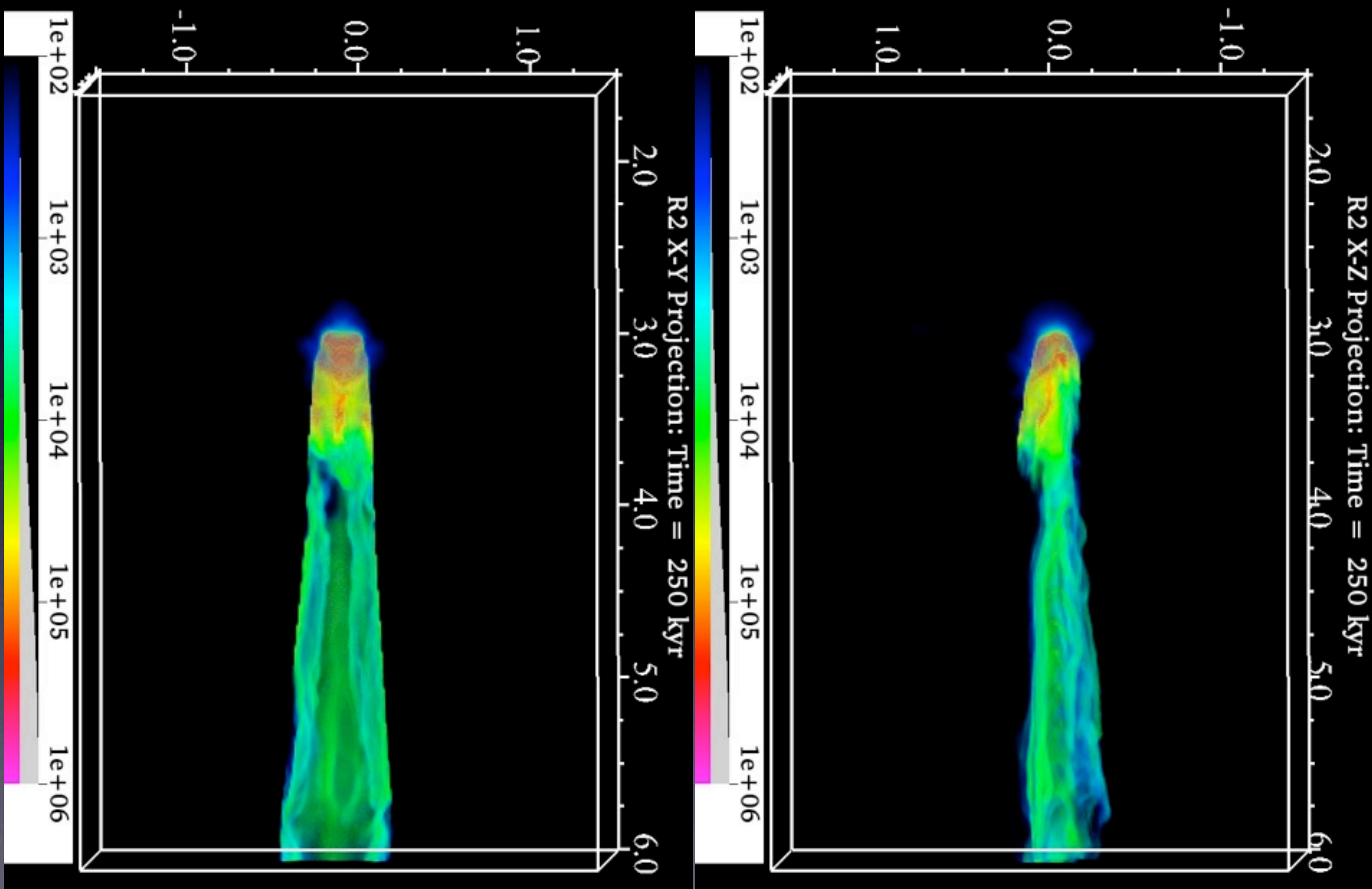

Weak, Perpendicular B-field - 300kyr

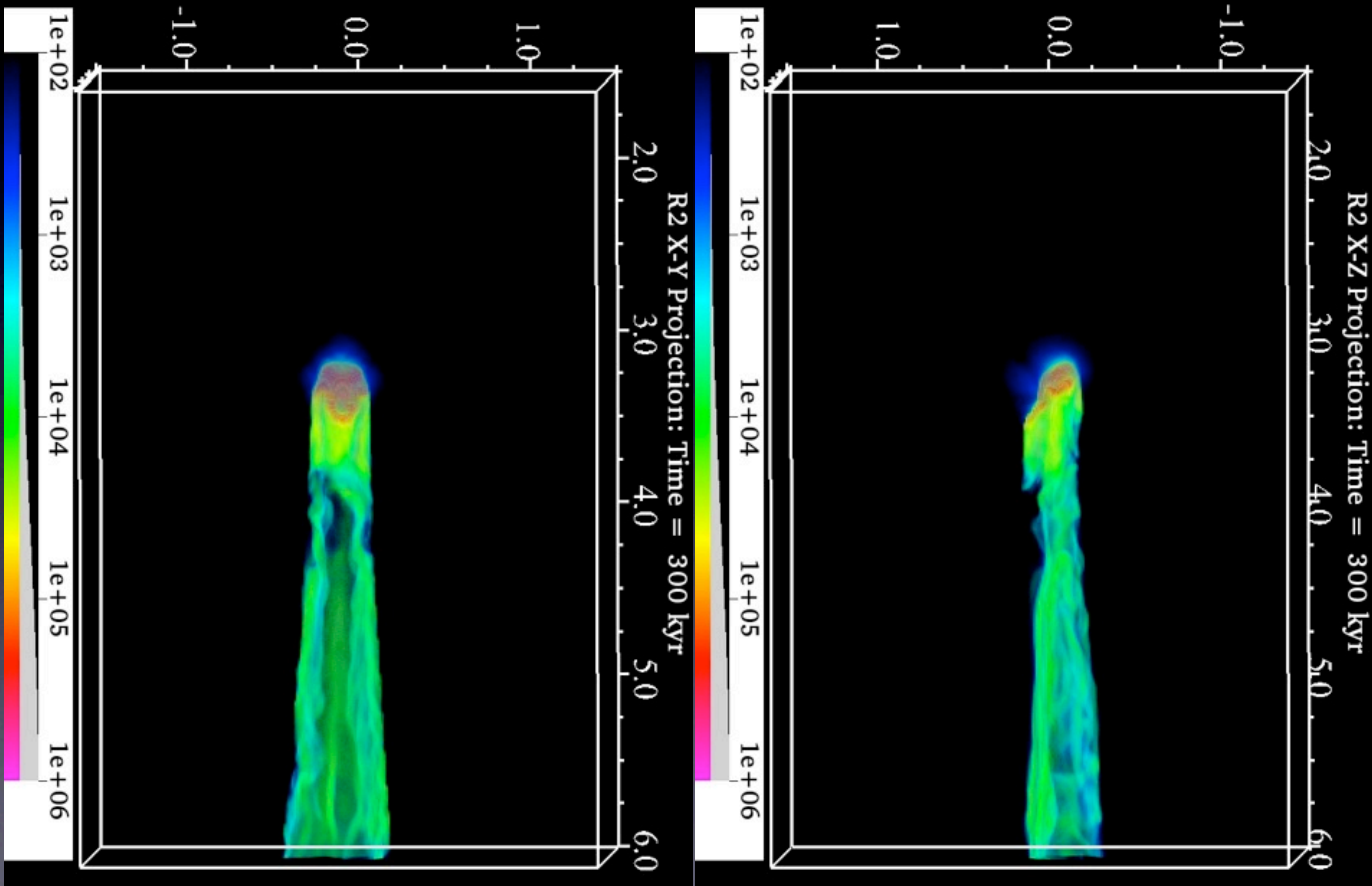

Weak, Perpendicular B-field - 350kyr

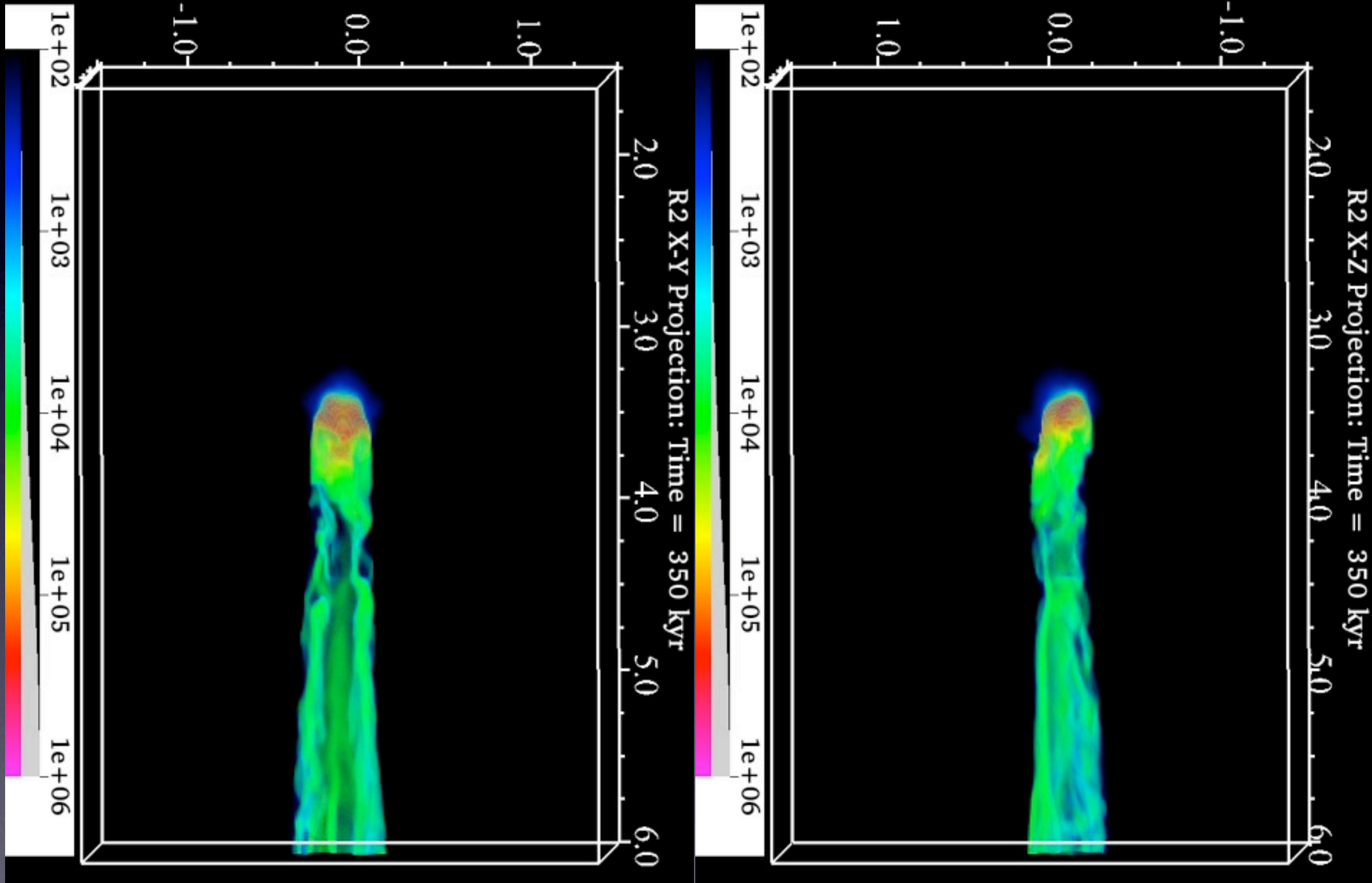

Weak, Perpendicular B-field - 400kyr

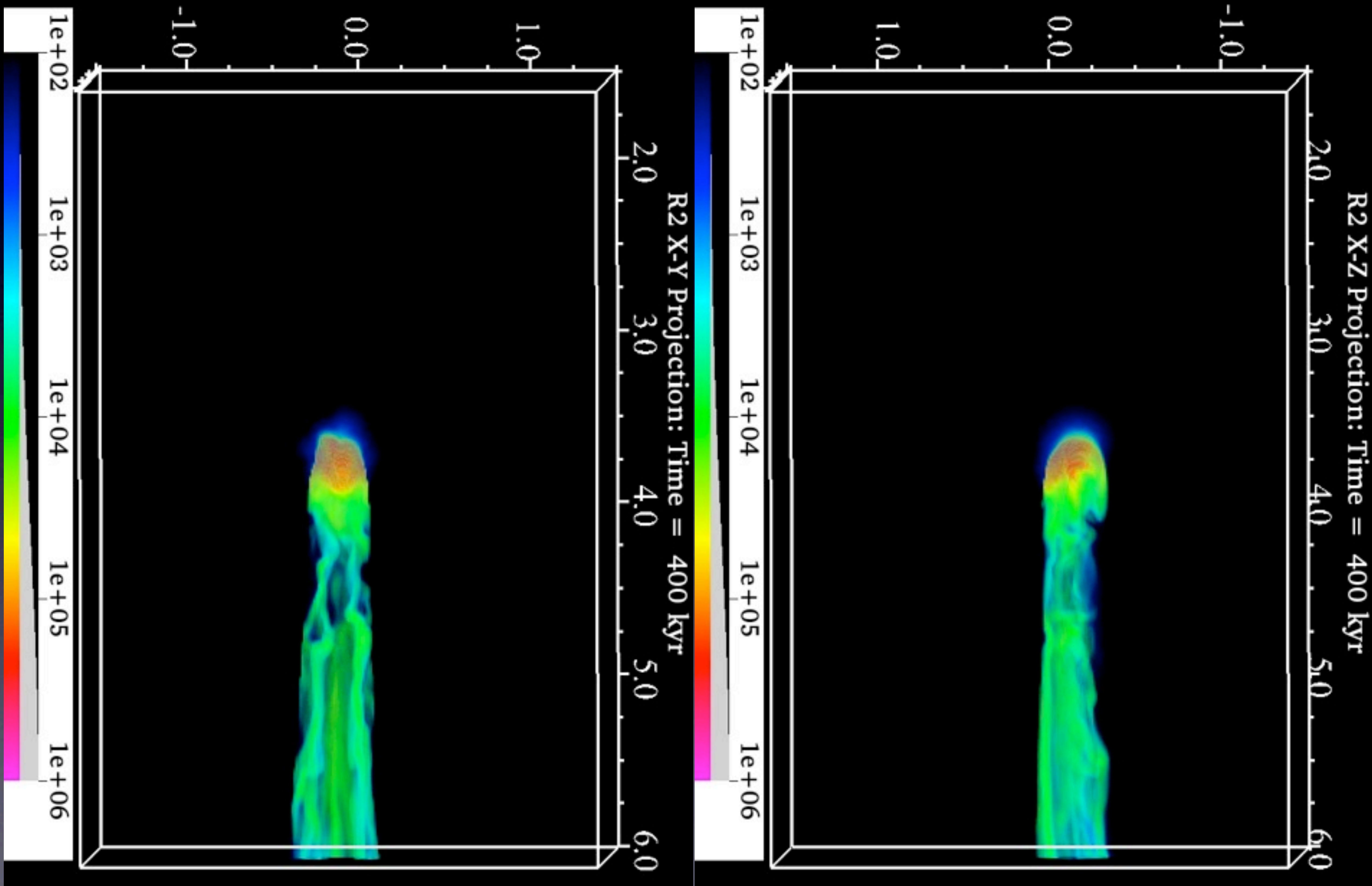

Weak, Perpendicular B-field - 450 kyr

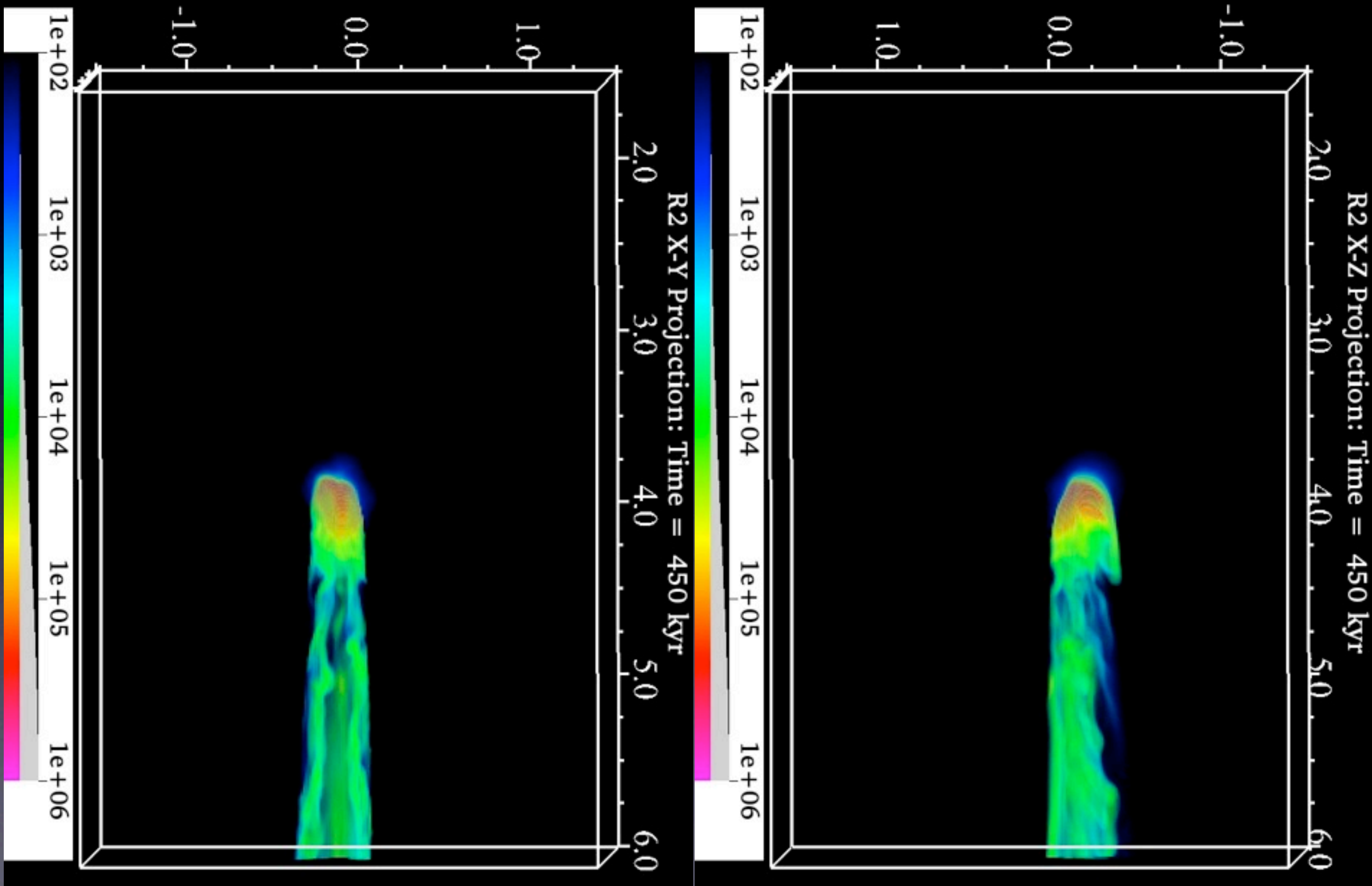

Weak, Perpendicular B-field - 500 kyr

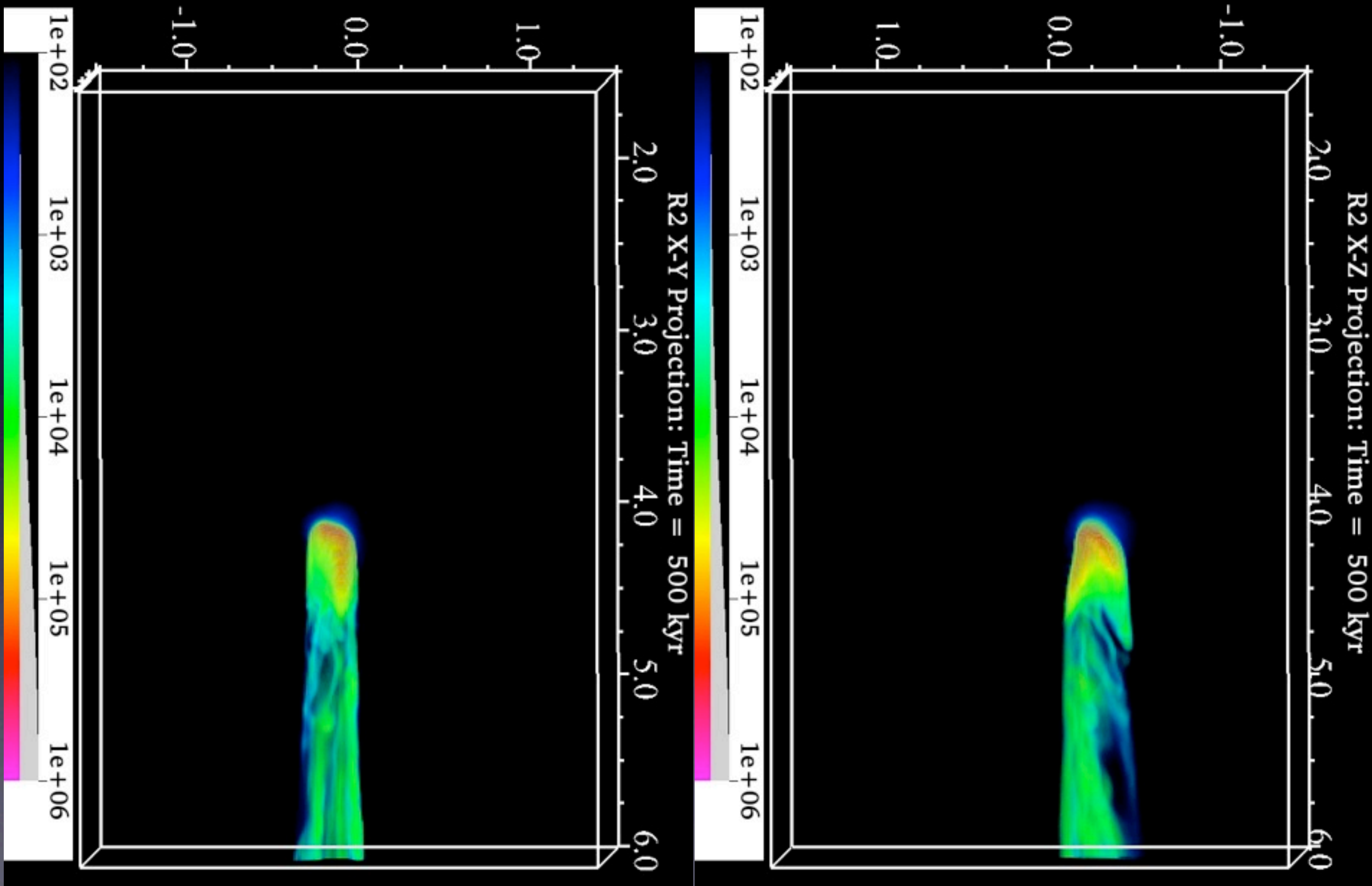

Medium strength, perpendicular B-field

Medium, Perpendicular B-field - 25 kyr

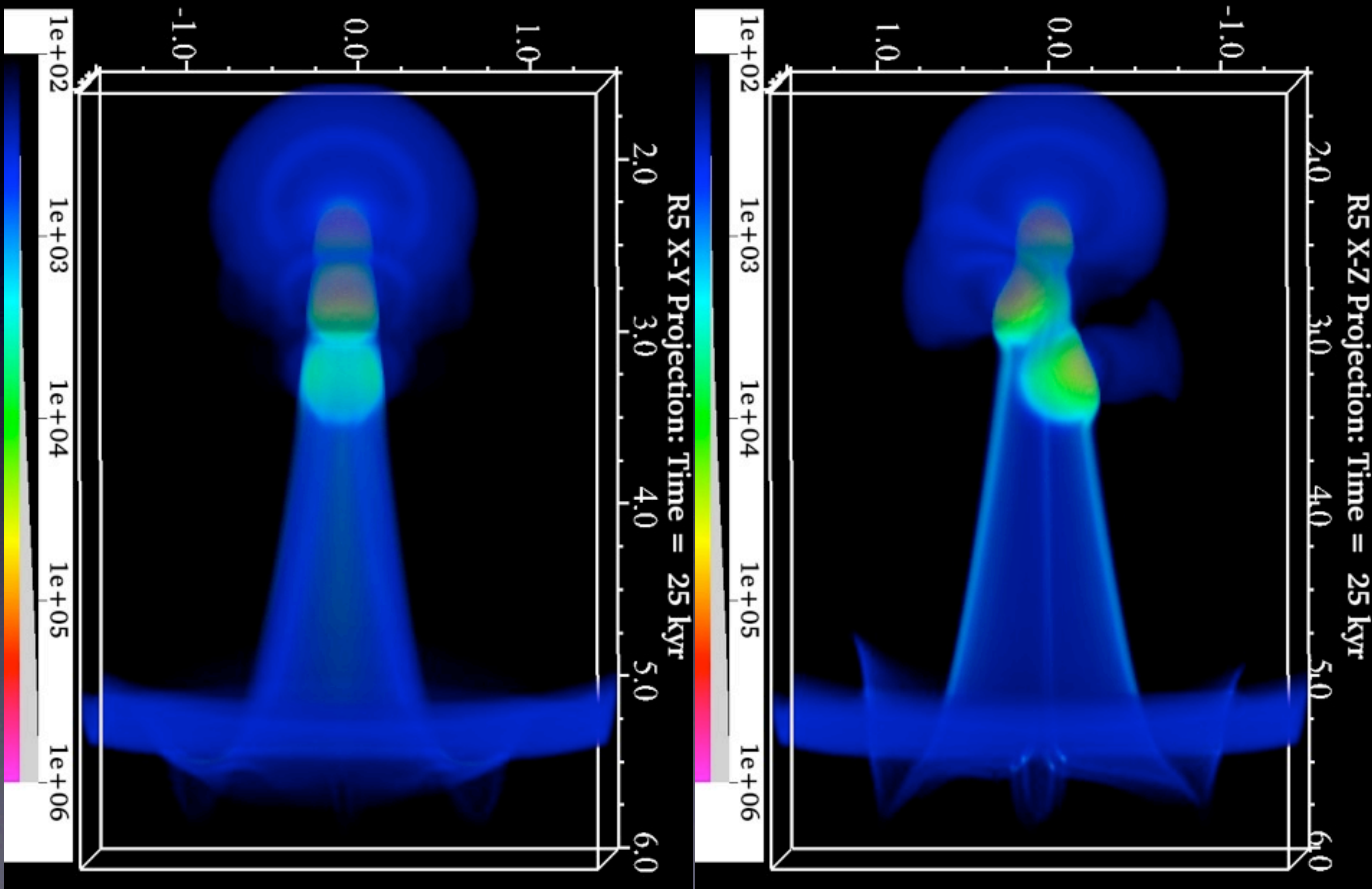

Medium, Perpendicular B-field - 50 kyr

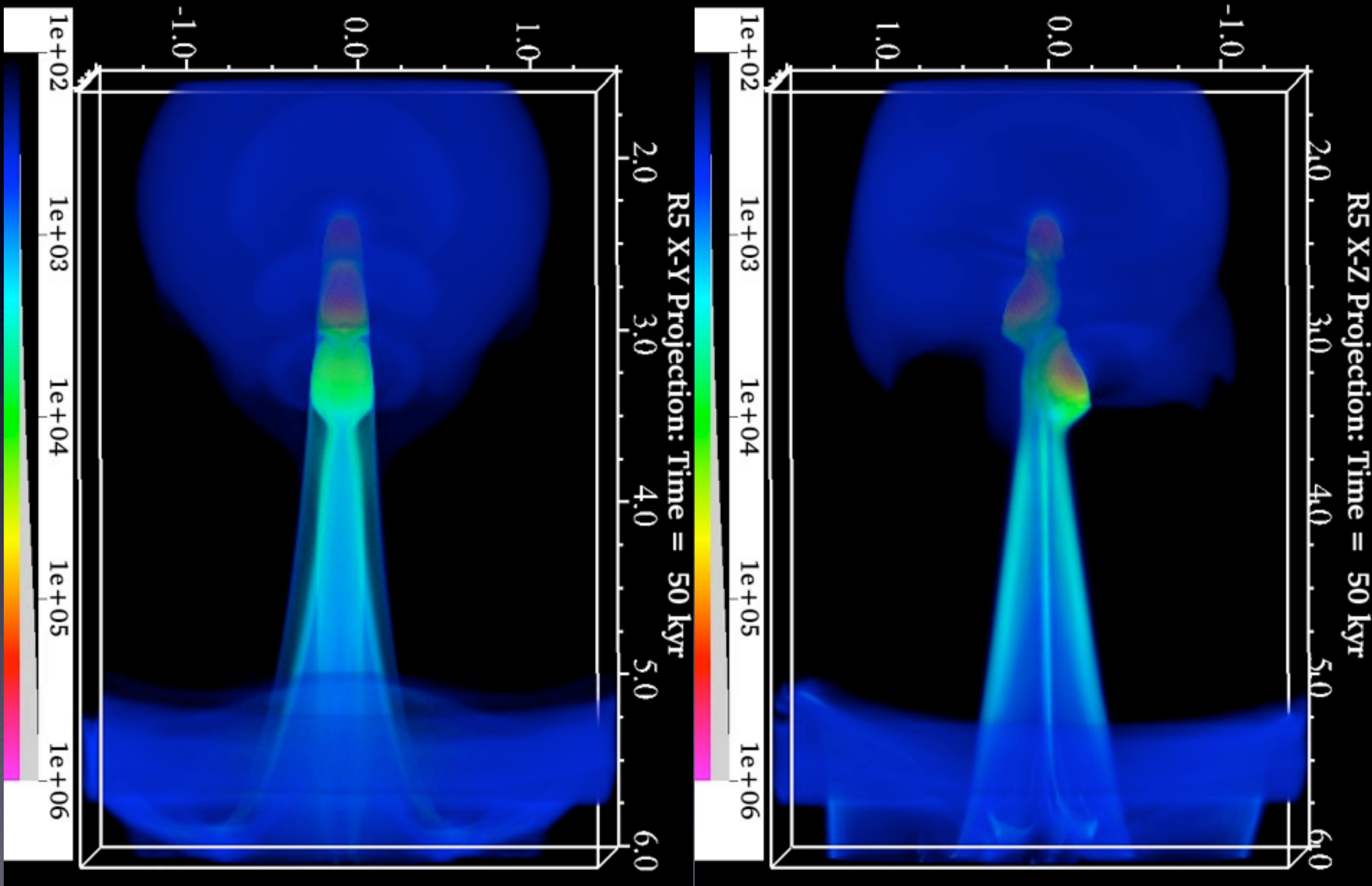

Medium, Perpendicular B-field - 100 kyr

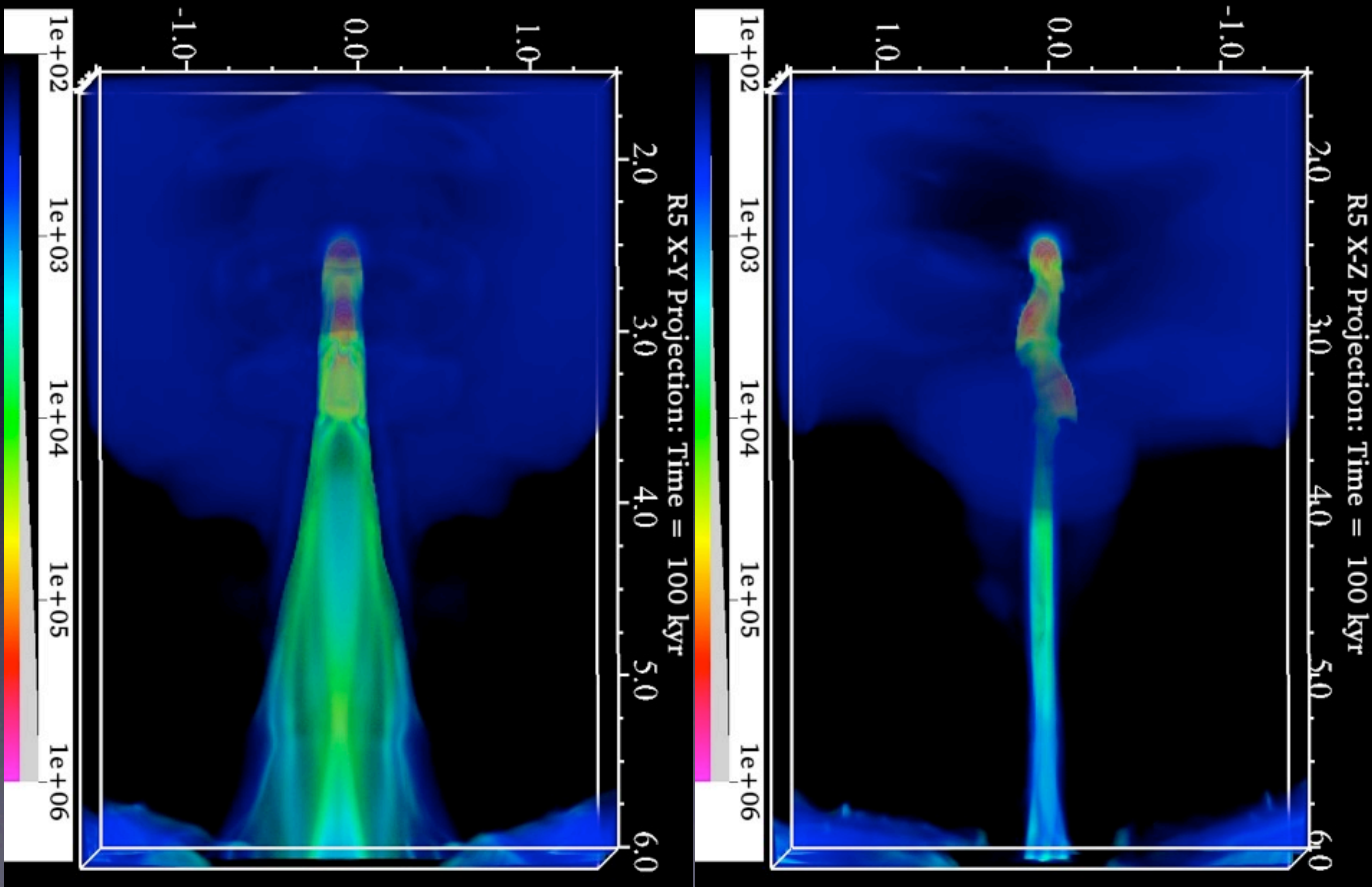

Medium, Perpendicular B-field - 150 kyr

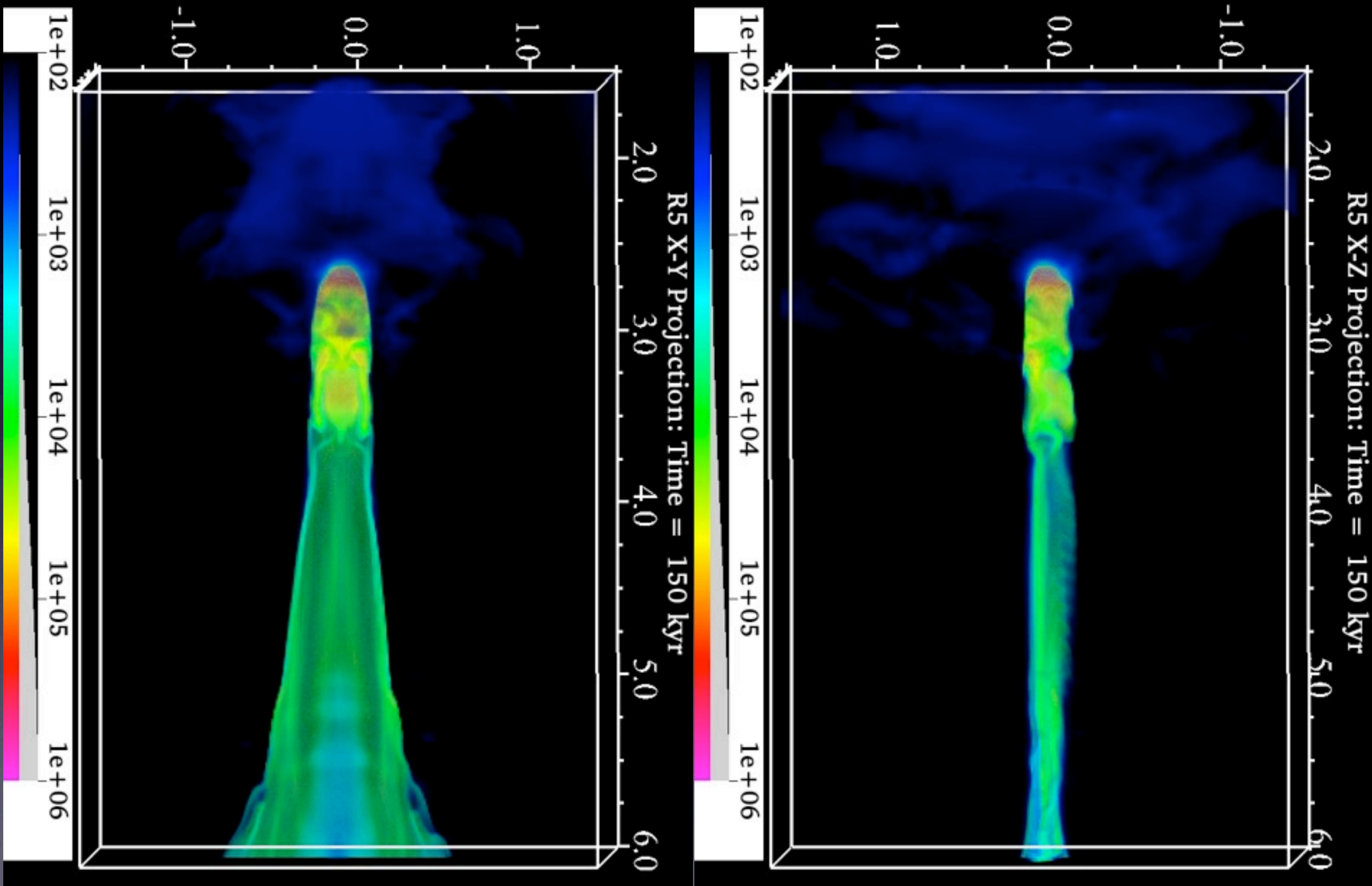

Medium, Perpendicular B-field - 200 kyr

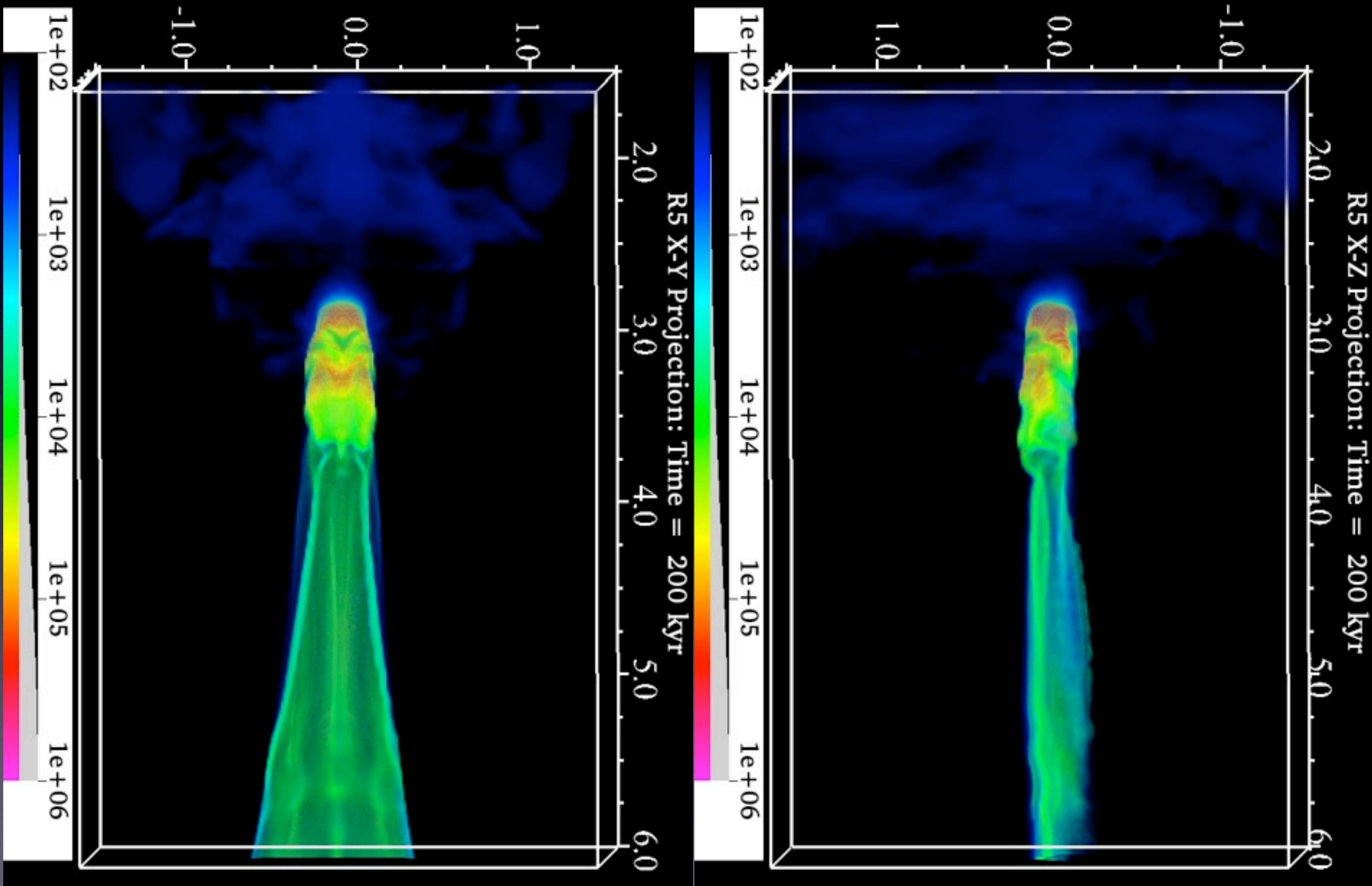

Medium, Perpendicular B-field - 250 kyr

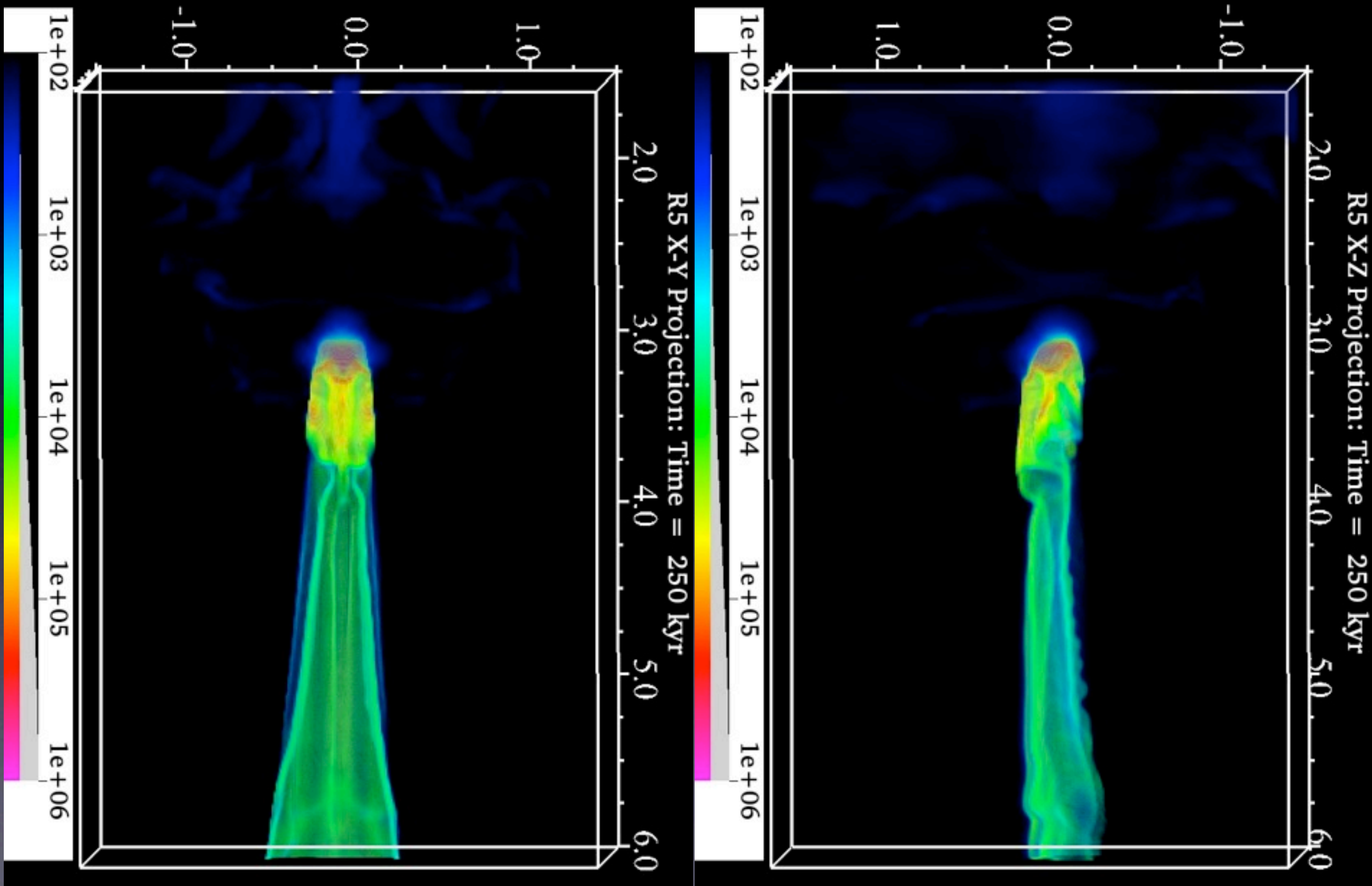

Medium, Perpendicular B-field - 300 kyr

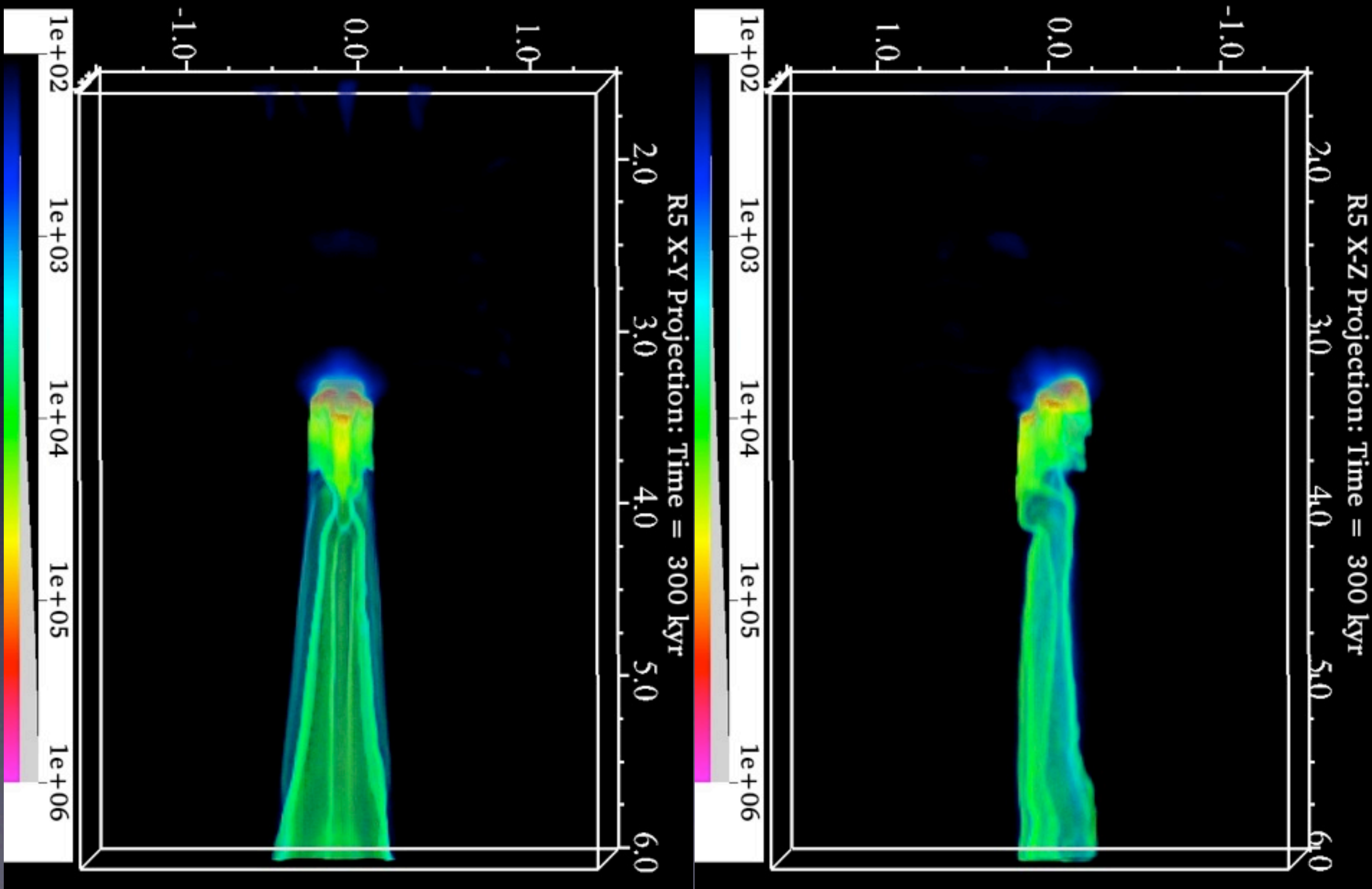

Medium, Perpendicular B-field - 350 kyr

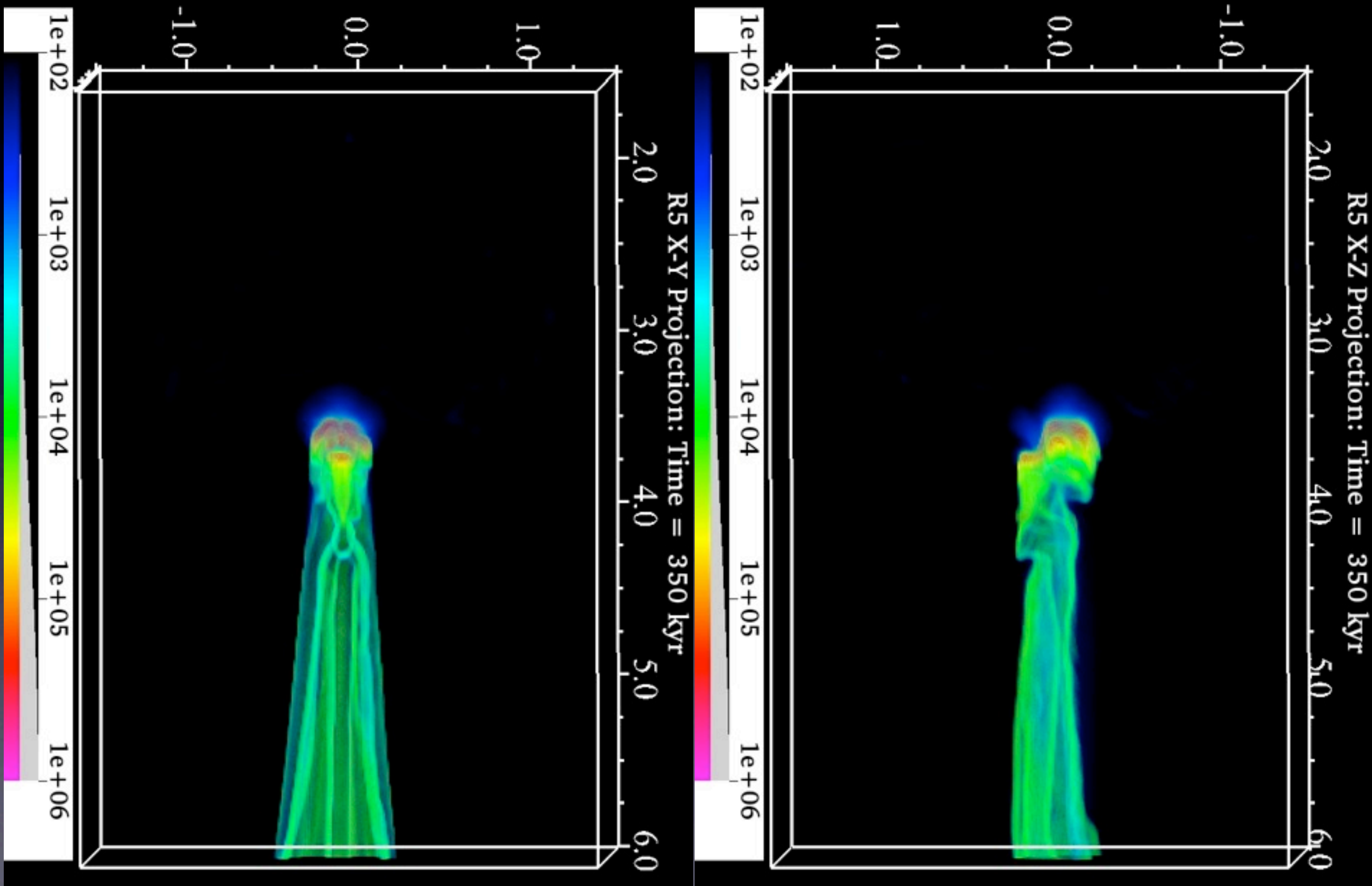

Medium, Perpendicular B-field - 400 kyr

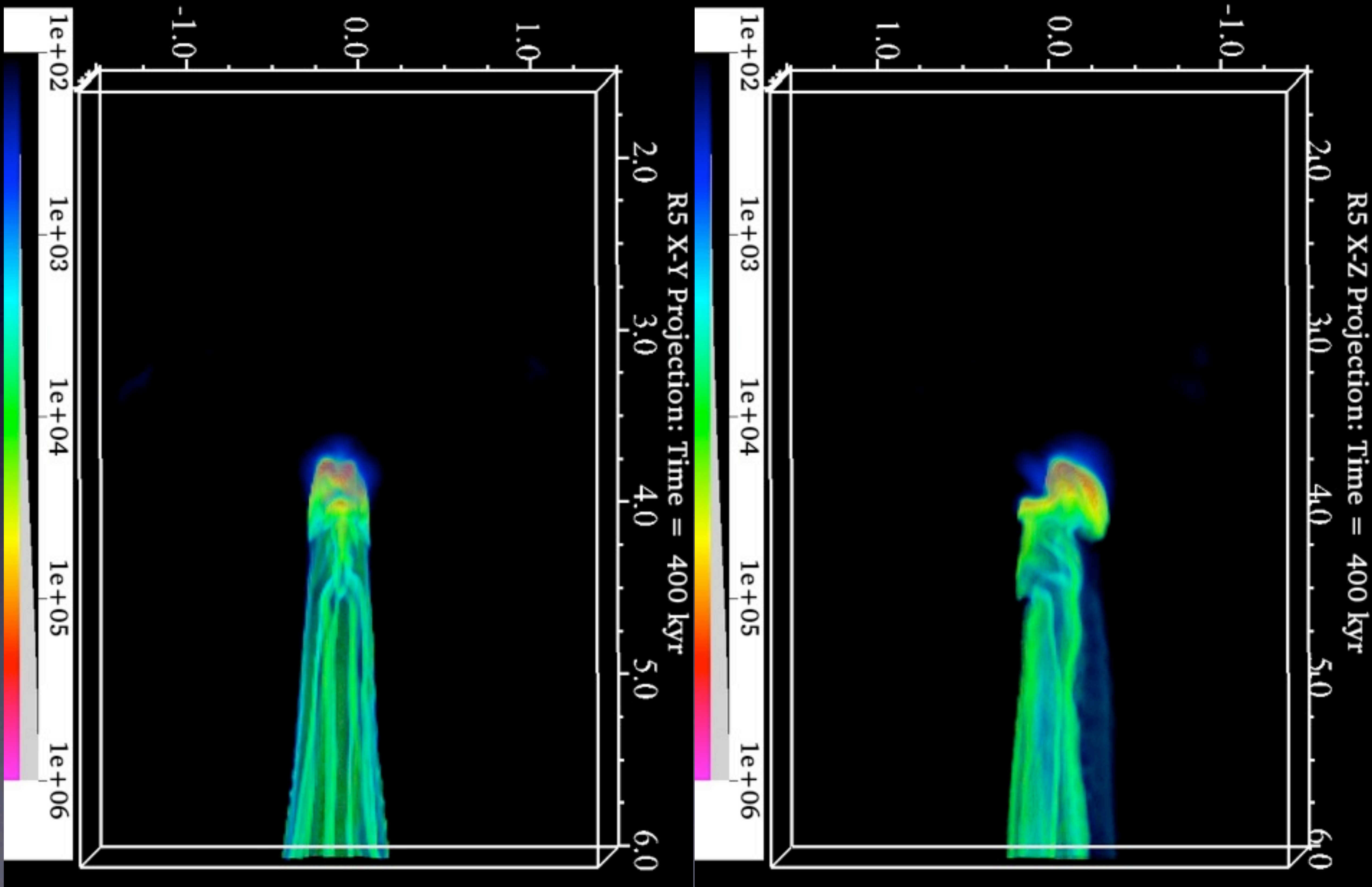

Medium, Perpendicular B-field - 450 kyr

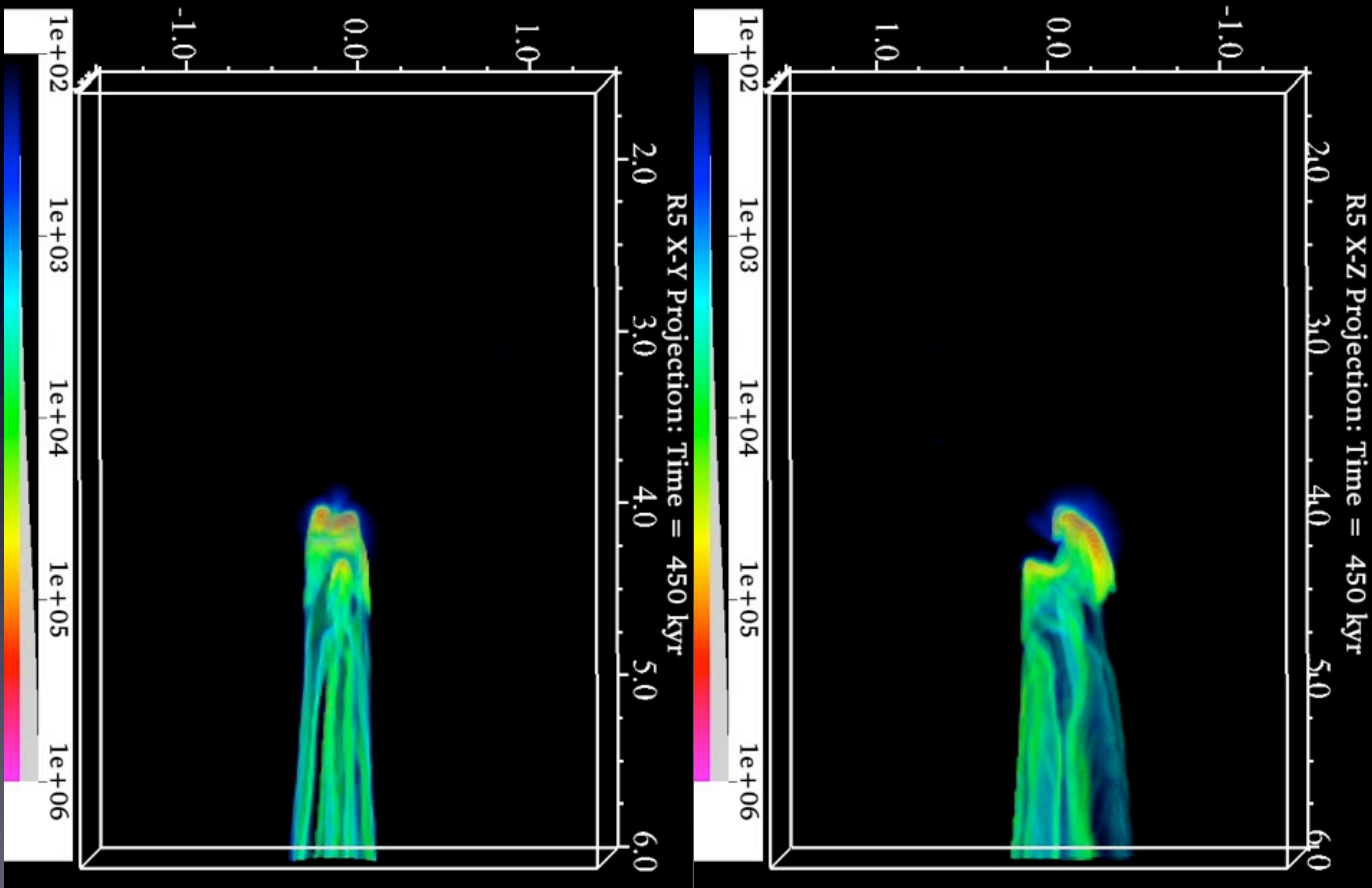

Medium, Perpendicular B-field - 500 kyr

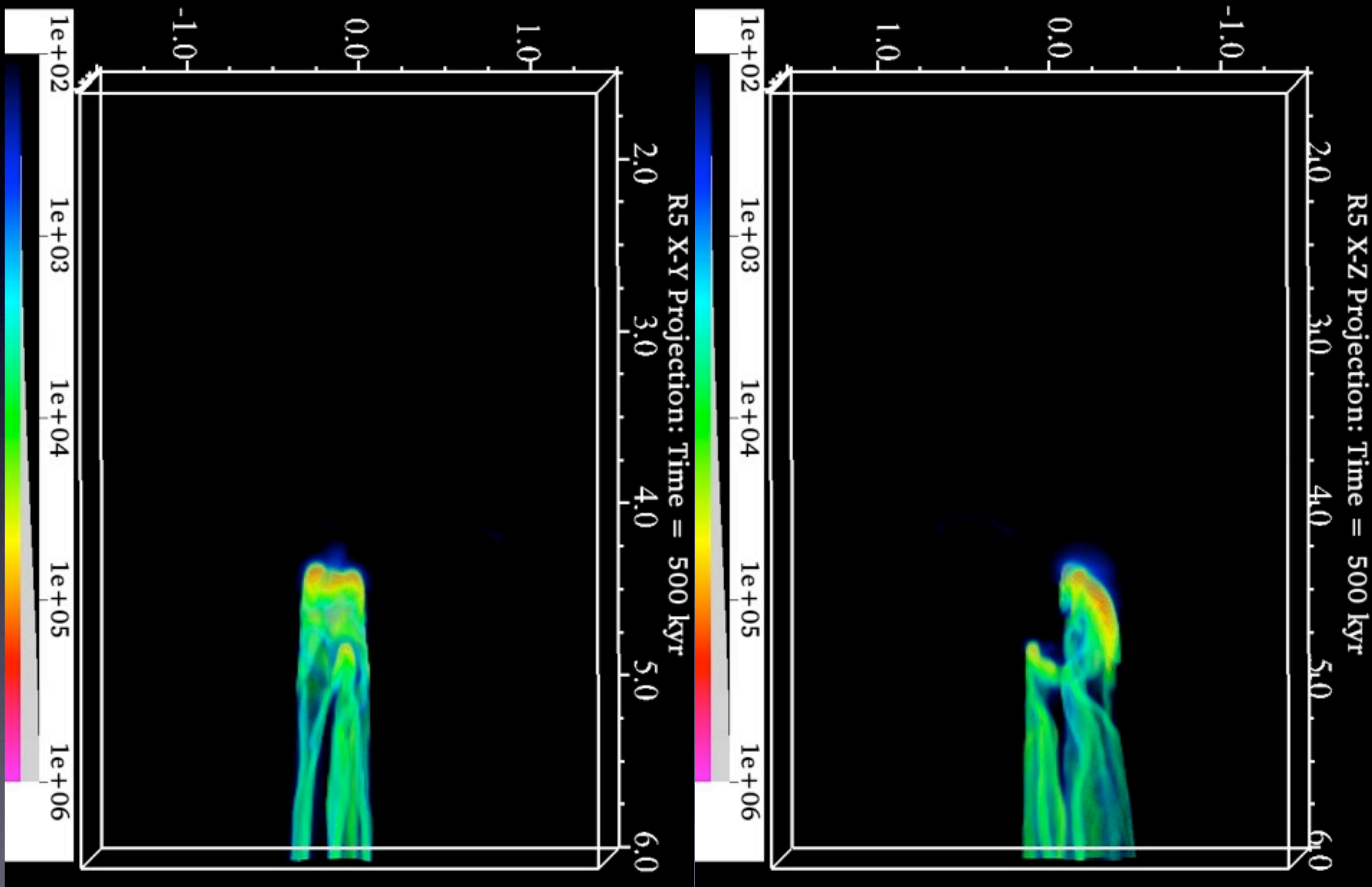

Strong, perpendicular B-field

Strong, Perpendicular B-field - 25 kyr

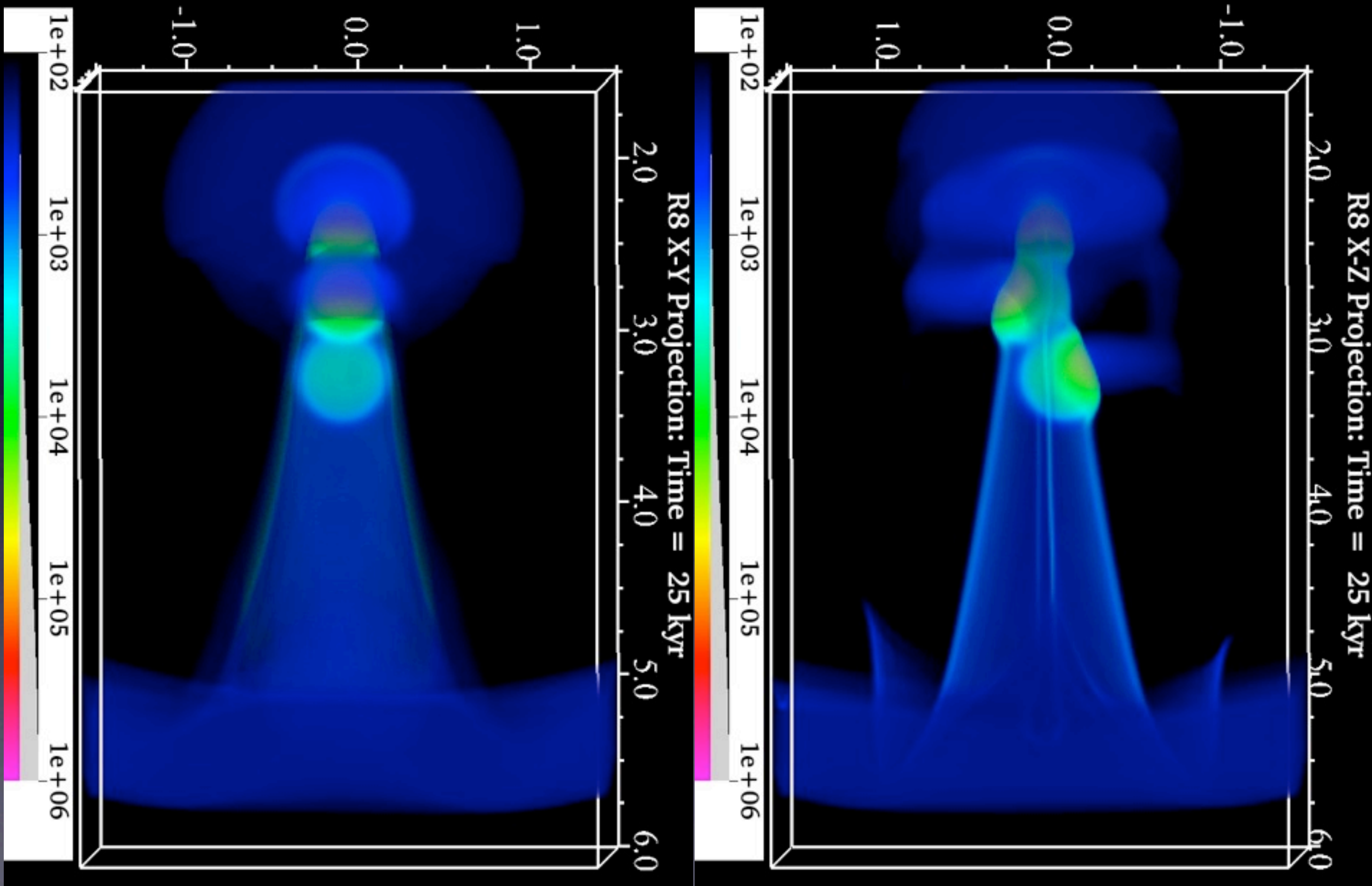

Strong, Perpendicular B-field - 50 kyr

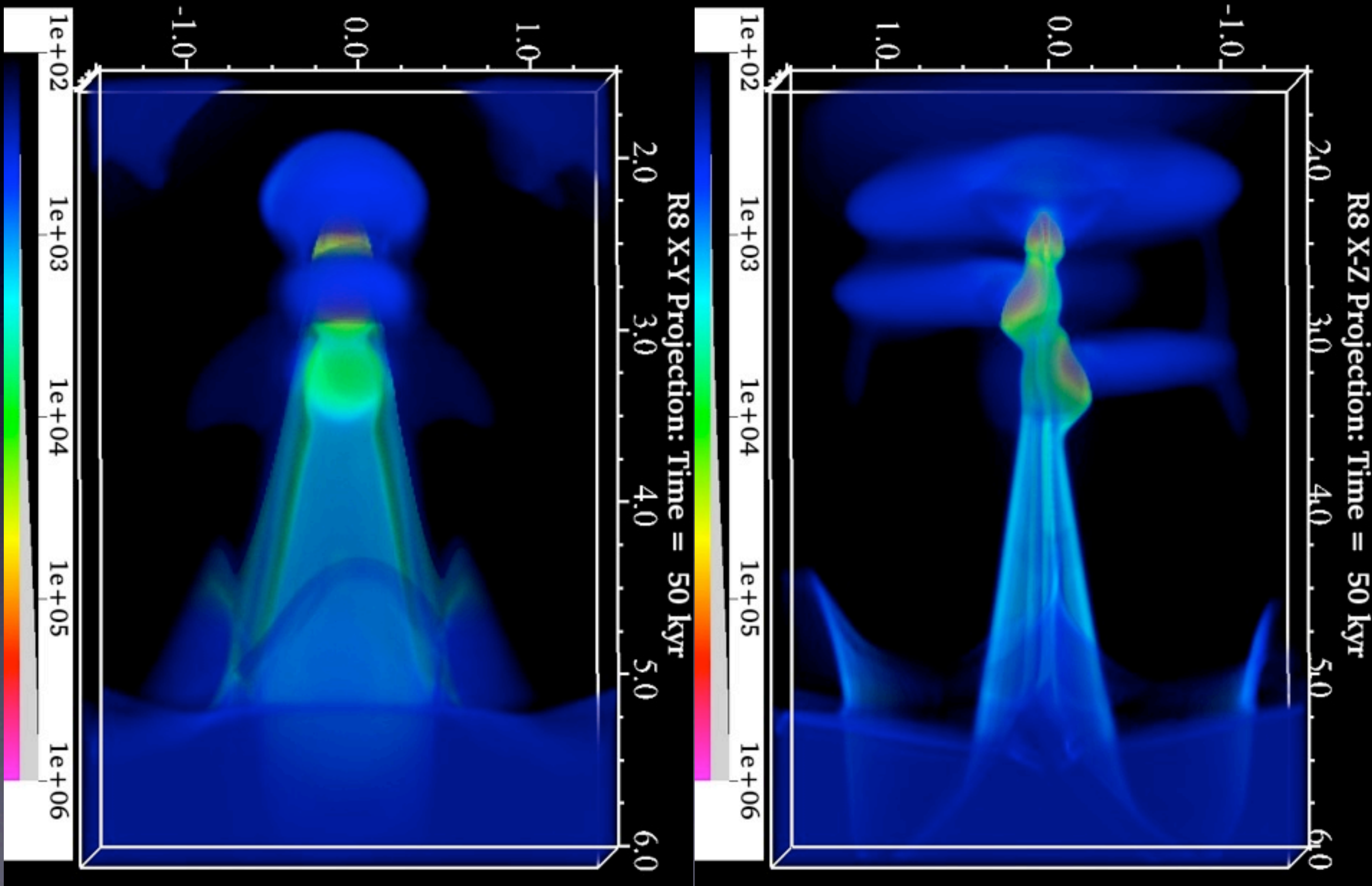

Strong, Perpendicular B-field - 100 kyr

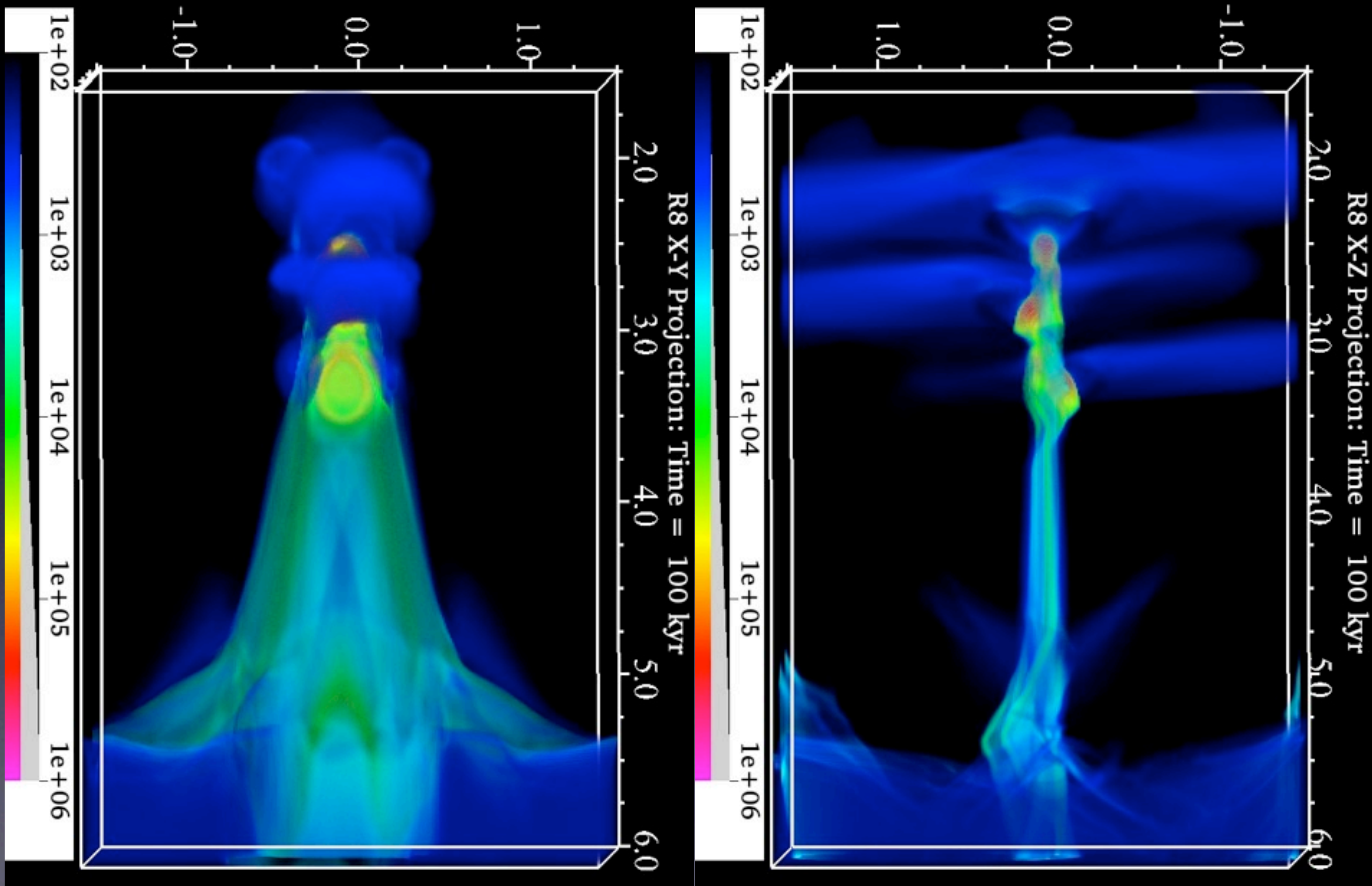

Strong, Perpendicular B-field - 150 kyr

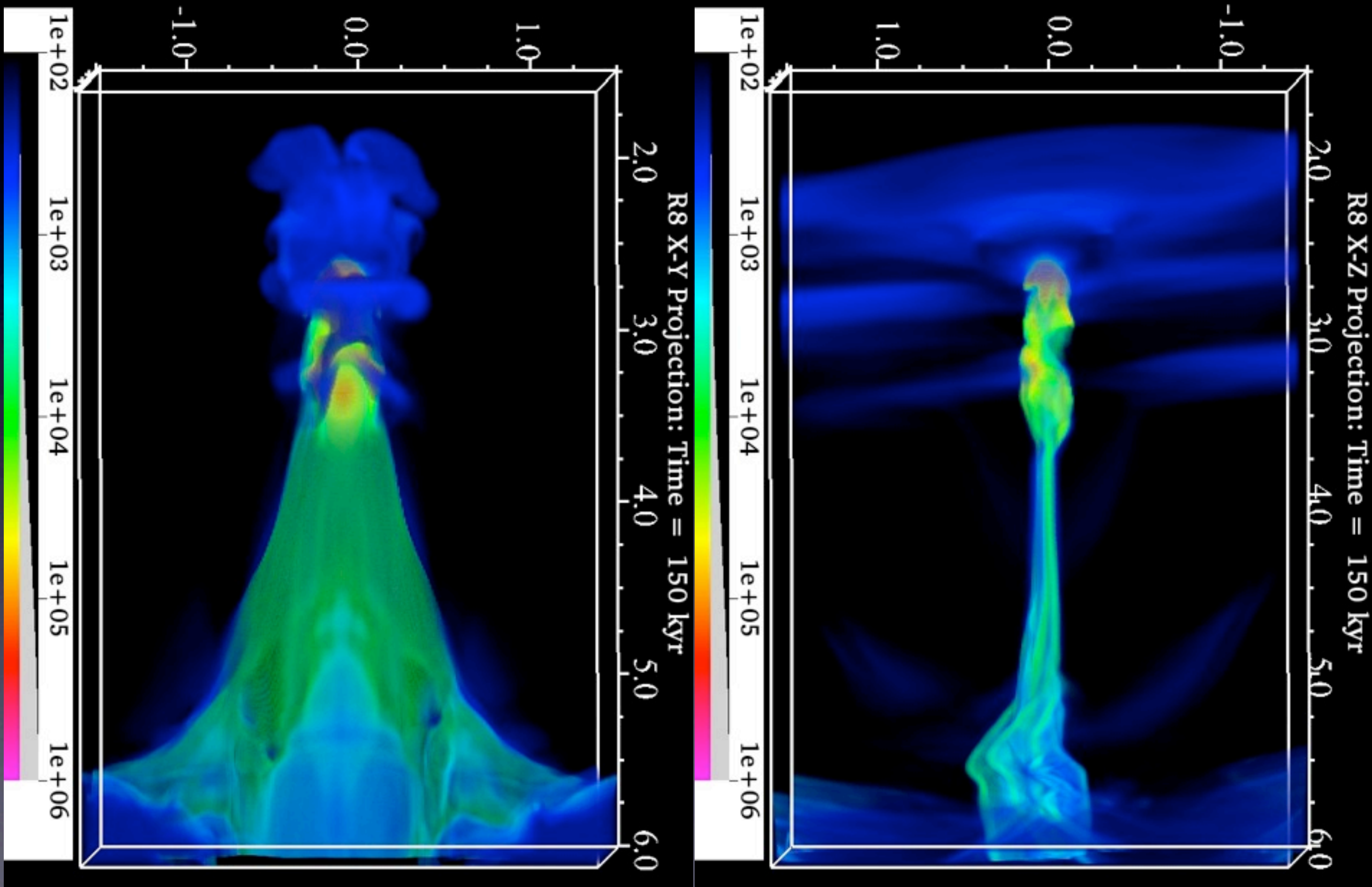

Strong, Perpendicular B-field - 200 kyr

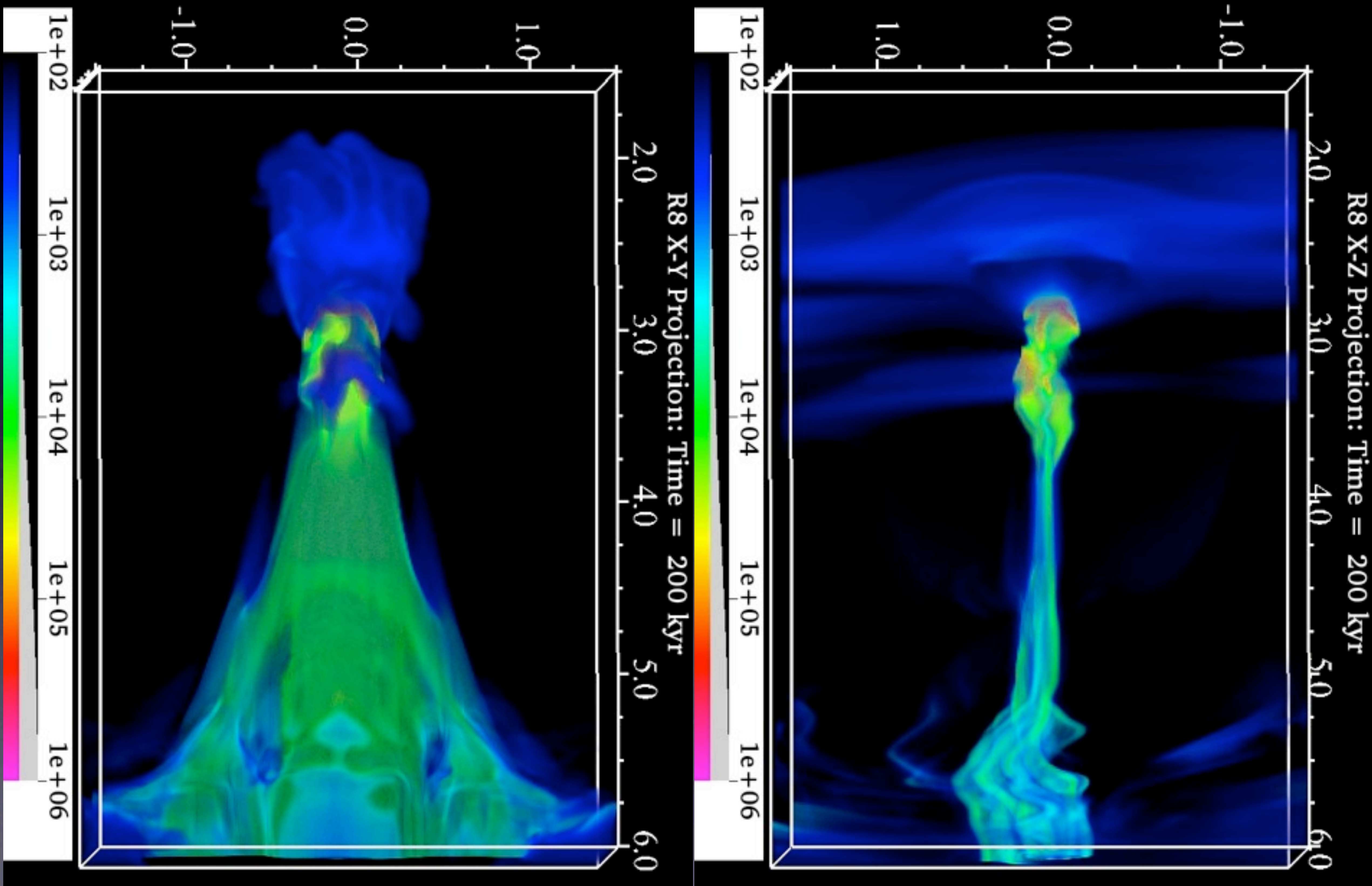

Strong, Perpendicular B-field - 250 kyr

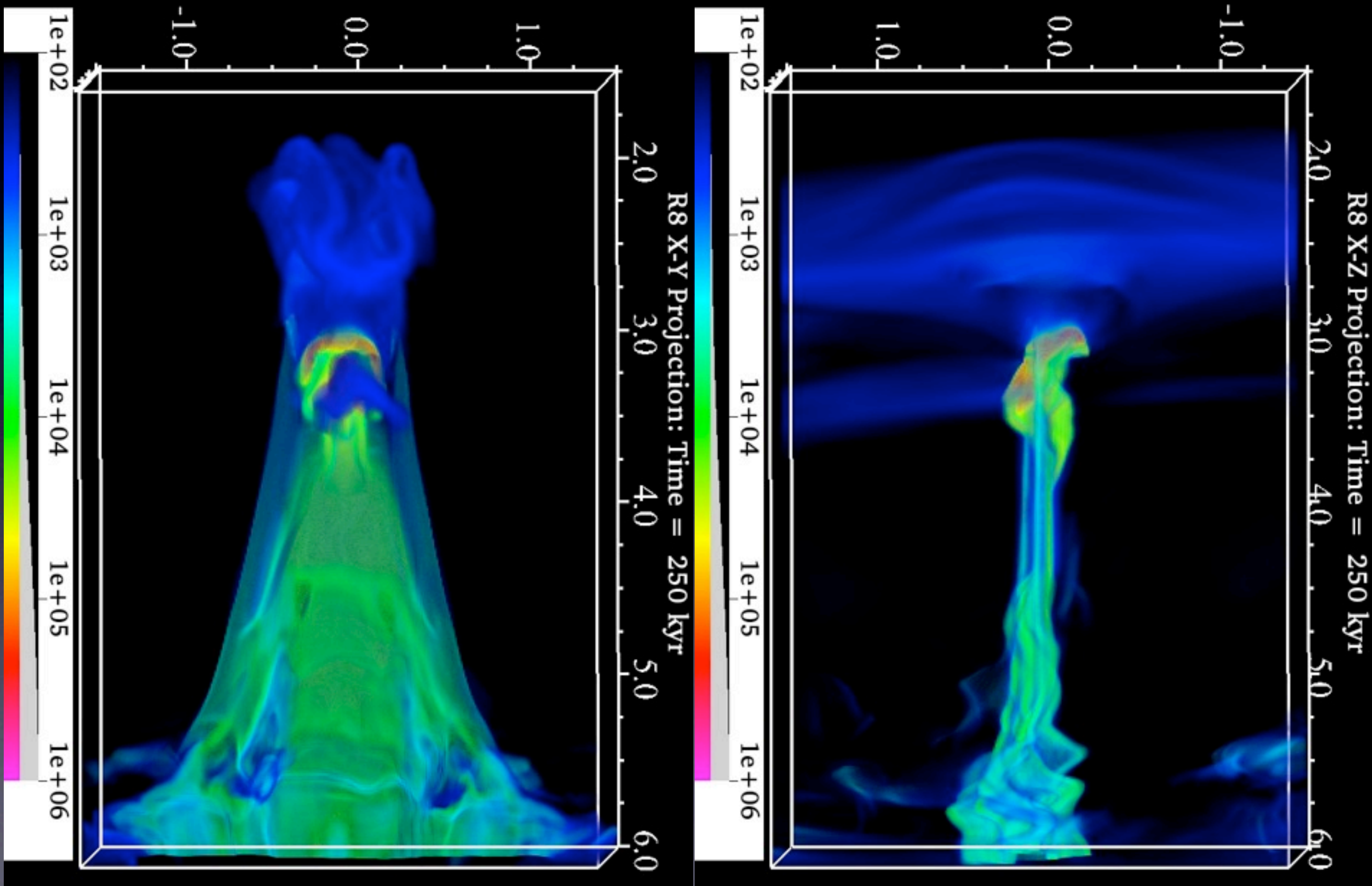

Midplane Slice, 250kyr

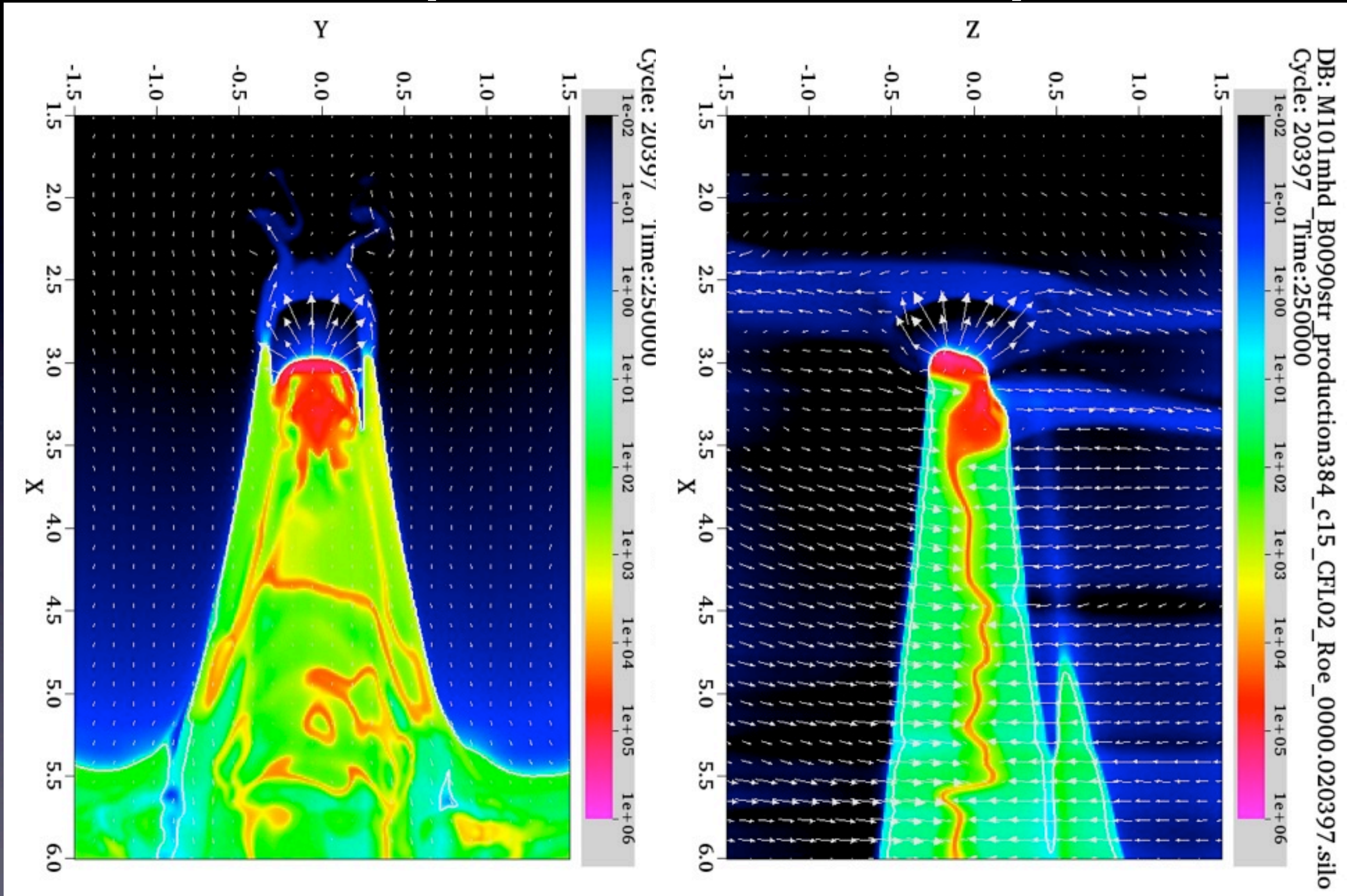

Projection: B-orientation and N(H)

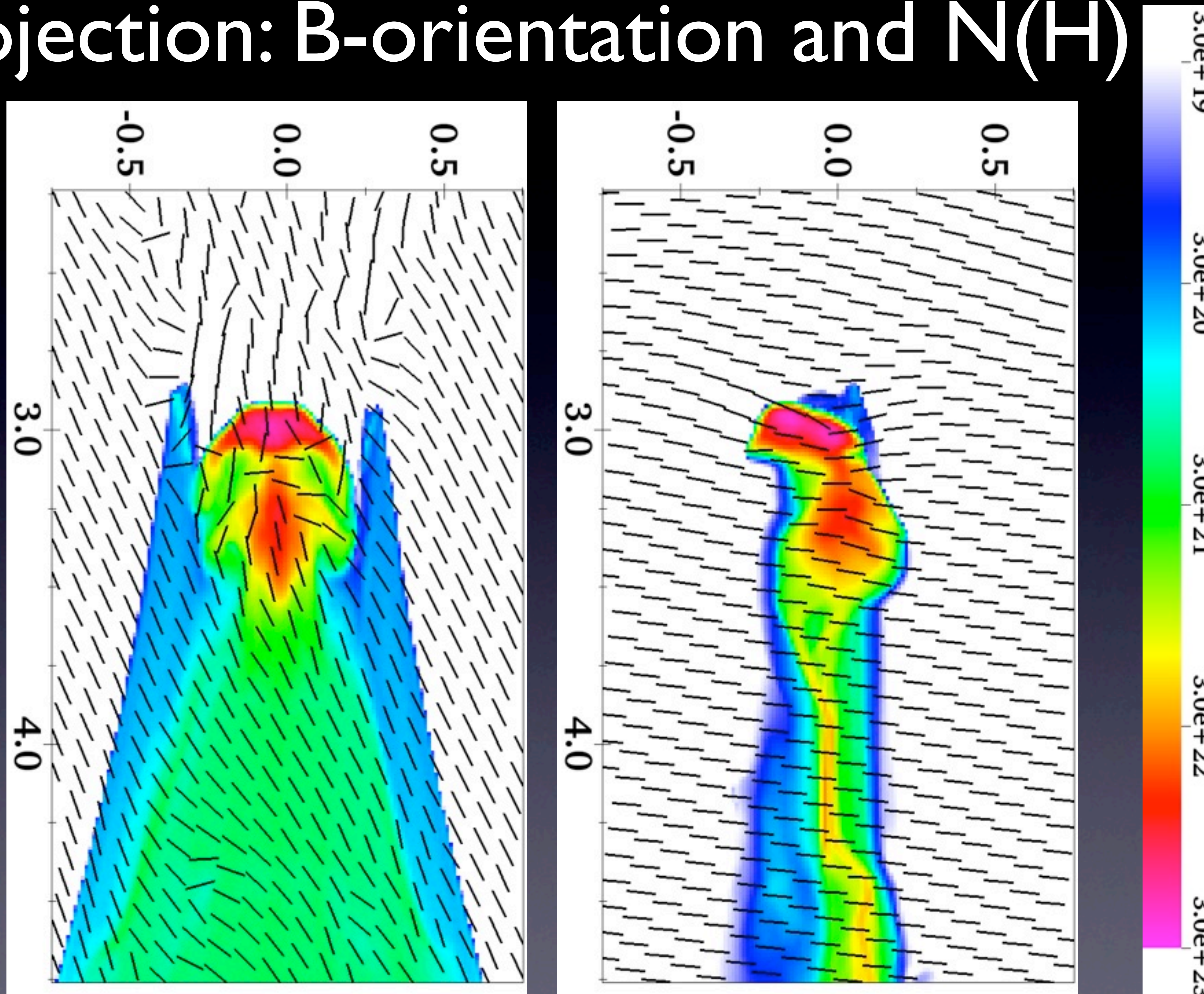

Strong, Perpendicular B-field - 300 kyr

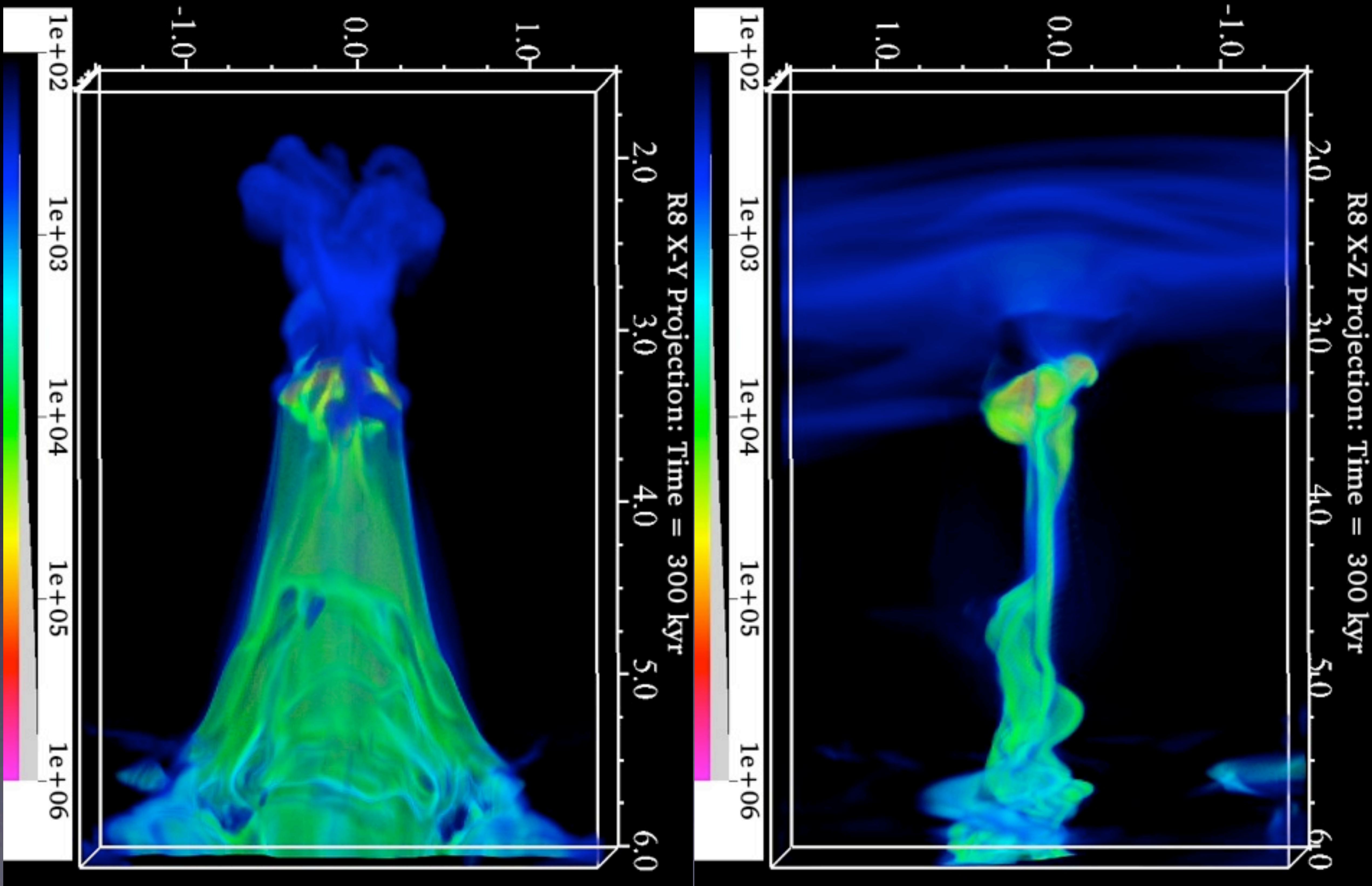

Strong, Perpendicular B-field - 350 kyr

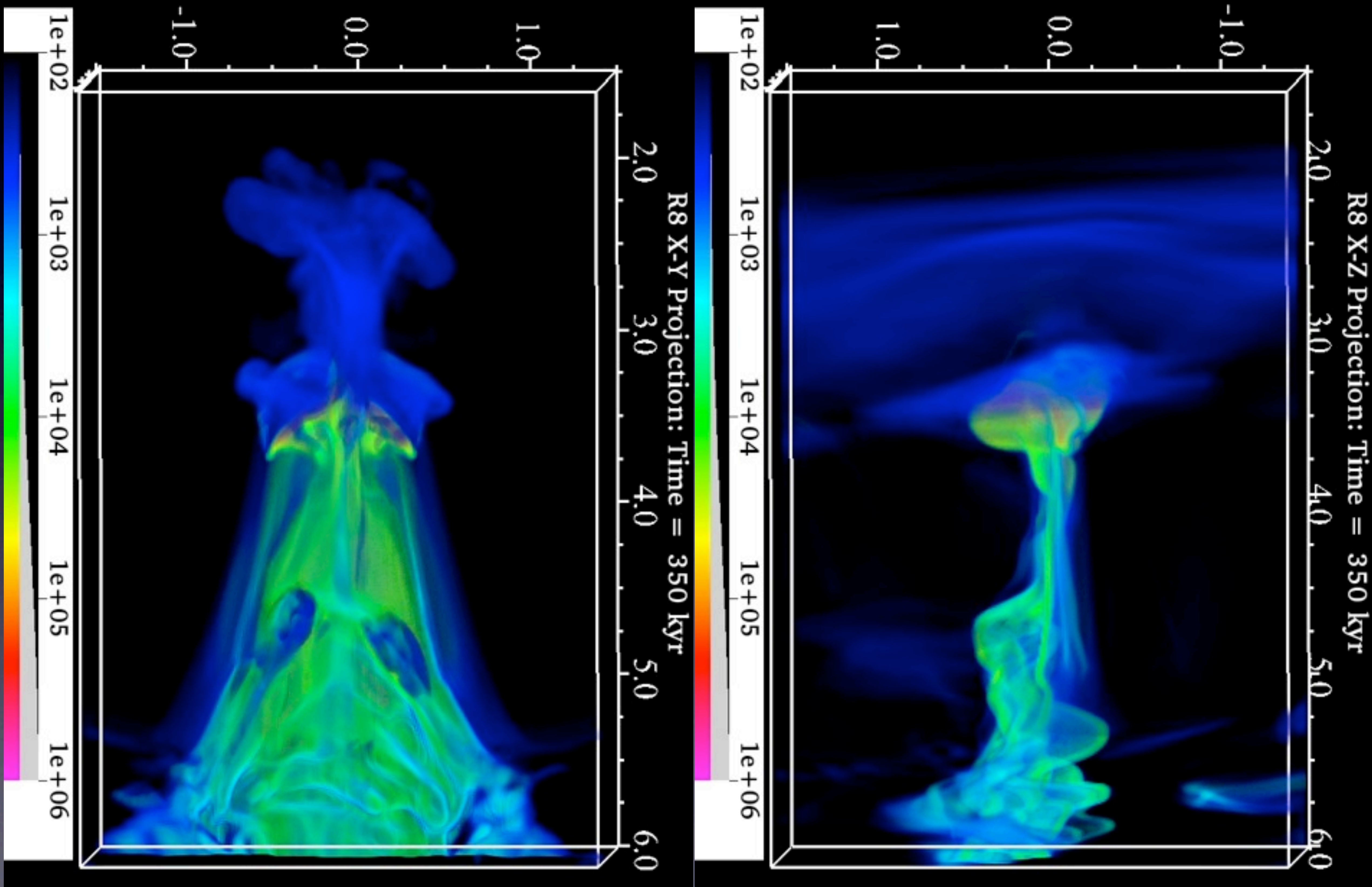

Strong, Perpendicular B-field - 400 kyr

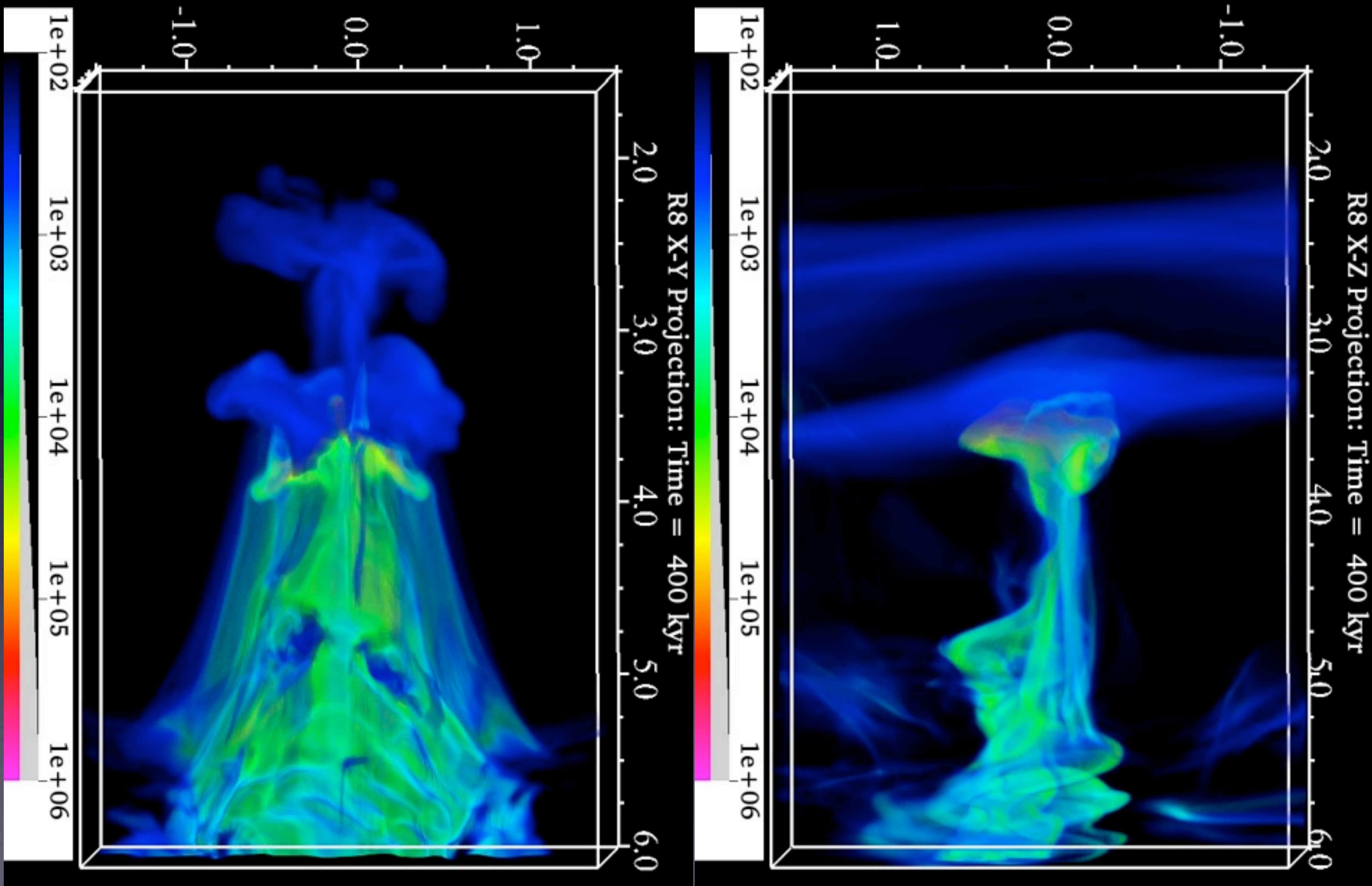

Midplane Slice, 400kyr

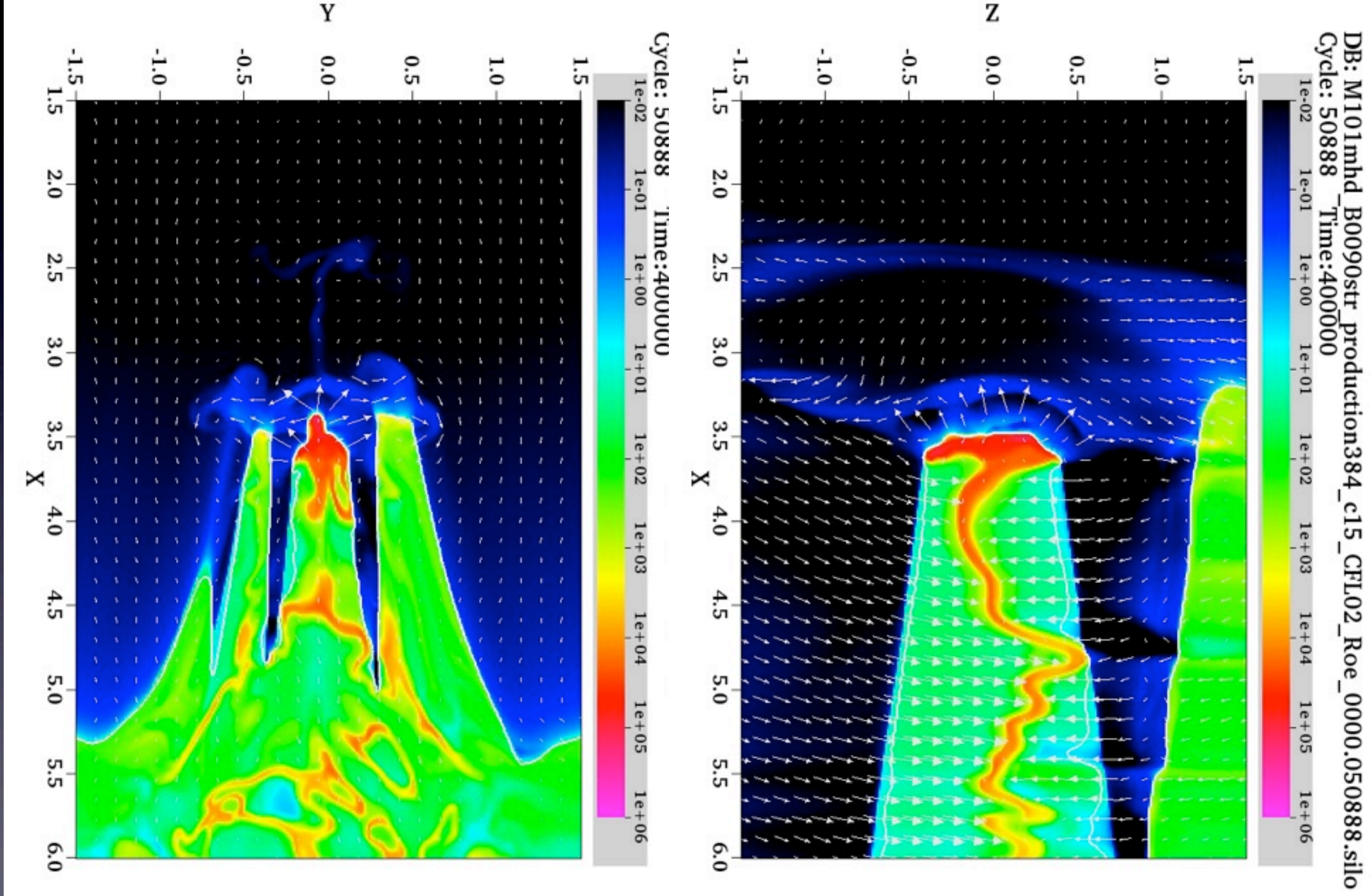

Projection: B-orientation and N(H)

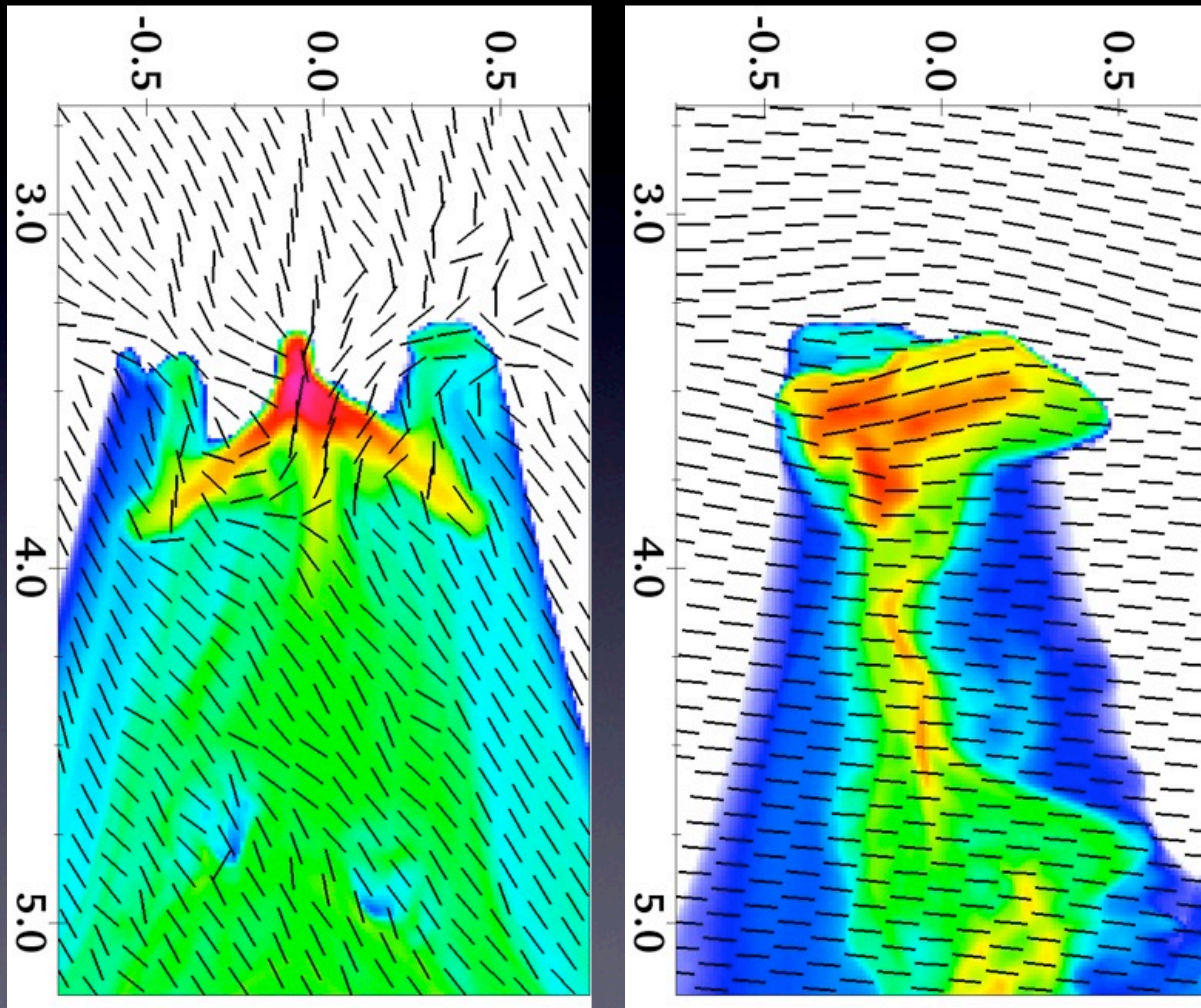

Strong, parallel B-field

Strong, Parallel B-field - 25 kyr

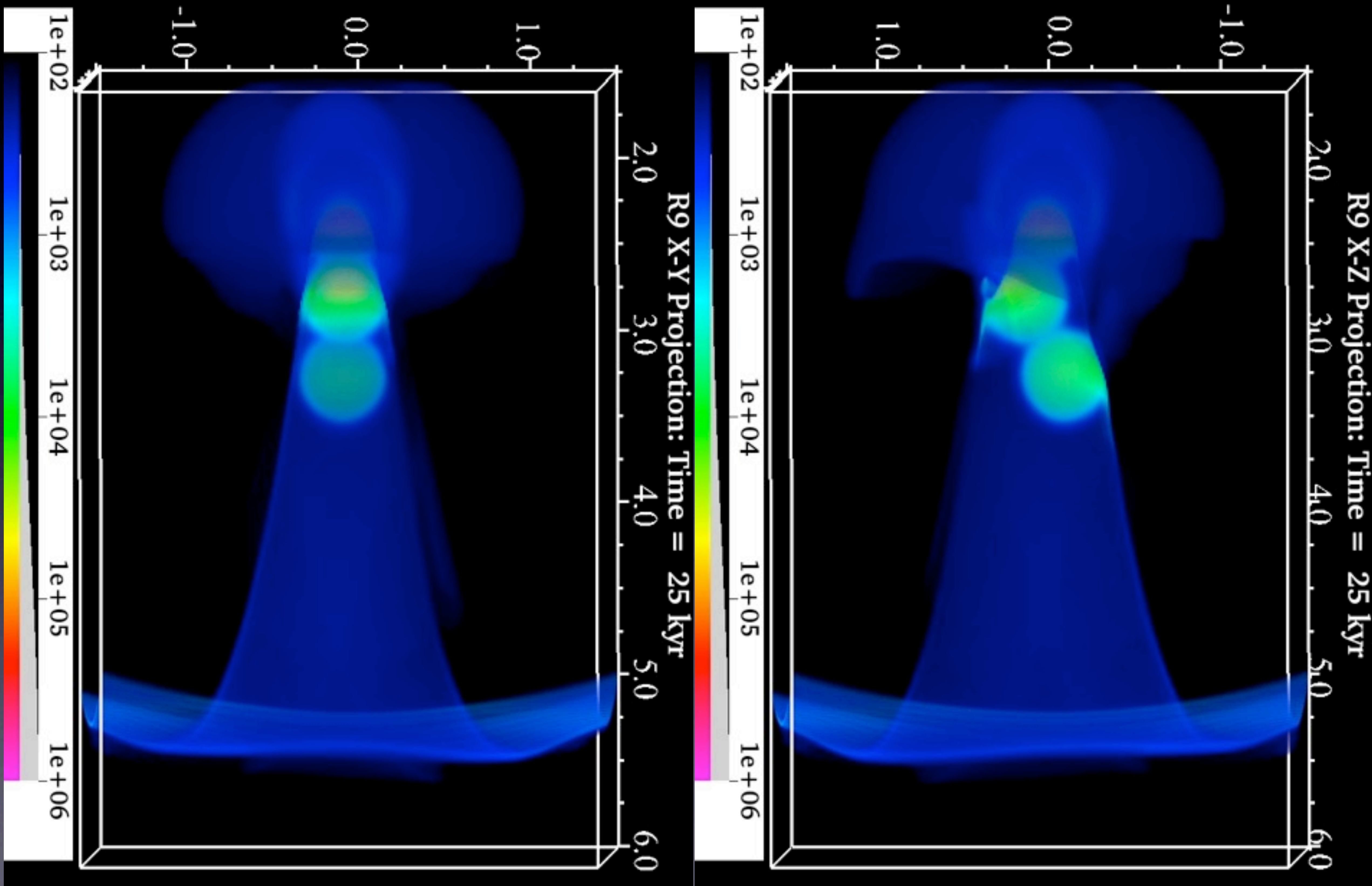

Strong, Parallel B-field - 50 kyr

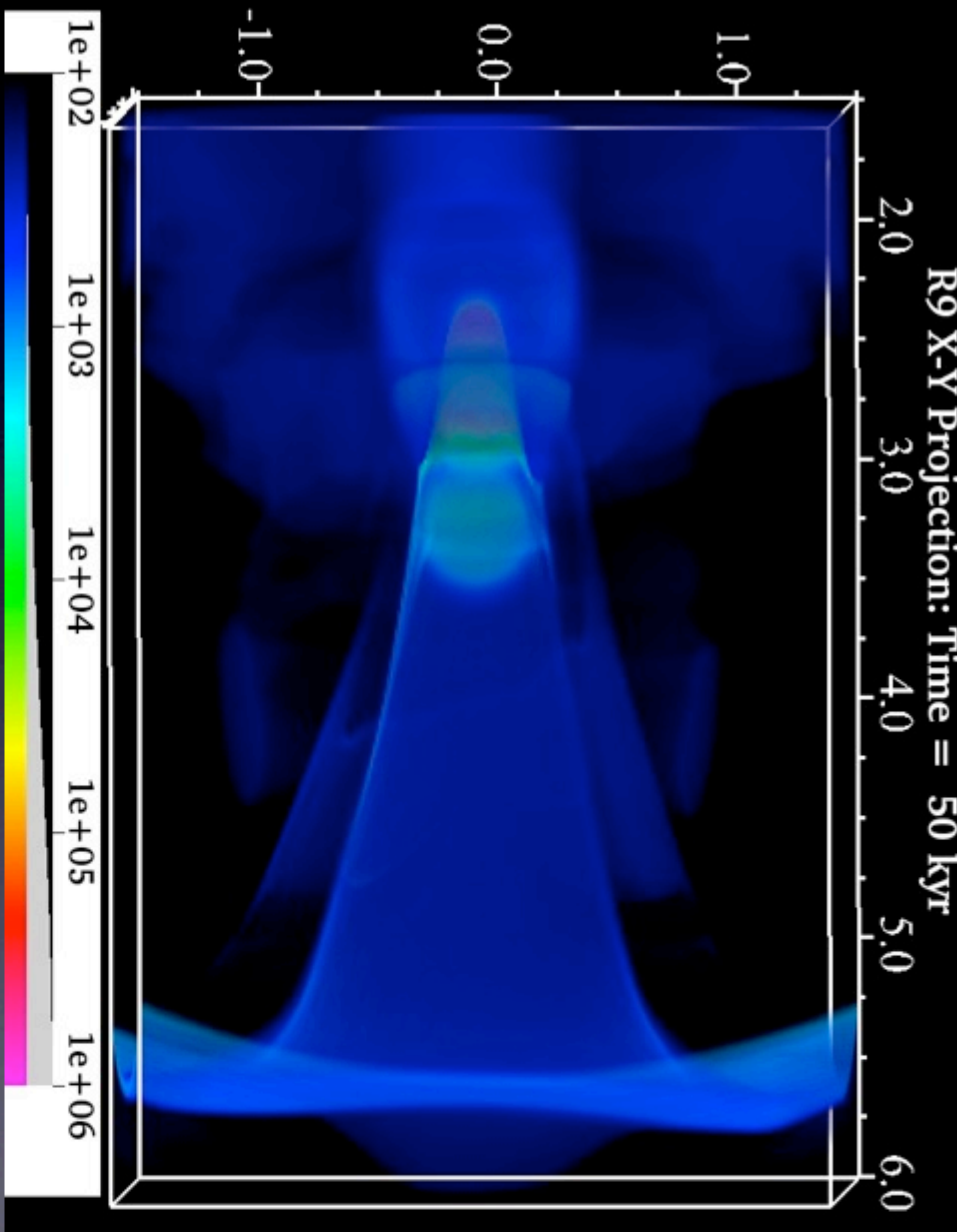

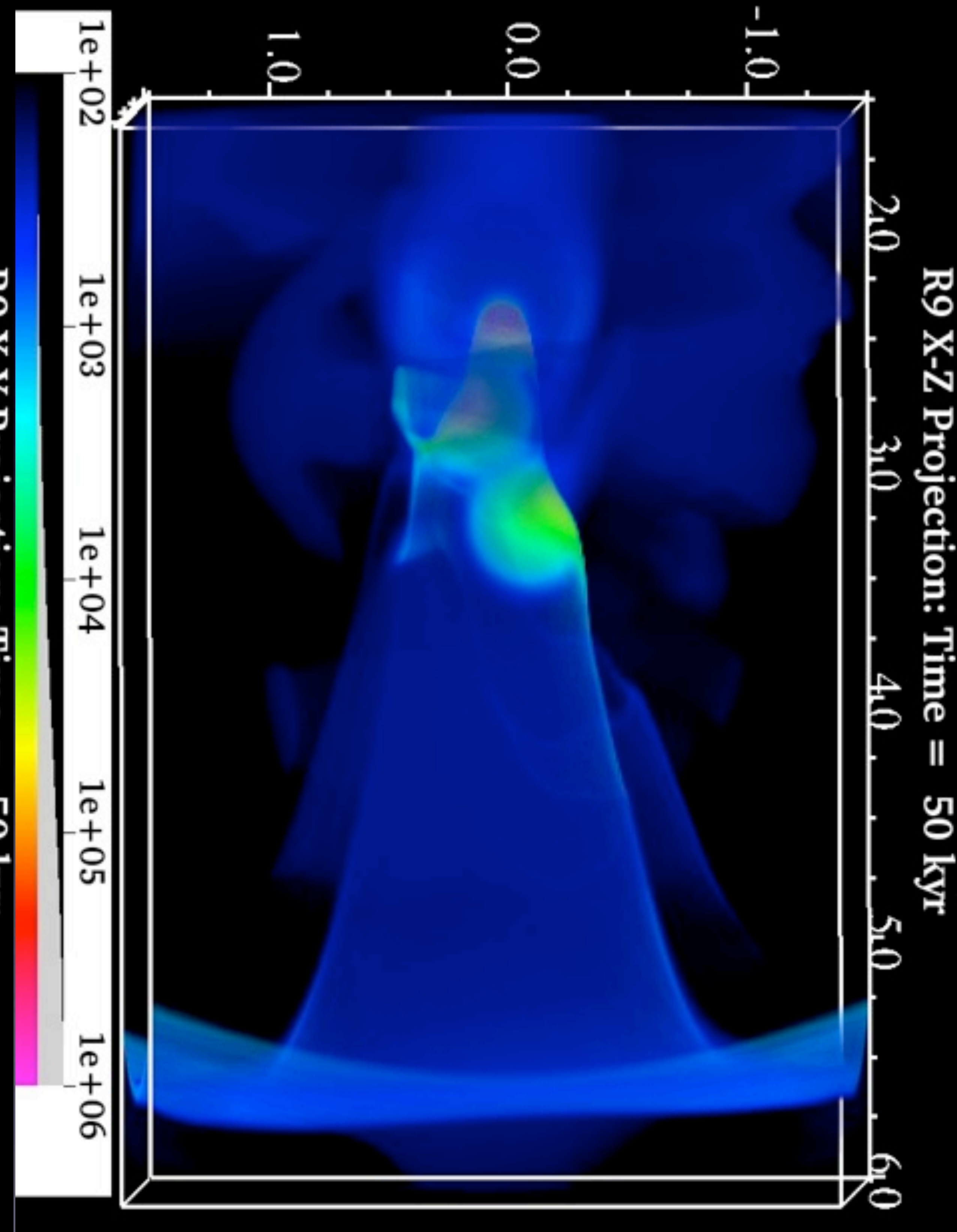

Strong, Parallel B-field - 75 kyr

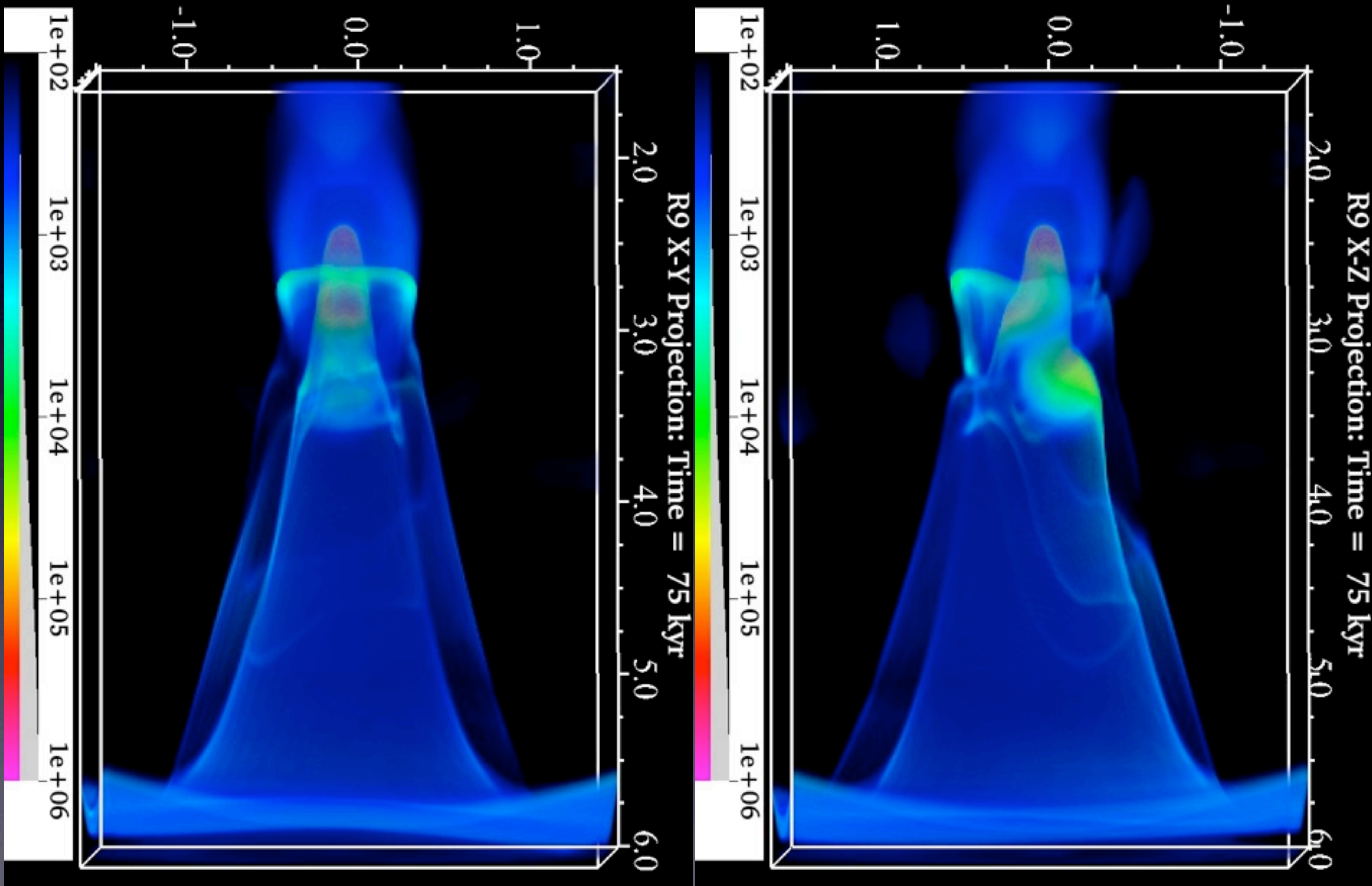

Strong, Parallel B-field - 100 kyr

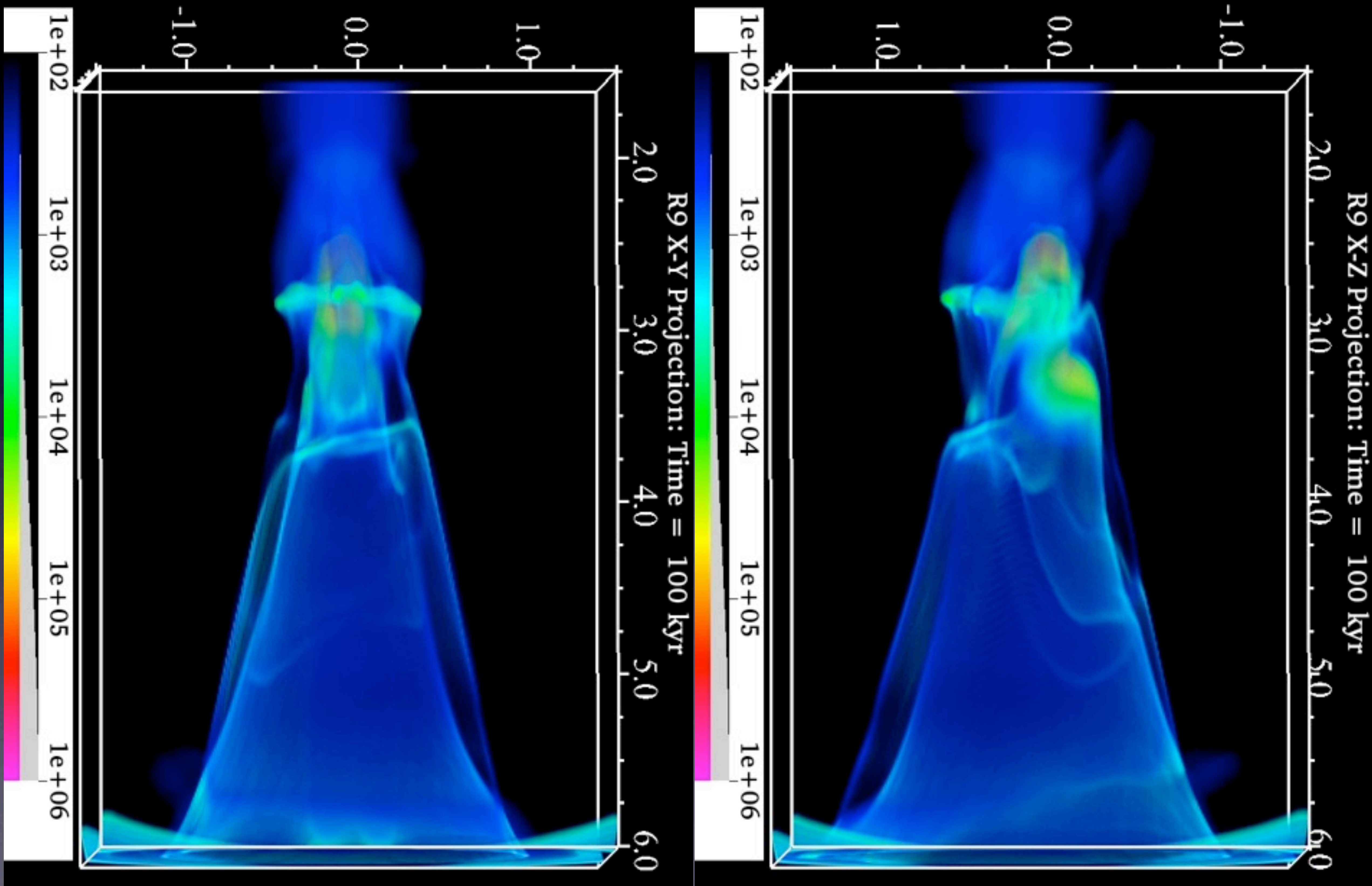

Strong, Parallel B-field - 150 kyr

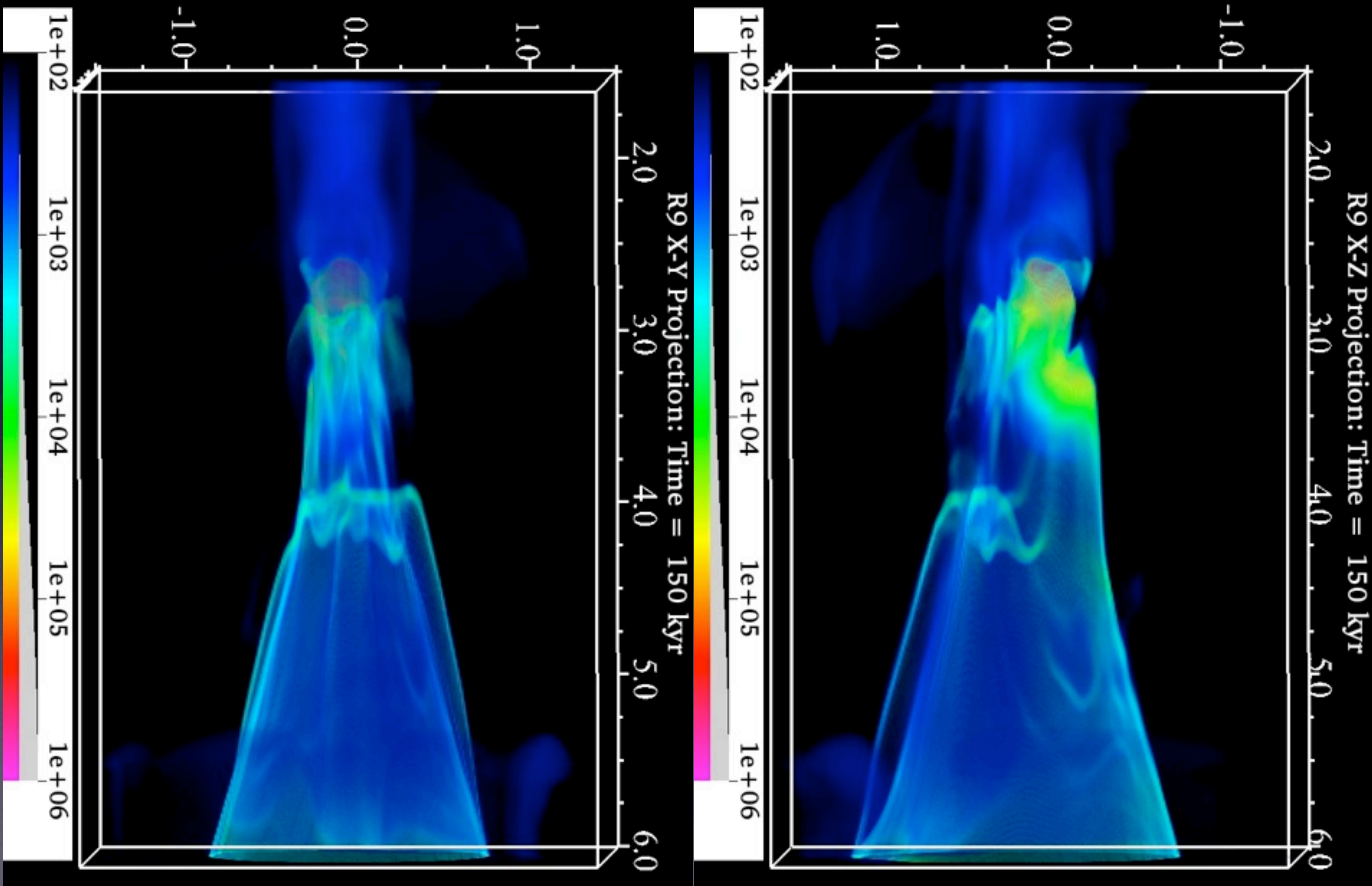

Strong, Parallel B-field - 200 kyr

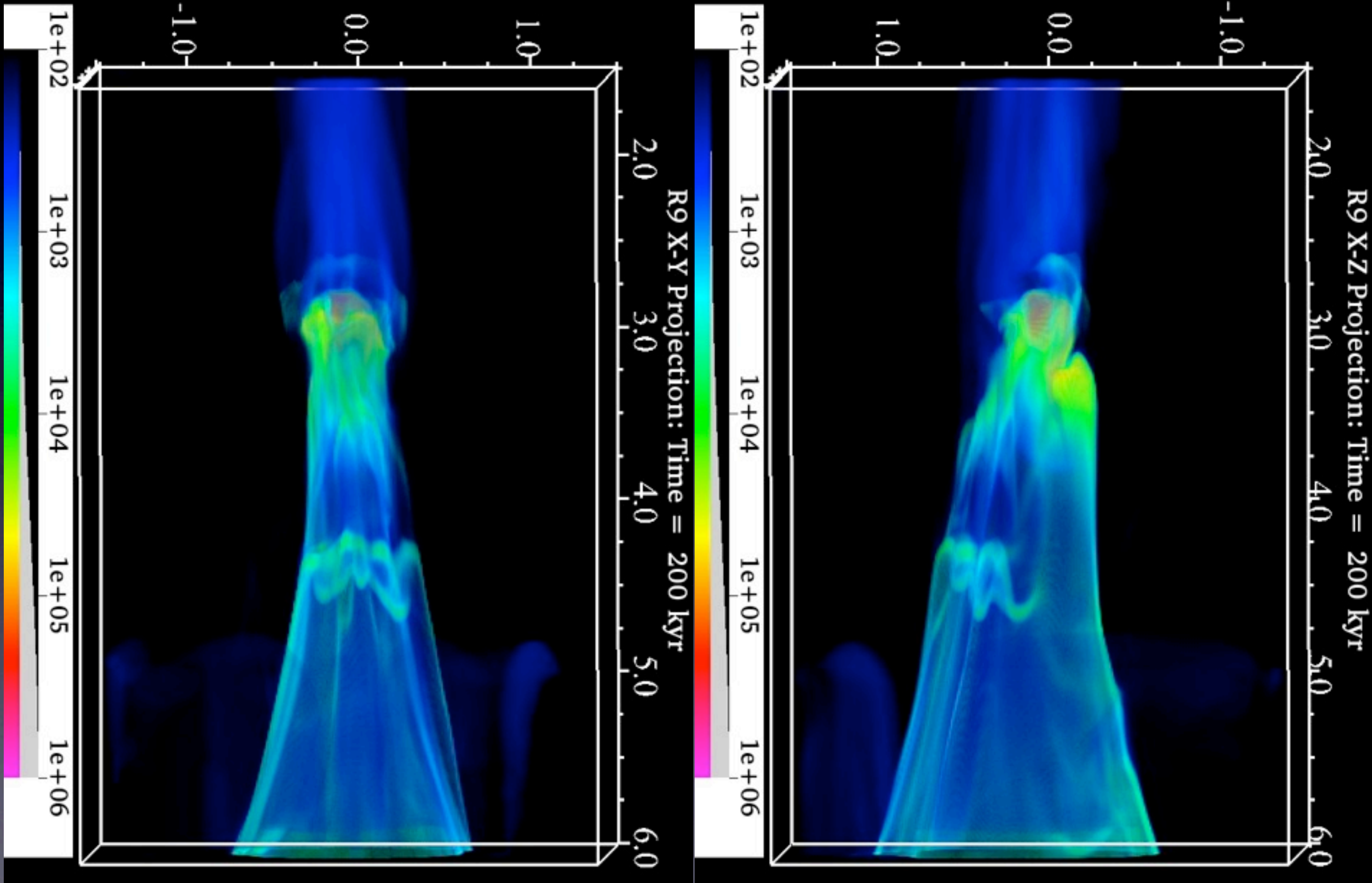

Strong, Parallel B-field - 300 kyr

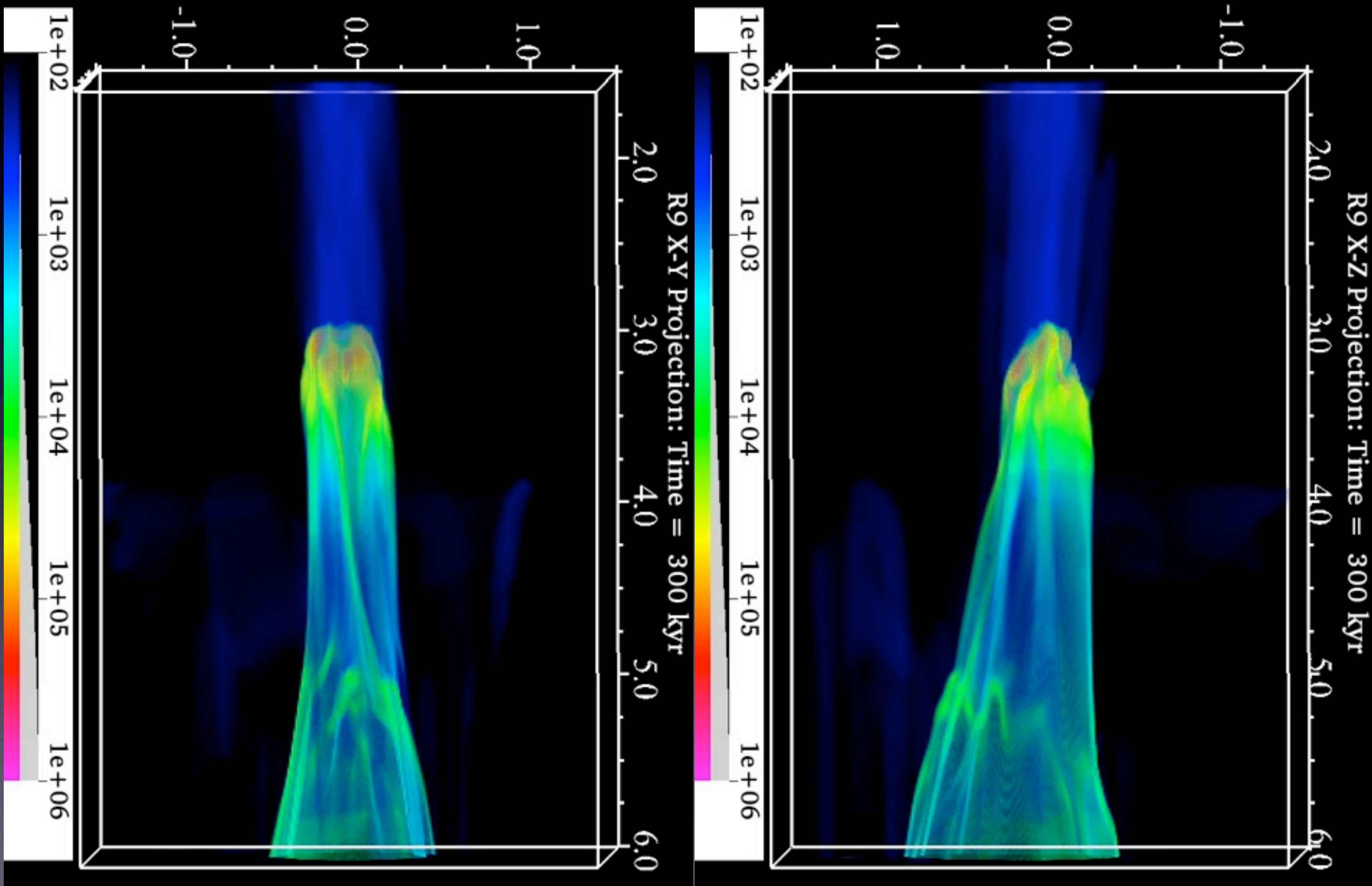

Strong, Parallel B-field - 400 kyr

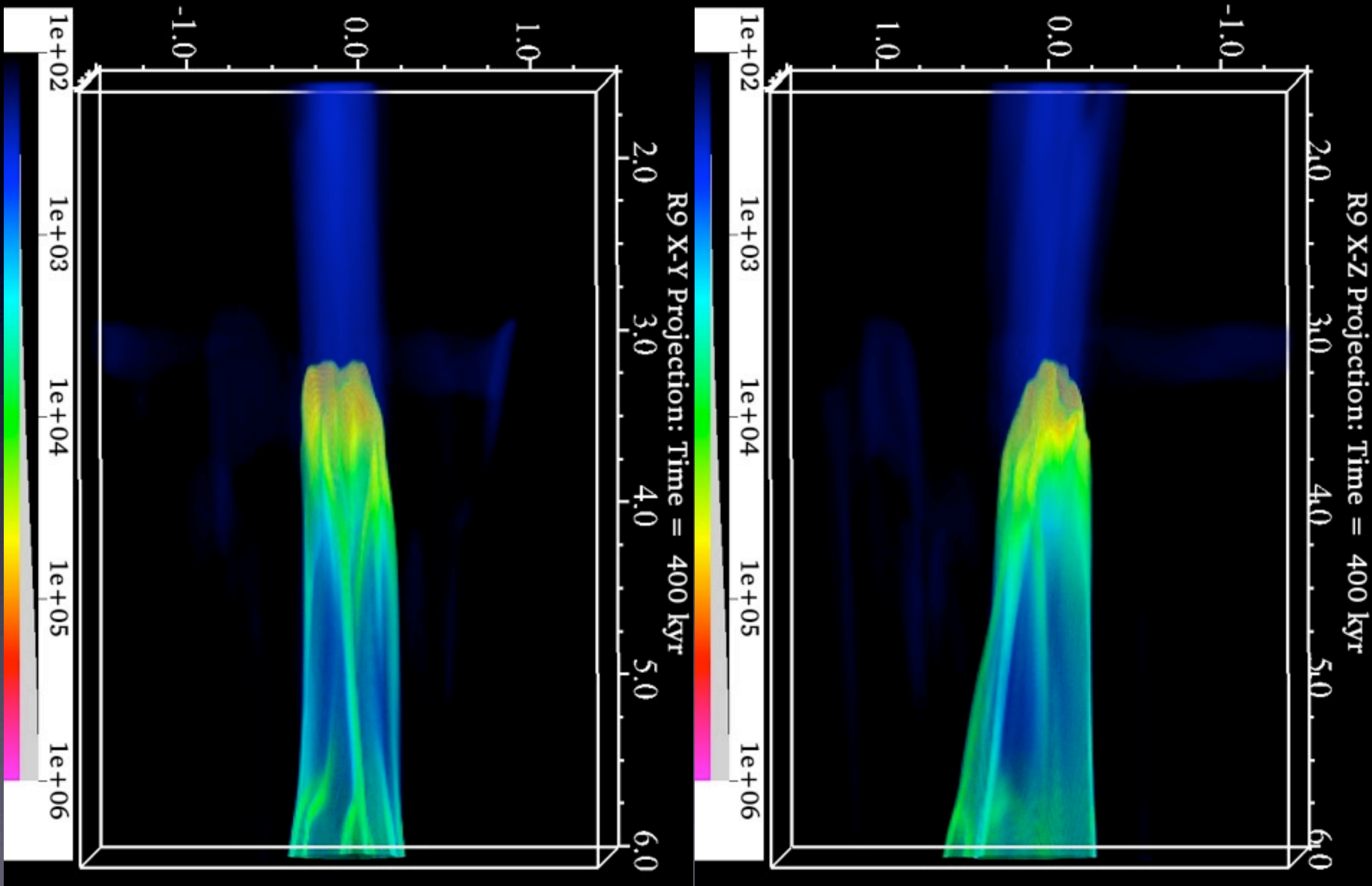

Strong parallel field, 400kyr

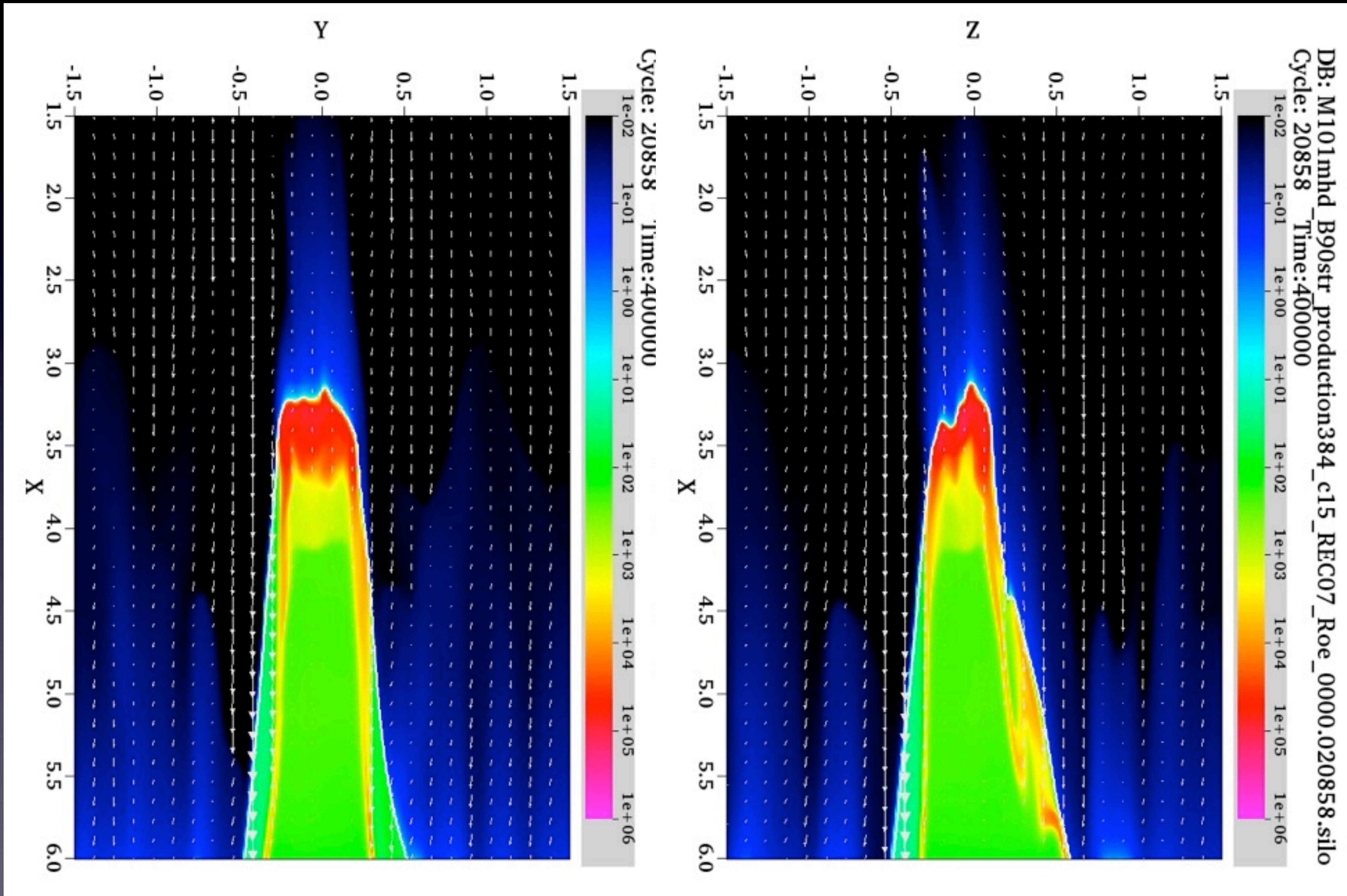

Projection: B-orientation and N(H)

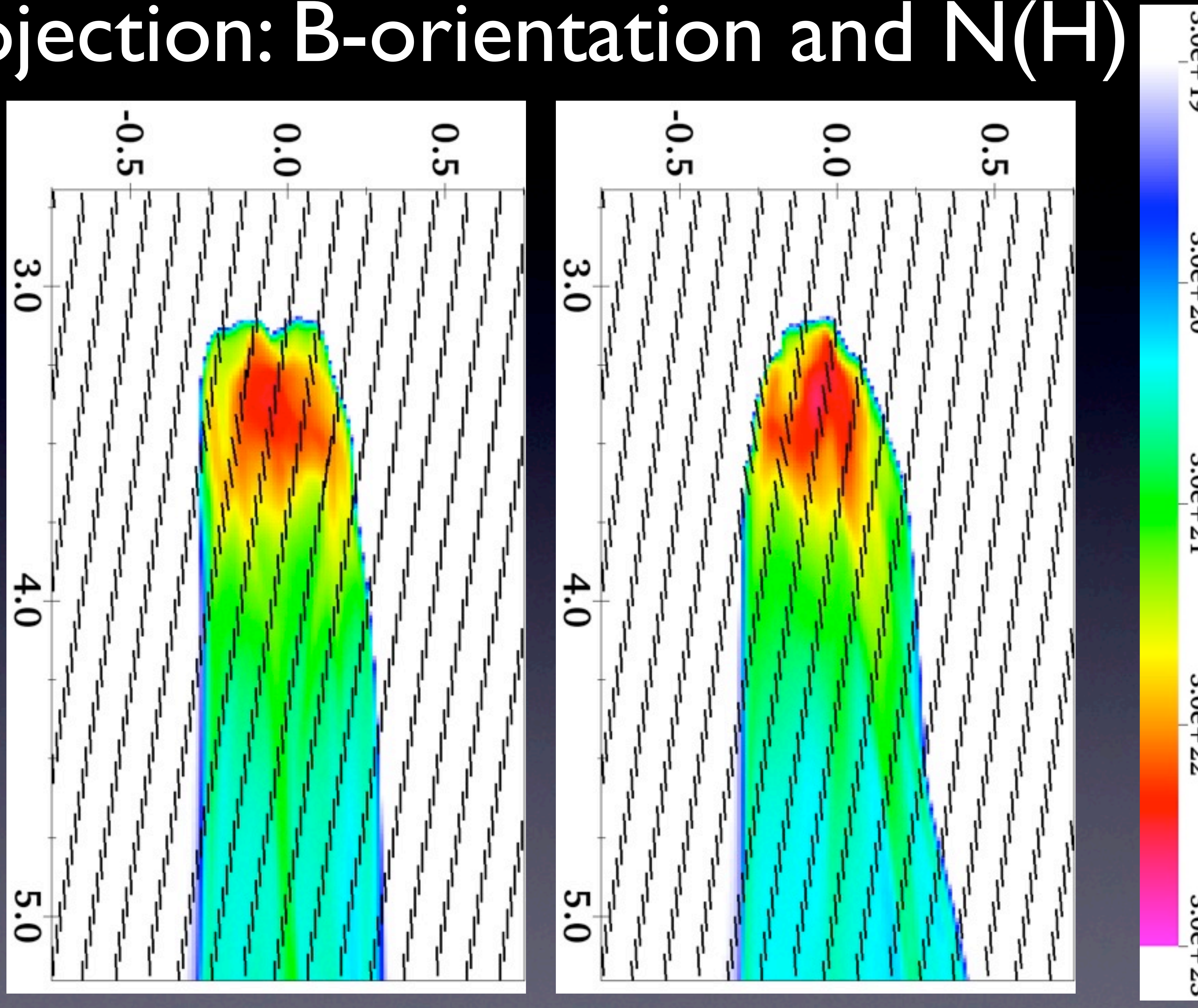

Hα Emission from perpendicular field models

- Calculated by integrating lines of sight through the simulation box with an emissivity appropriate for Hα, and absorption by dust.

Comparison of Hα Emission (25 kyr)

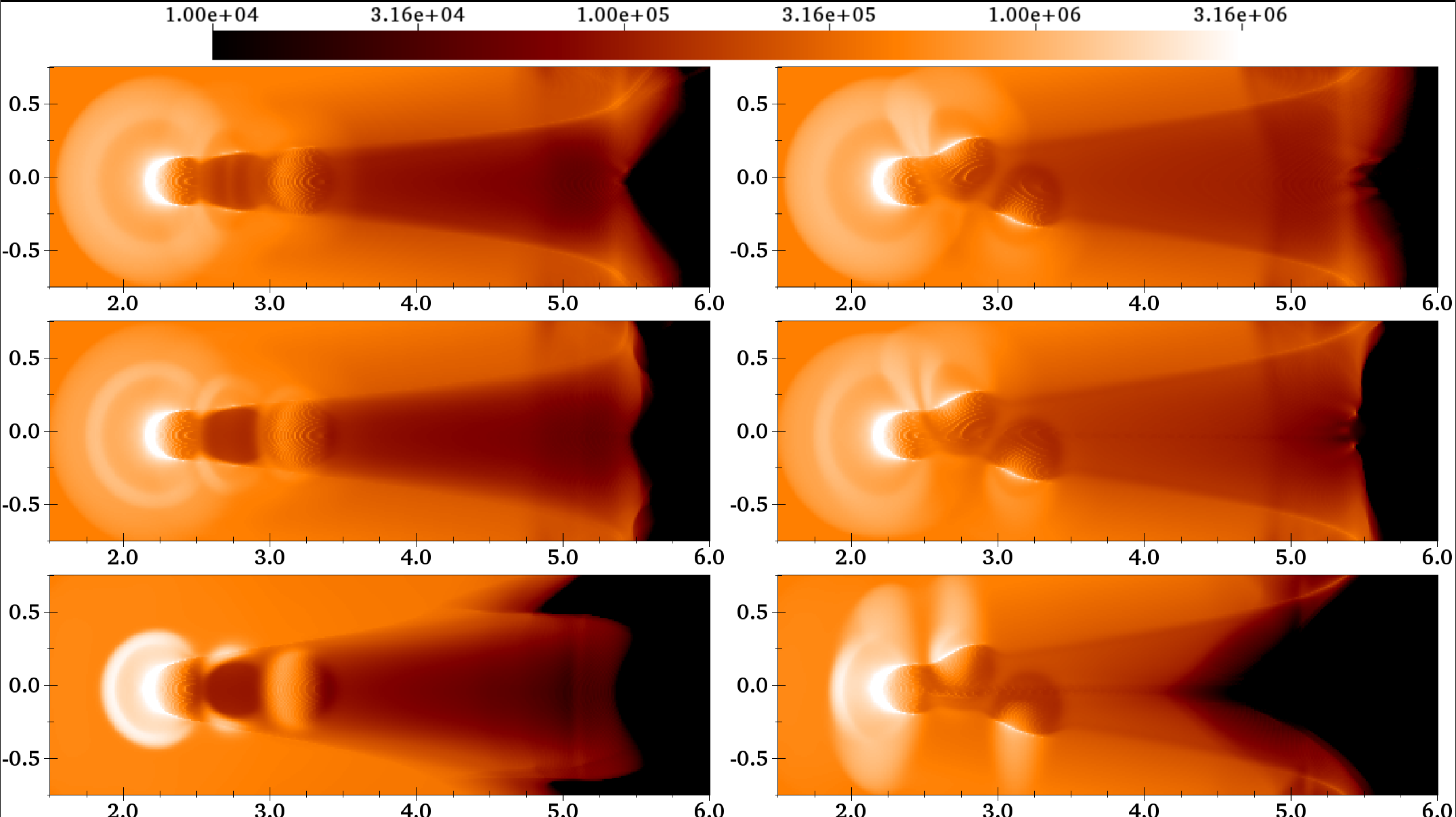

Left: x-y, LOS= -z; Right: x-z, LOS= y. Top to bottom: R2 (weak), R5 (medium), R8 (strong field).

Comparison of Hα Emission (100 kyr)

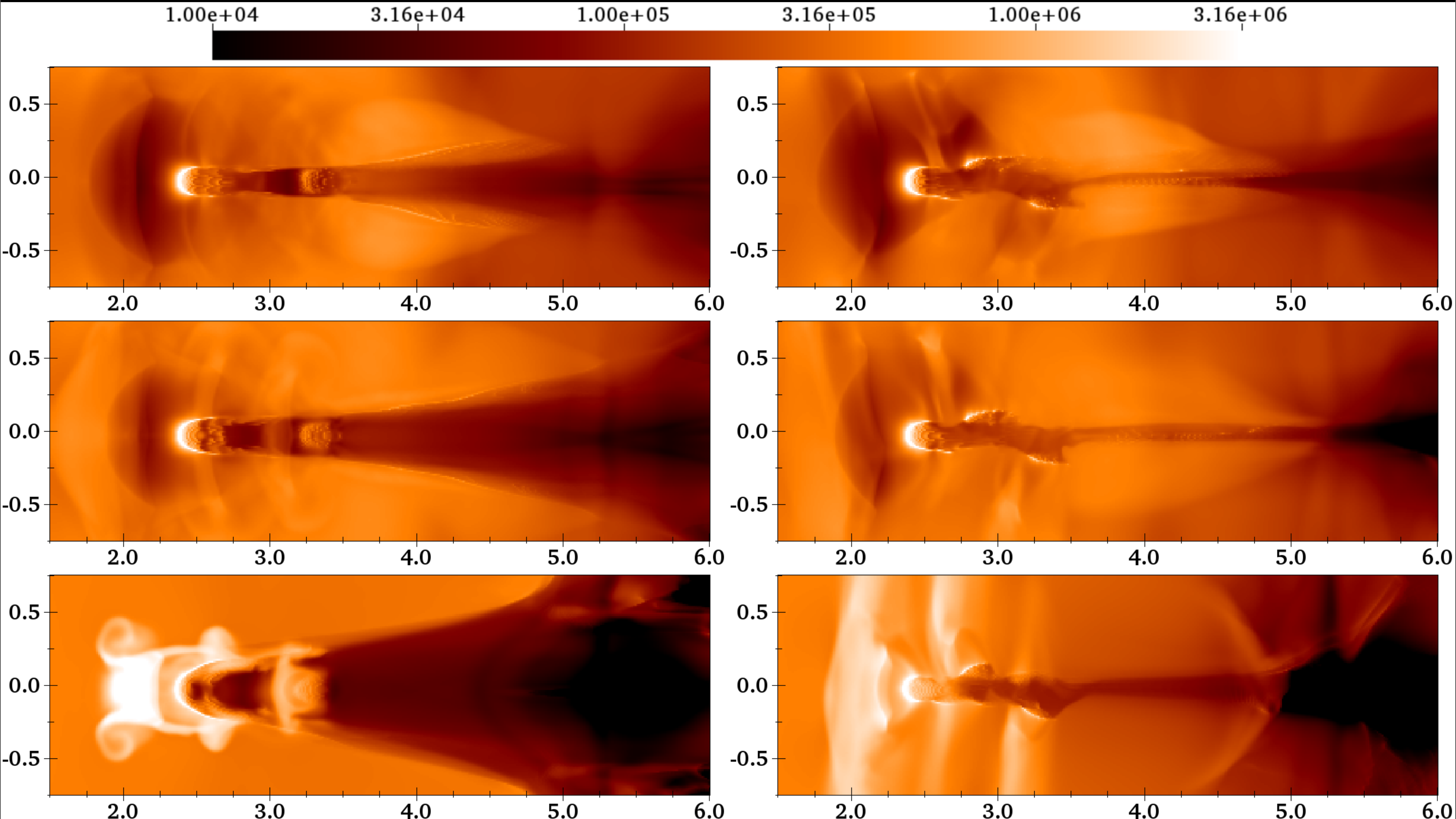

Left: x-y, LOS= -z; Right: x-z, LOS= y. Top to bottom: R2 (weak), R5 (medium), R8 (strong field).

Comparison of Hα Emission (200 kyr)

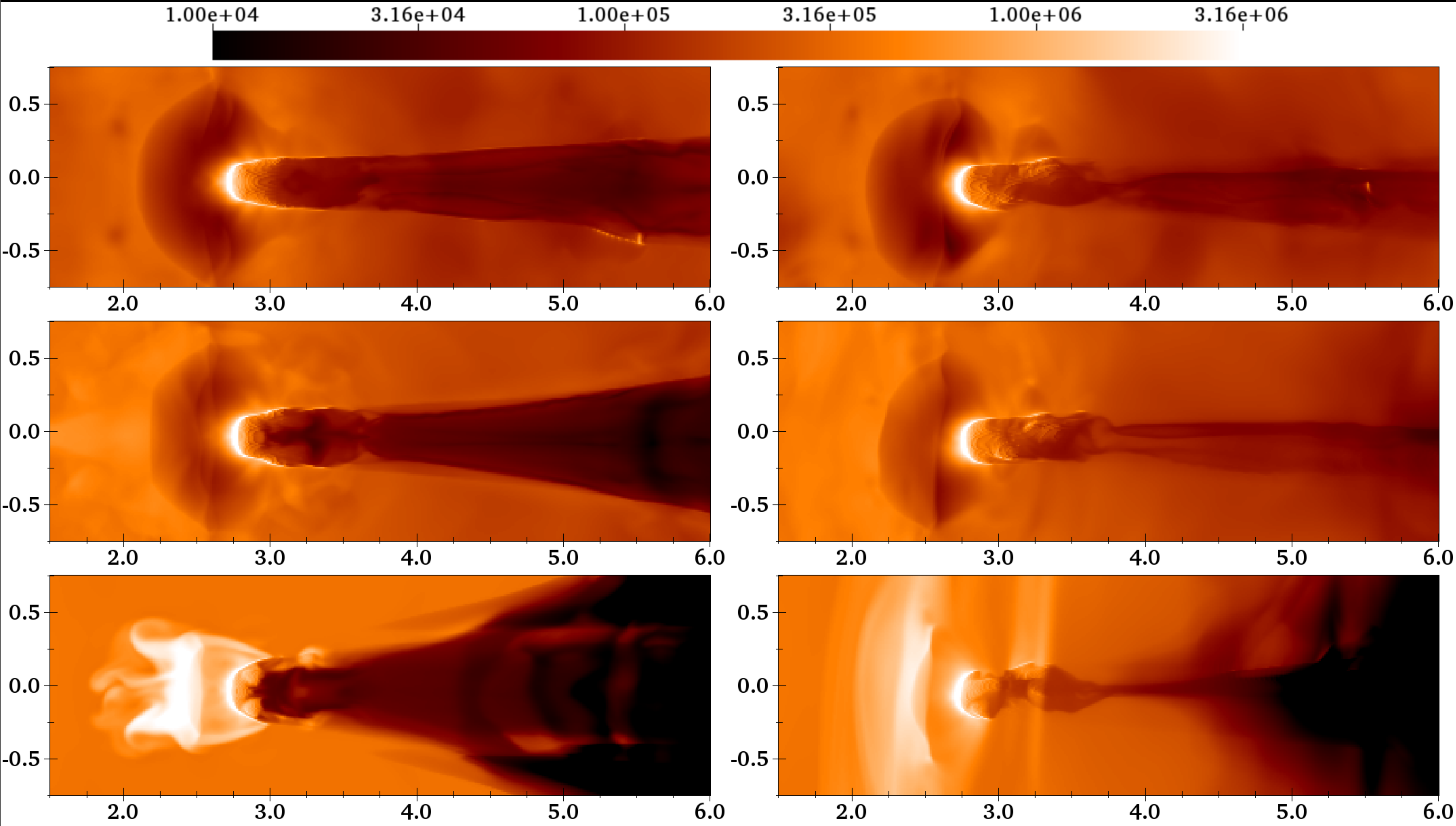

Left: x-y, LOS= -z; Right: x-z, LOS= y. Top to bottom: R2 (weak), R5 (medium), R8 (strong field).

Comparison of Hα Emission (300 kyr)

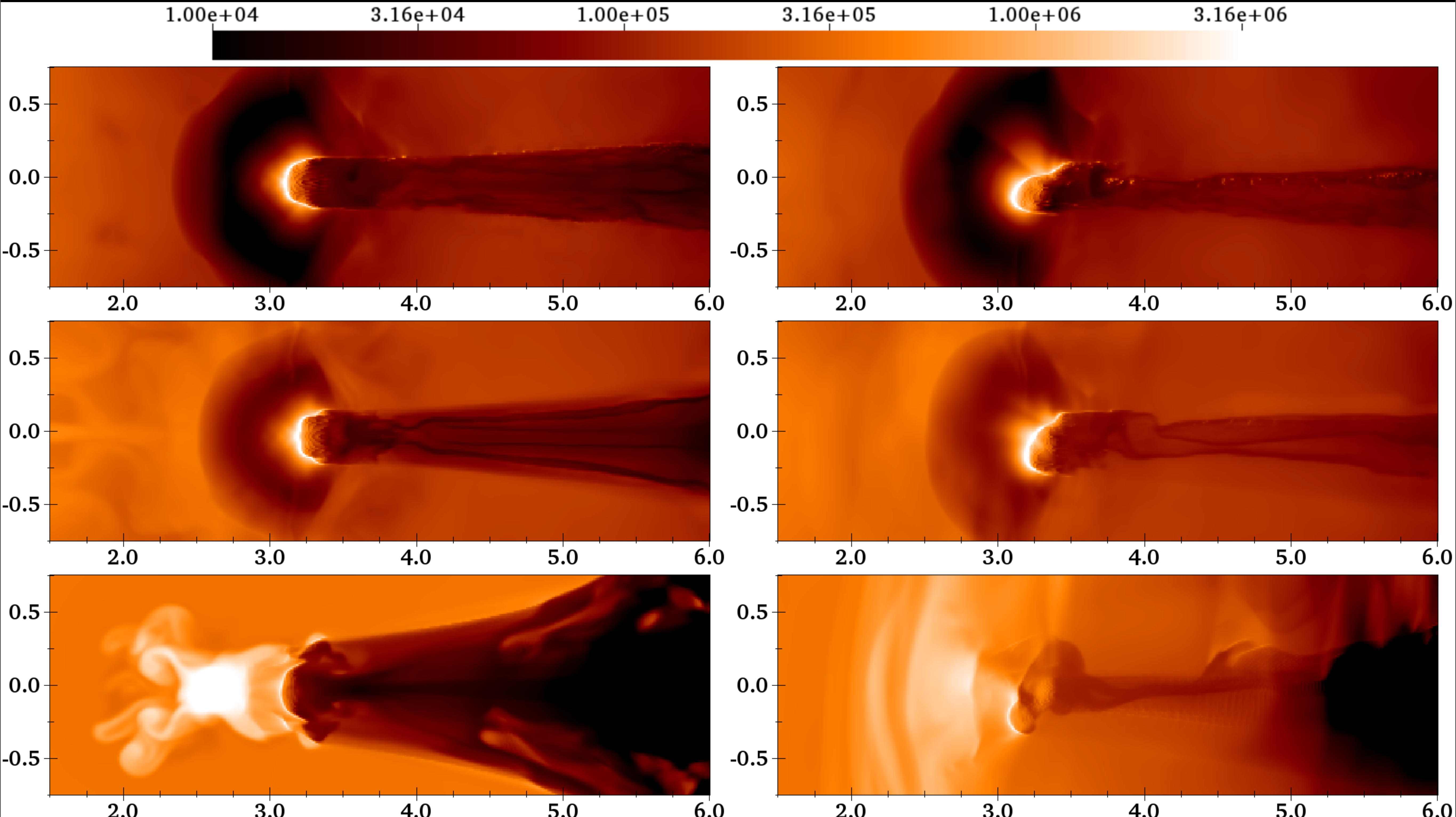

Left: x-y, LOS= -z; Right: x-z, LOS= y. Top to bottom: R2 (weak), R5 (medium), R8 (strong field).

Comparison of Hα Emission (400 kyr)

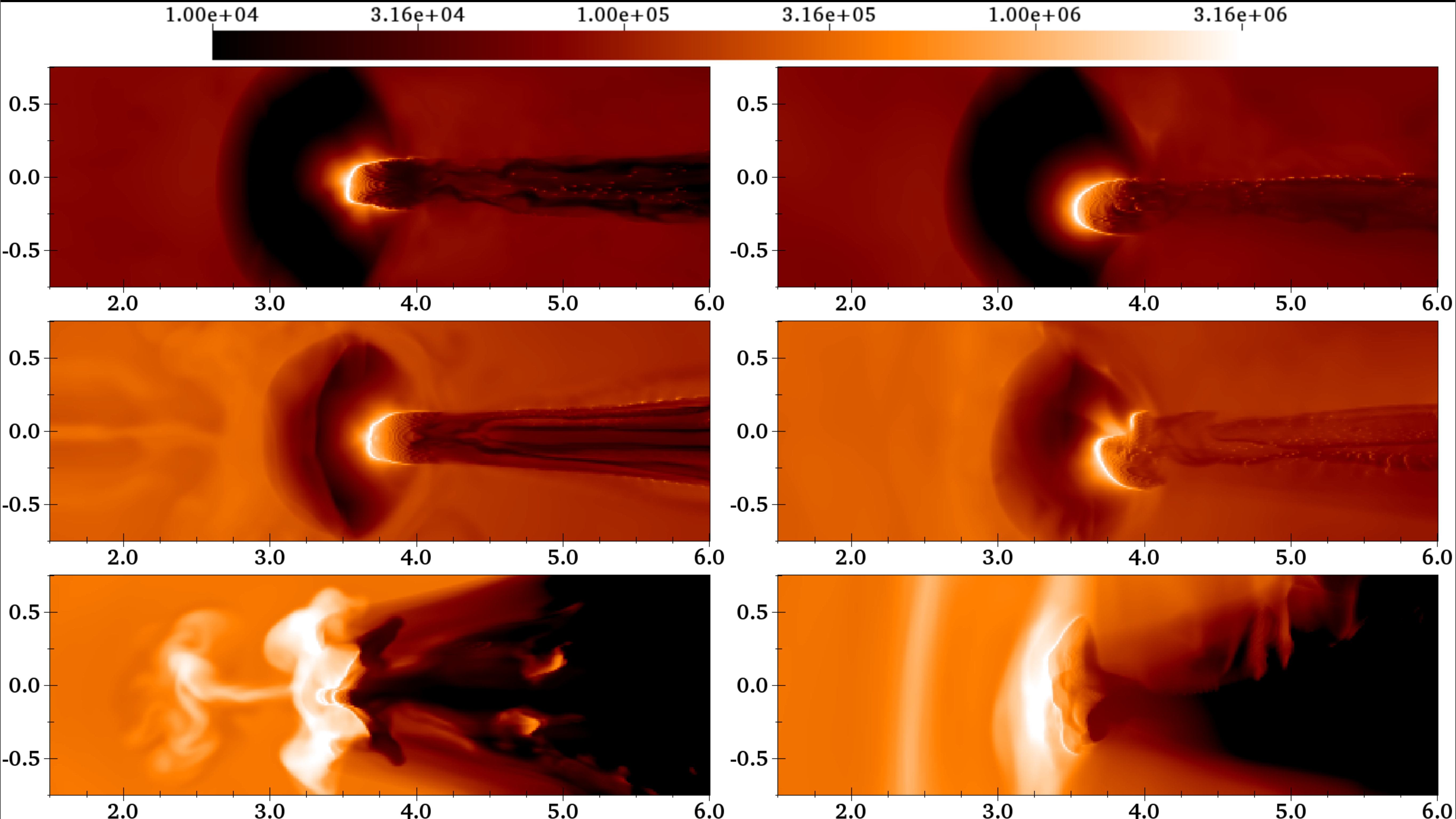

Left: x-y, LOS= -z; Right: x-z, LOS= y. Top to bottom: R2 (weak), R5 (medium), R8 (strong field).

Hα: comparison between parallel and perpendicular strong B-fields

100 kyr

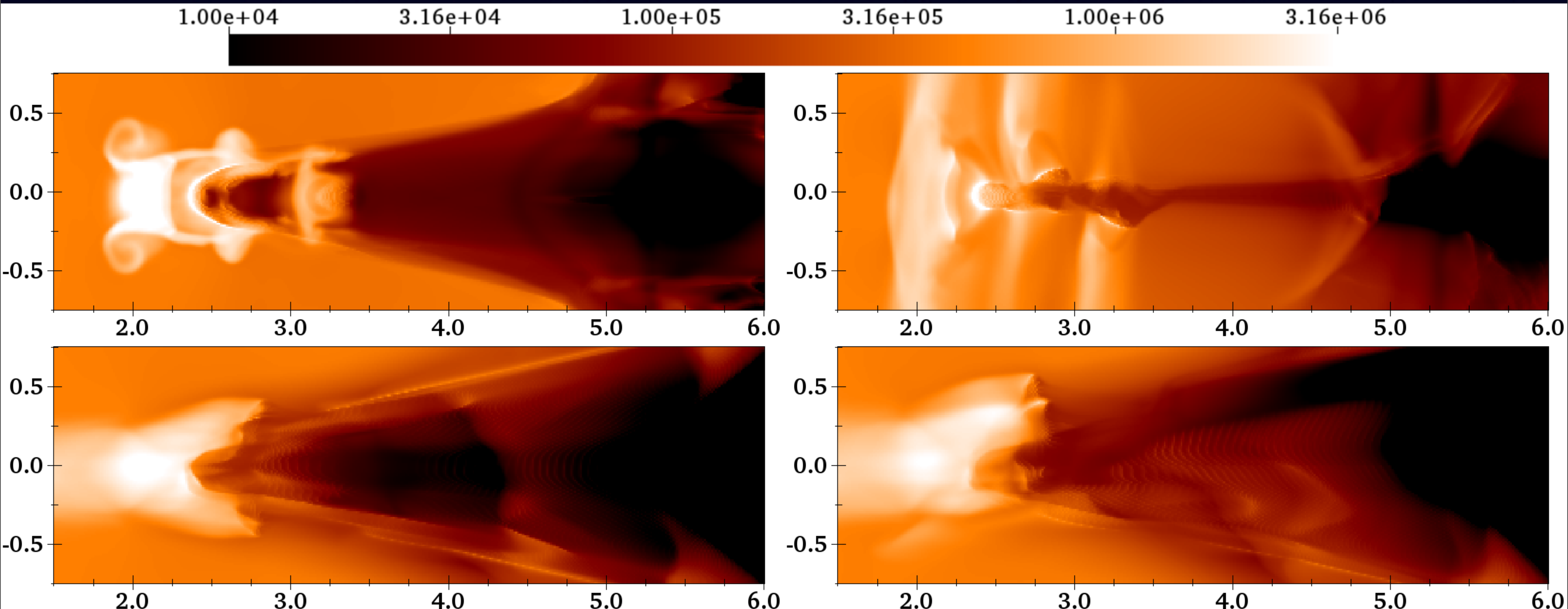

Left: x-y, LOS= -z; Right: x-z, LOS= y.   Top is R8 (perpendicular B-field) bottom is R9 (parallel B-field).

Hα Emission: comparison between parallel and perpendicular B-fields

200 kyr

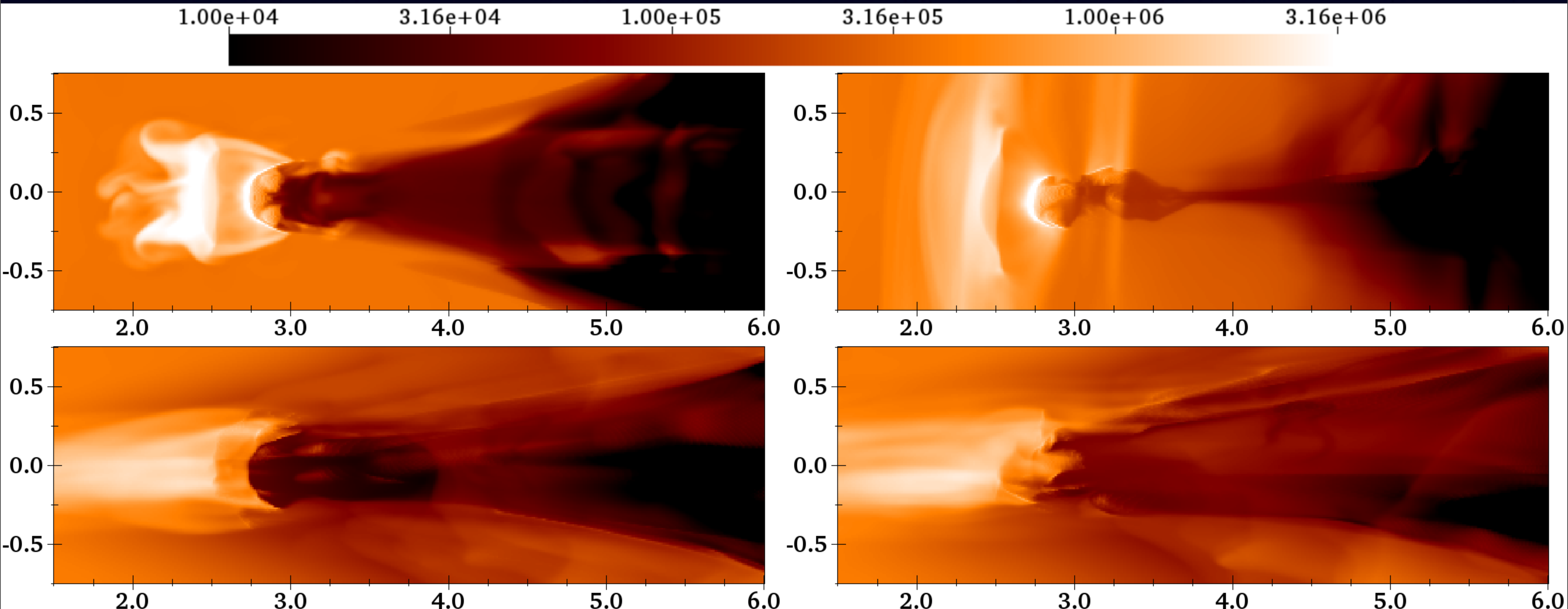

Left: x-y, LOS= -z; Right: x-z, LOS= y. Top is R8 (perpendicular B-field) bottom is R9 (parallel B-field).

Hα Emission: comparison between parallel and perpendicular B-fields

400 kyr

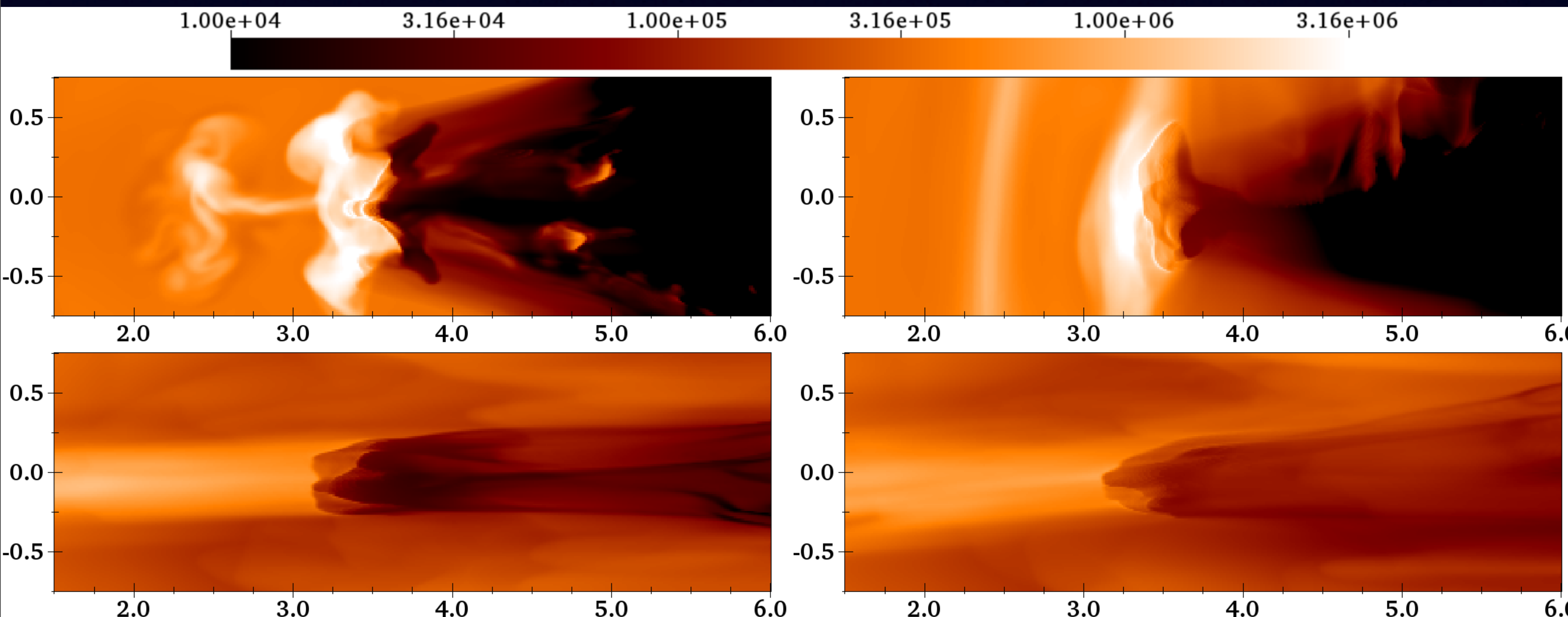

Left: x-y, LOS= -z; Right: x-z, LOS= y. Top is R8 (perpendicular B-field) bottom is R9 (parallel B-field).

Comparison to Observations

- B-field strengths not measured in any pillars, and orientation only measured in Eagle nebula pillars.
- Strong B-field leaves signature in photoevaporation flow, most obvious in Hα emission.

Weak B-field model at 400 kyr

- B-field in pillar/globule is now aligned with pillar's axis.
- Field around tail region influence by "cooling flow" into shadowed region.
- Radial field from photoevaporation flow.
- Also seen in medium strength case.
- Aligned field component increases dramatically in strength.

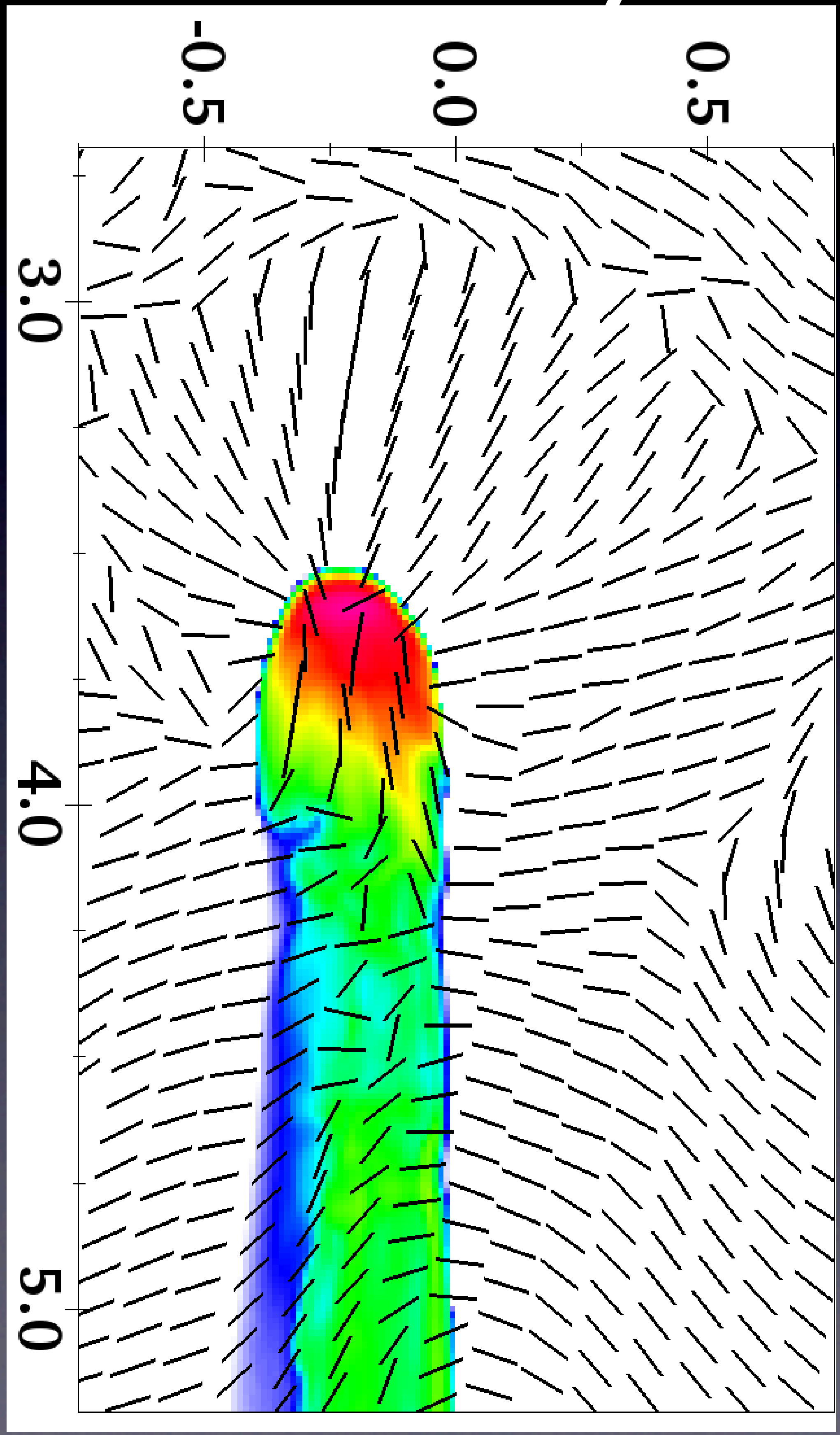

Parallel Field Evolution

- x-component of B in dense gas is shown as function of time.
- Weak field (R2) re-orients almost completely.
- Medium field (R5) changes significantly.
- Strong field (R8) basically unchnaged
- Basic agreement with Henney+(2009) models.

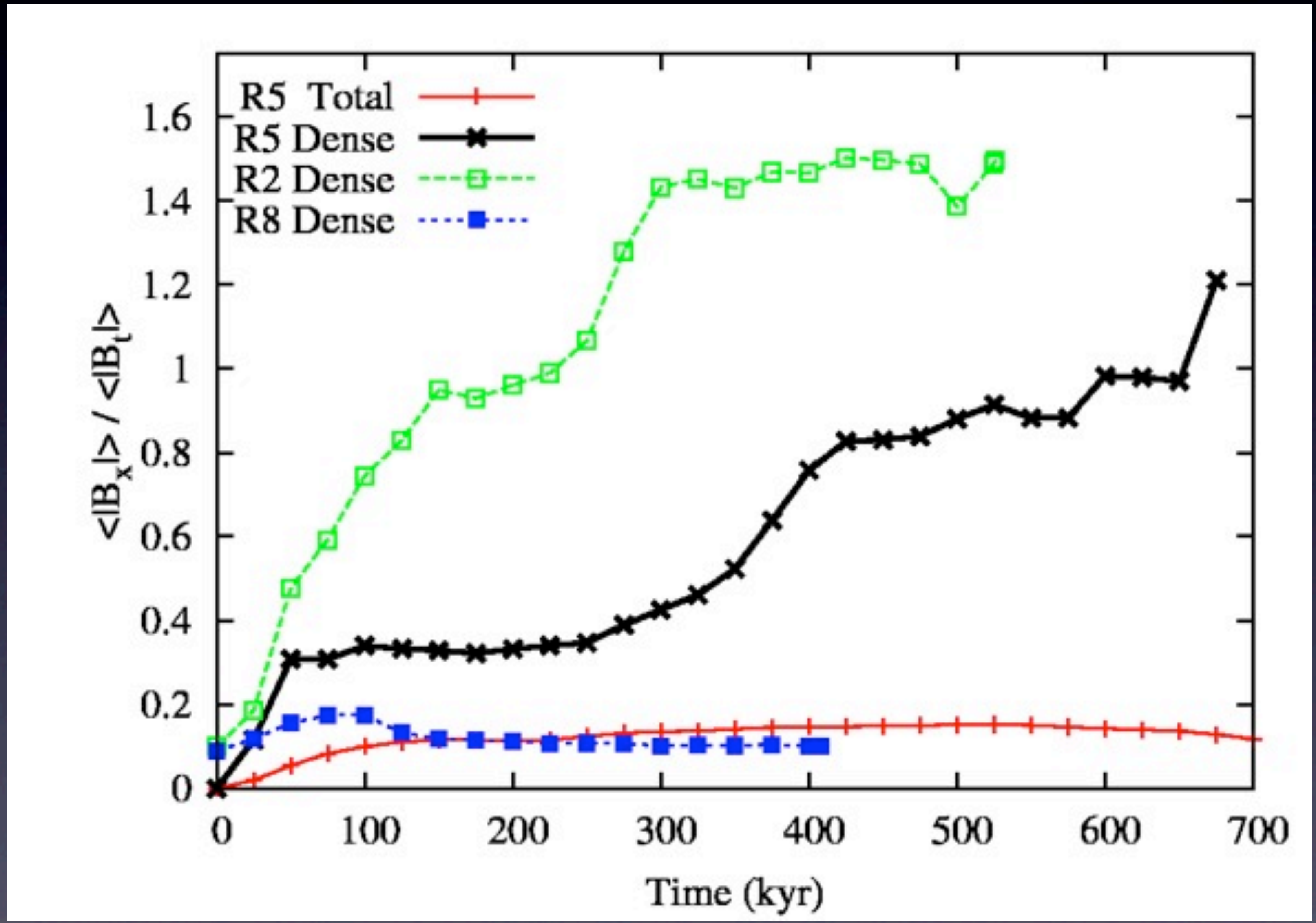

Eagle Nebula (Sugitani+,2007)

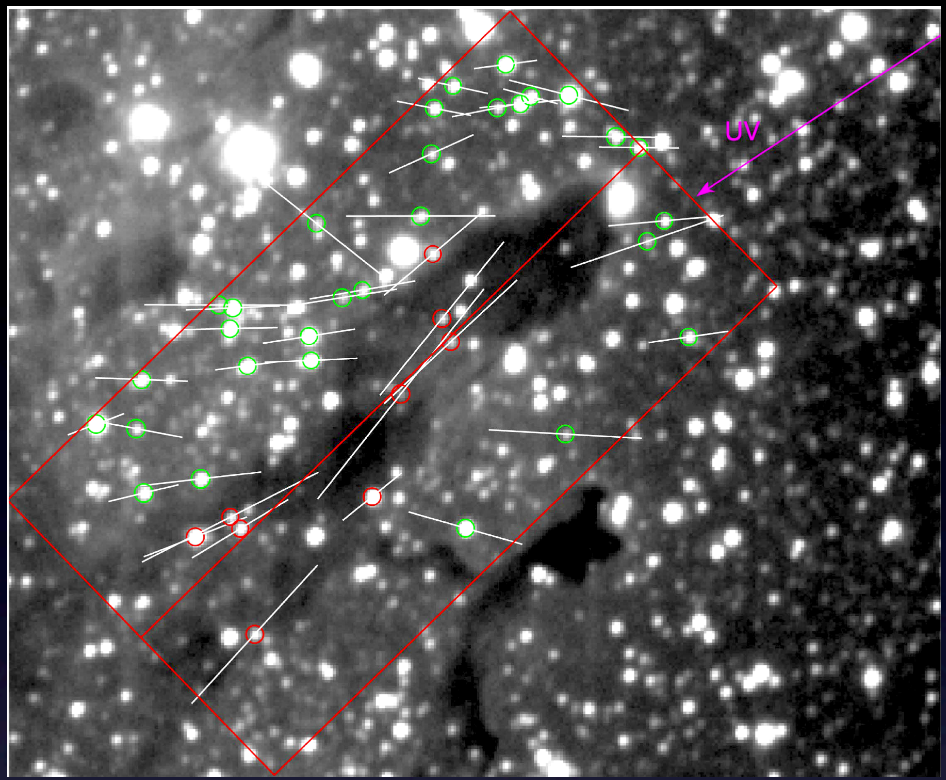

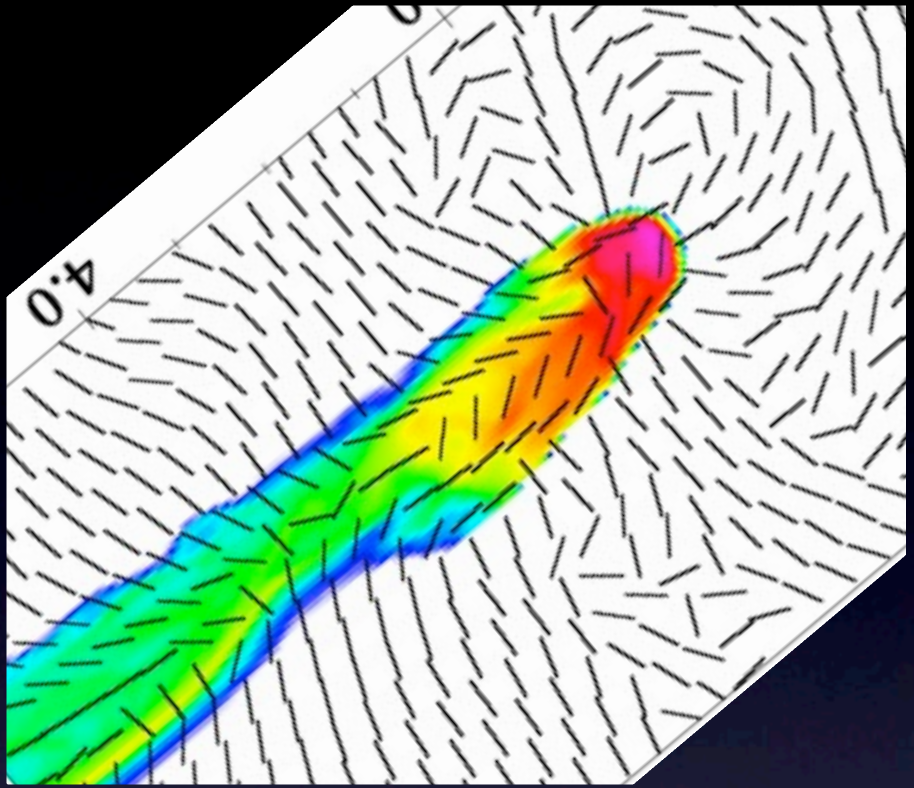

- 18 and 53 μG simulations can match Sugitani+(2007) observations, but 160 μG field model does not.
- This field orientation also seen in some cometary globules (Sridharan+1996, Bhatt 1999, Bhatt+2004).
- What is the dependence on initial conditions?
- Arthur+(2011,MNRAS) have shown that pillars formed from turbulent magnetised initial conditions already had different field orientations compared to surrounding lower density gas.
- May be poor constraint on initial conditions or formation mechanism.

NGC6357 and Pismis 24

- HST press release image (lines to trace ionised gas).
- Credit: NASA, ESA, and J. Maíz Apellániz (IAA, Spain)

- Bohigas et al. (2004, AJ, 127,2826).
- Continuum subtracted Hα image.
- “Bright Ridge” is the brightest feature on image.
- Hα emissivity, $I \sim n_e\, n(H+) / T_e$
- If isothermal, $I \sim n_e\, n(H+)$
- Conclude that the ridge contains the densest concentration of ionised gas.
- Magnetically confined?
- Or ram-pressure?

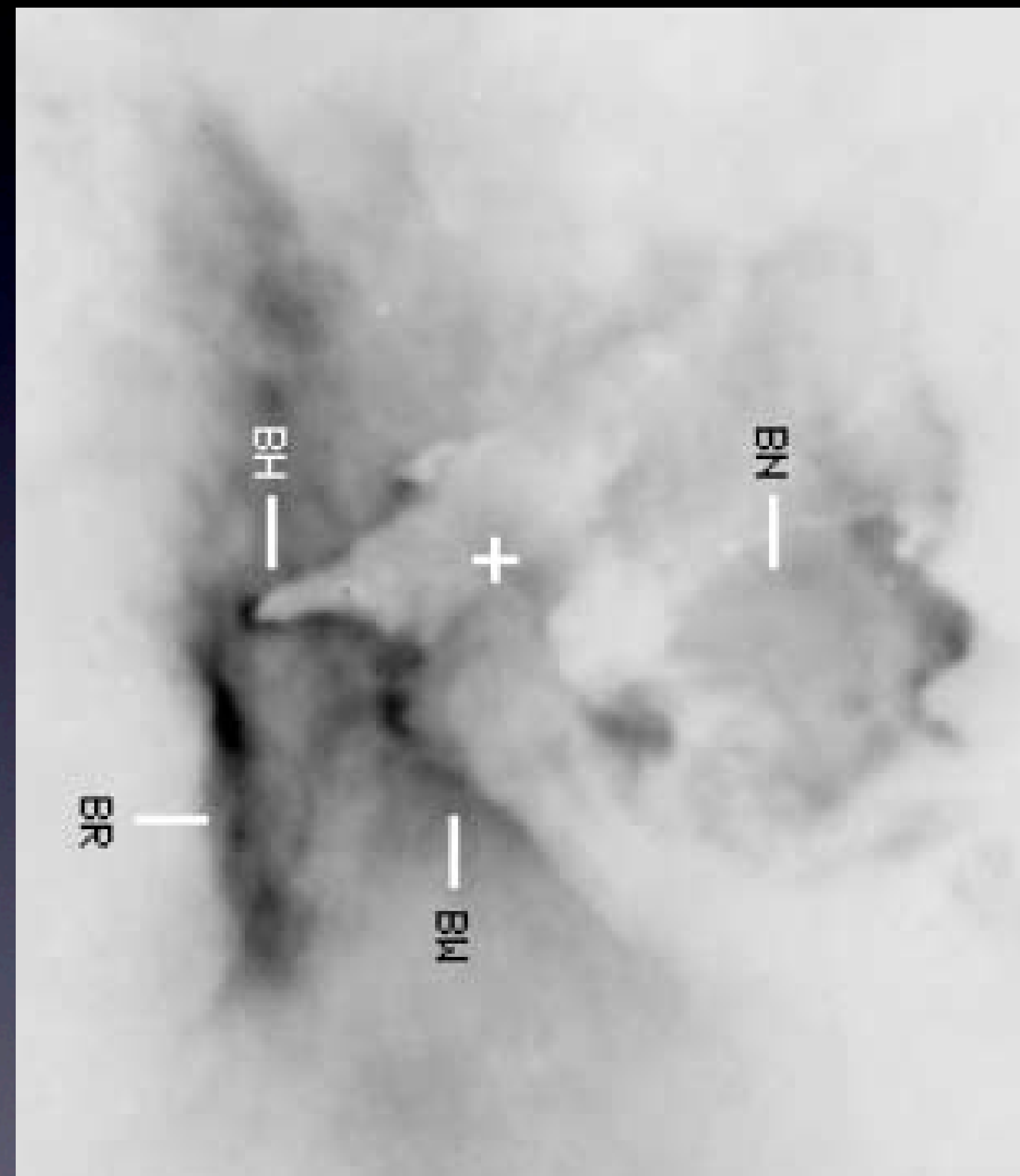

More Hα: NGC 3603 from HST

- Another linear feature above bright rim of elephant trunk.
- Photoevaporation flow confined by something. . .
- . . . gas pressure, ram pressure, or magnetic field?

Credit: NASA, ESA, R.O'Connell, F. Paresce, E. Young, Hubble Heritage Team

Conclusions

- Observations of elephant trunks can in principle constrain field strength in H II regions.
- A sufficiently strong magnetic field can
  (1) Prevent field alignment with pillar/globule.
  (2) Significantly change the structure which develops.
  (3) Confine the photoevaporation flow.
- Rocket effect tends to align magnetic field with radial direction (cf. Williams 2007, see also Henney+2009, Arthur+2011).
- Comparing our results to observations in M16 (Sugitani et al. 2007) suggests ambient field $B <= 50\ \mu G$.
- Ionised gas may give less model–dependent constraints.
- A simple one-D model can explain the formation of a bright bar/ridge of ionised gas in strongly magnetised models.
- Ram-pressure confinement could be distinguished by line-of-sight velocity information.

IC 1396 Details

- Hα image from Barentsen, Vink et al. (2011,MNRAS)
- IC 1396: age is ~2−3 Myr,
- diameter ~35 pc.
- Main exciting star is O6V,
- part of cluster Trumpler 37.
- Hα emission roughly spherical, but not smooth.
- Pillars, clumps, ridges
- Significantly more complex than RCW120; larger and older.

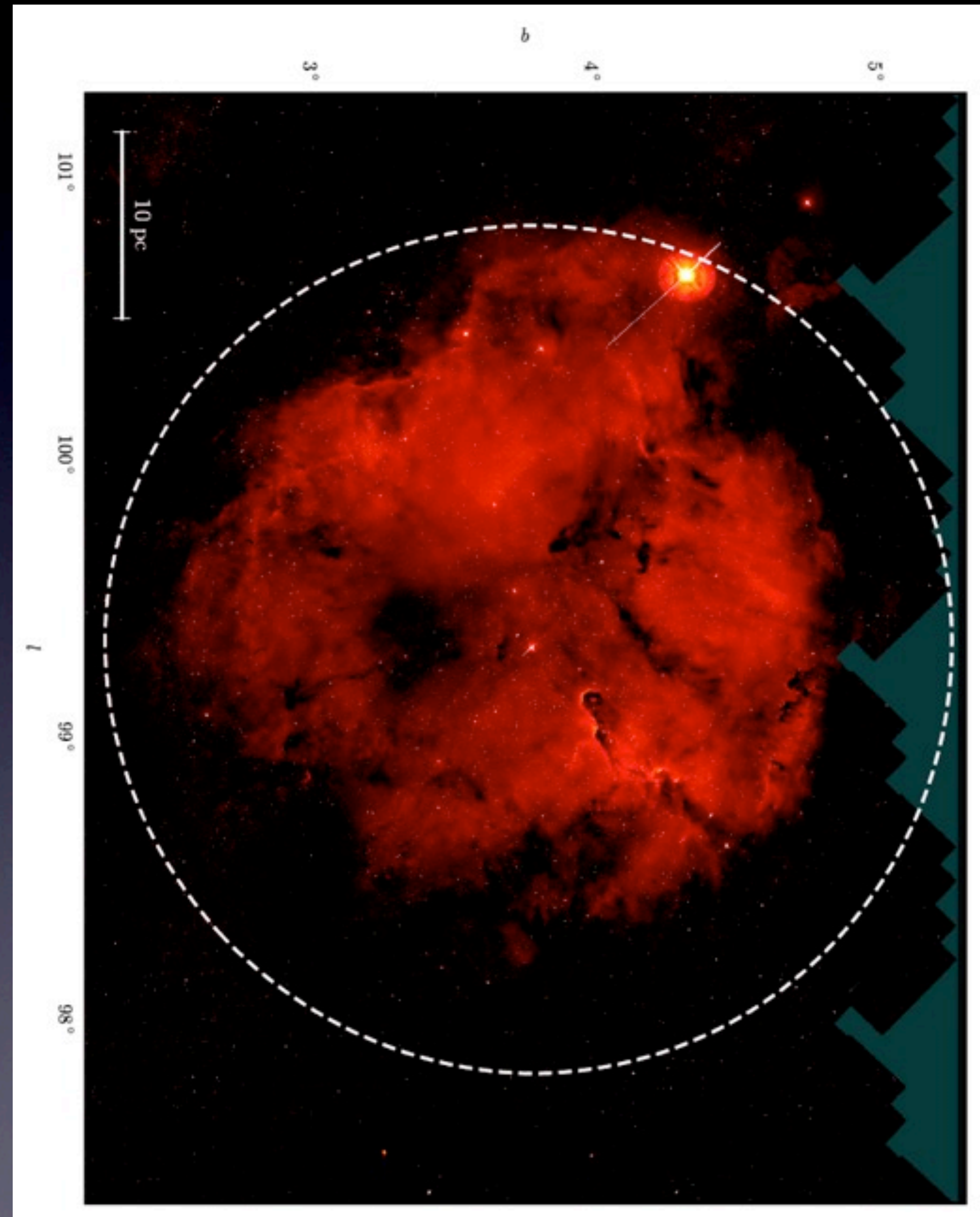

Second Order Explicit Algorithm

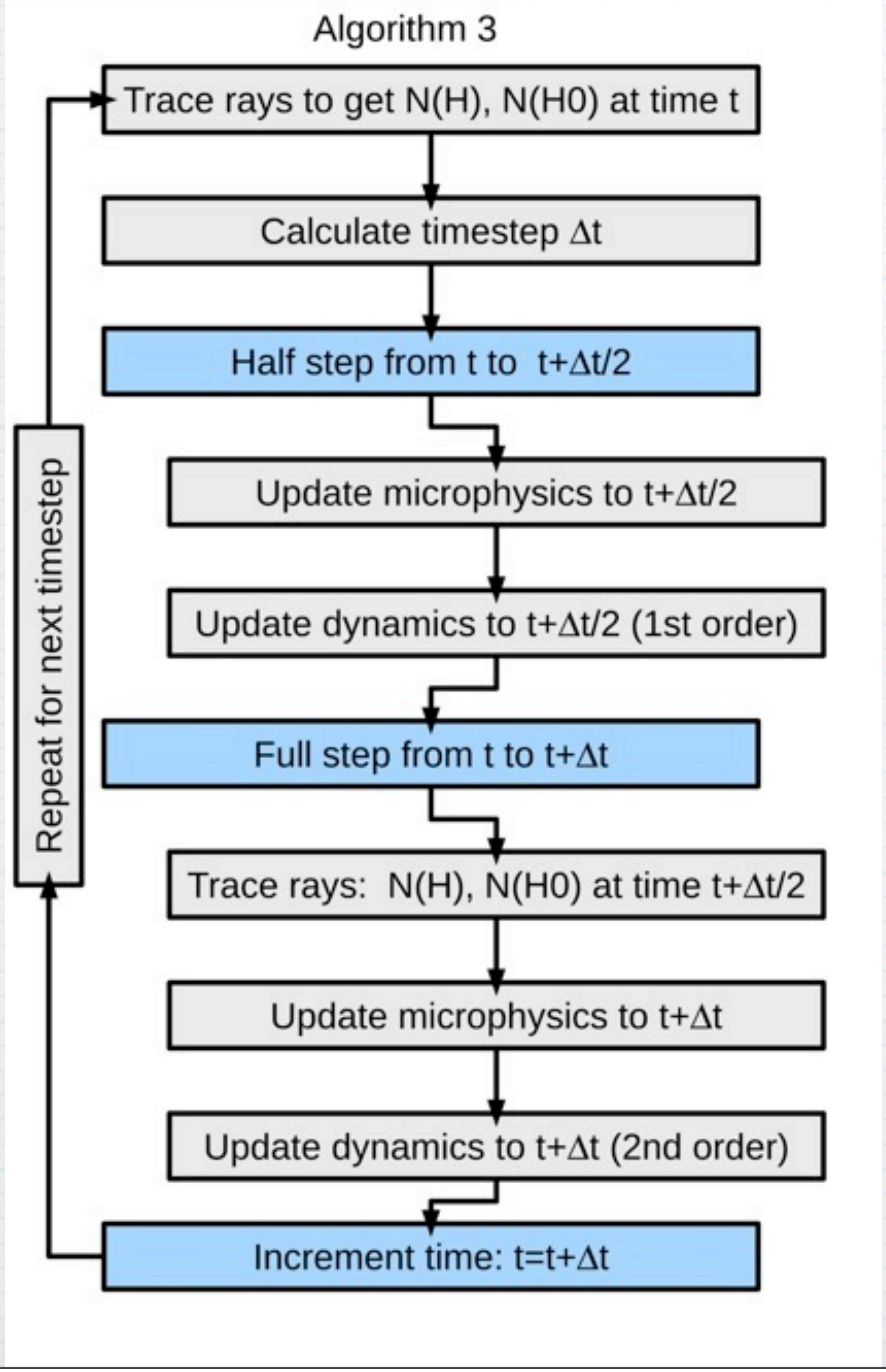

- 2 raytracings per step.
- Time-centred column densities mean photon conservation is 2nd order.
- Still explicit scheme.
- Fits in well with 2nd order dynamics update.
- Allows full ionisation of cell in 4 timesteps (8 raytracings).
- Still needs 4 steps for I-front to cross cell.

Planar, constant velocity, I-fronts

* Monochromatic radiation
* No recombinations
* I-front has constant velocity v=F/n(H0)
* 13 timestep criteria:
  0-4: dt=K.(1/ydot)
  5-8: dt=K.(y/ydot)
  9-12: dt=K.min(y/yd,E/Ed)
* Implicit A1 v. good by construction.
* A3 converges much faster than A2, error <1% very quickly.

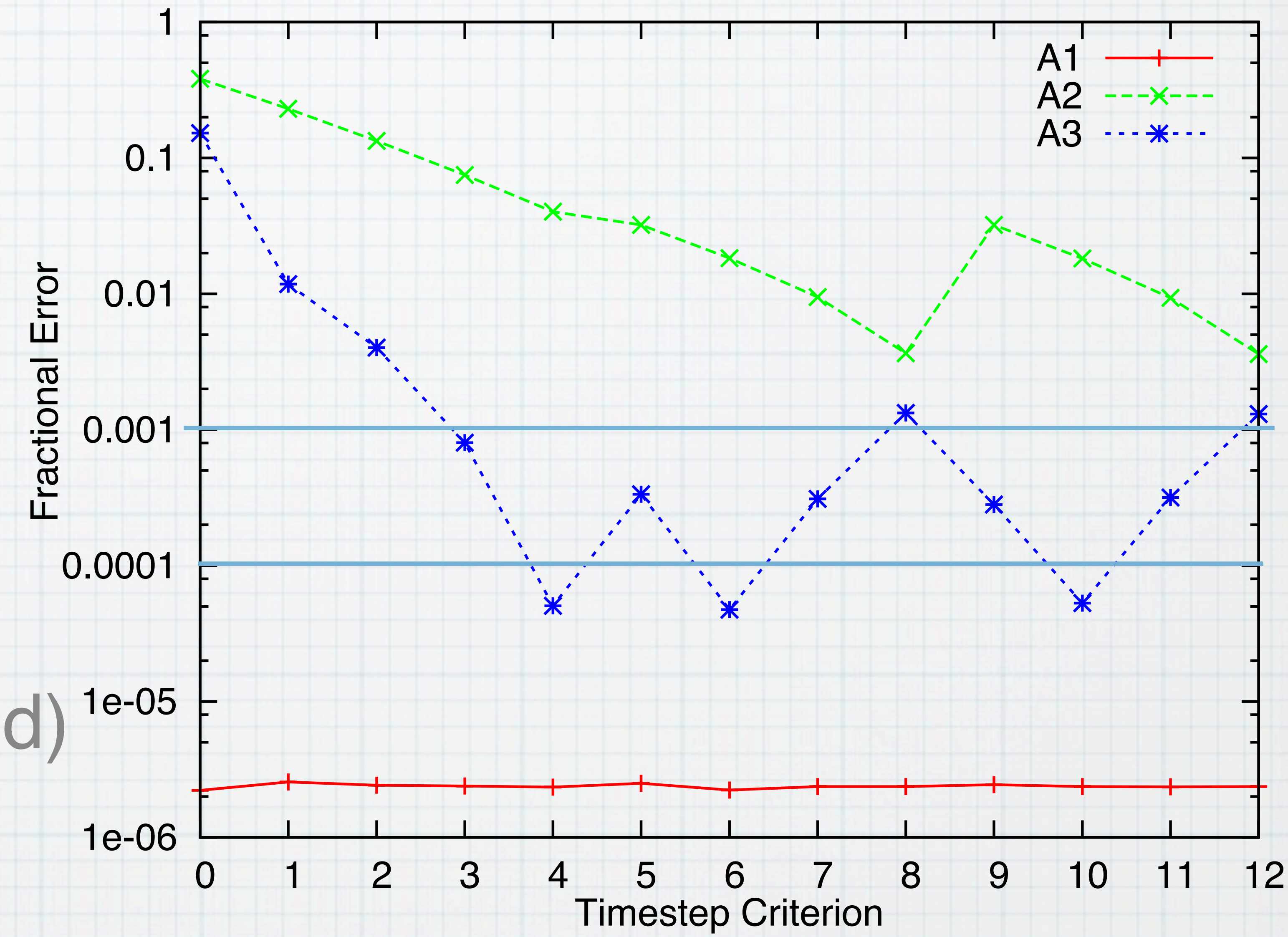

--> More restrictive dt -->

Accuracy vs. Runtime

- Multi-frequency radiation, no dynamics, 1D expansion of Stromgren sphere.
- L1 error after one recombination time, as function of calculation time.
- 4 different cell optical depths: dTau=1, 3, 10, and 30.

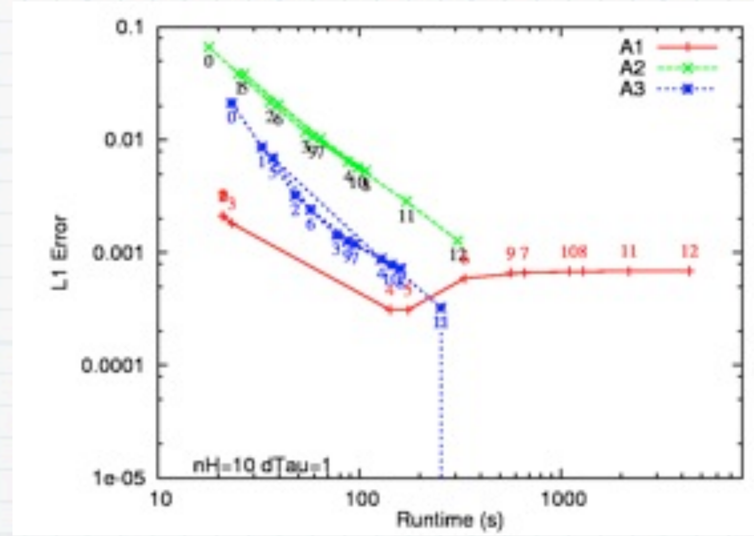

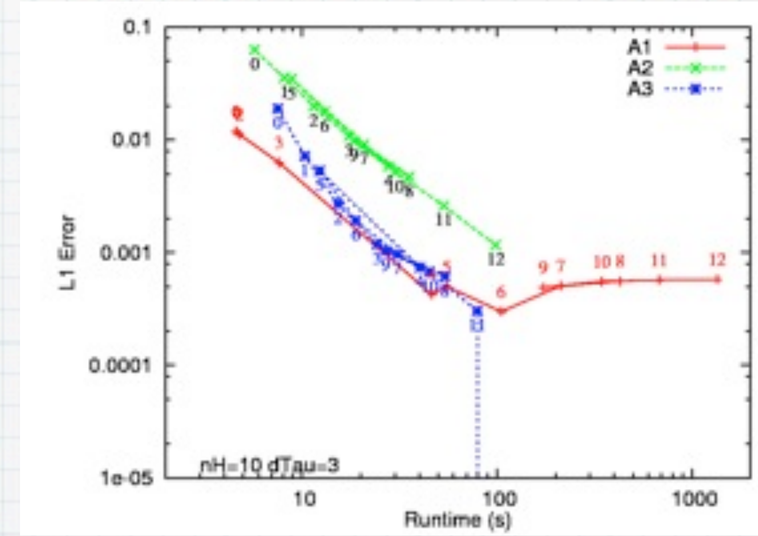

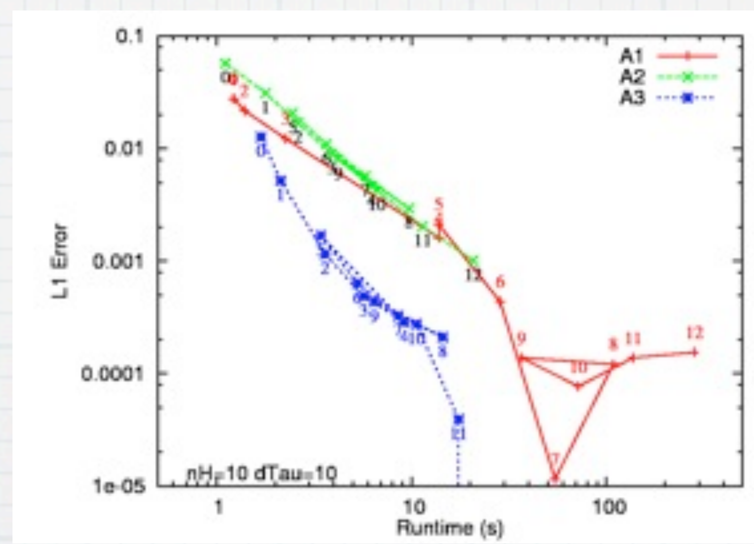

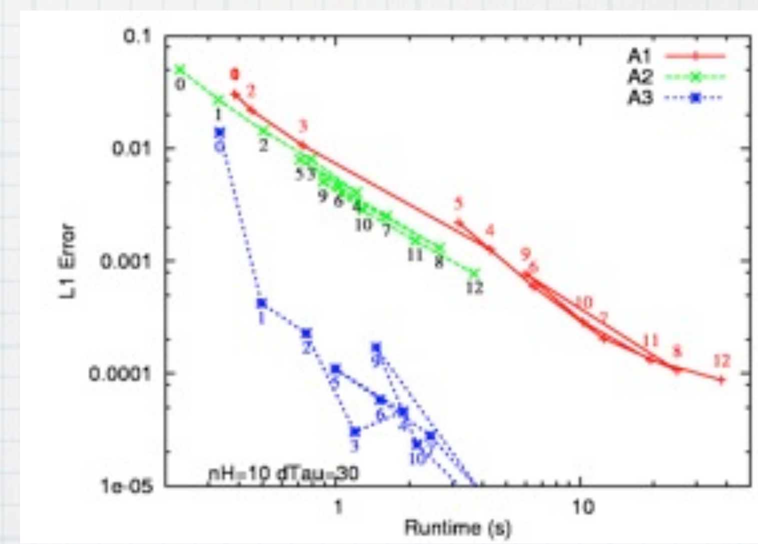

Accuracy vs. Runtime

* M ra n 1 S
* L re a c
* 4 d 1

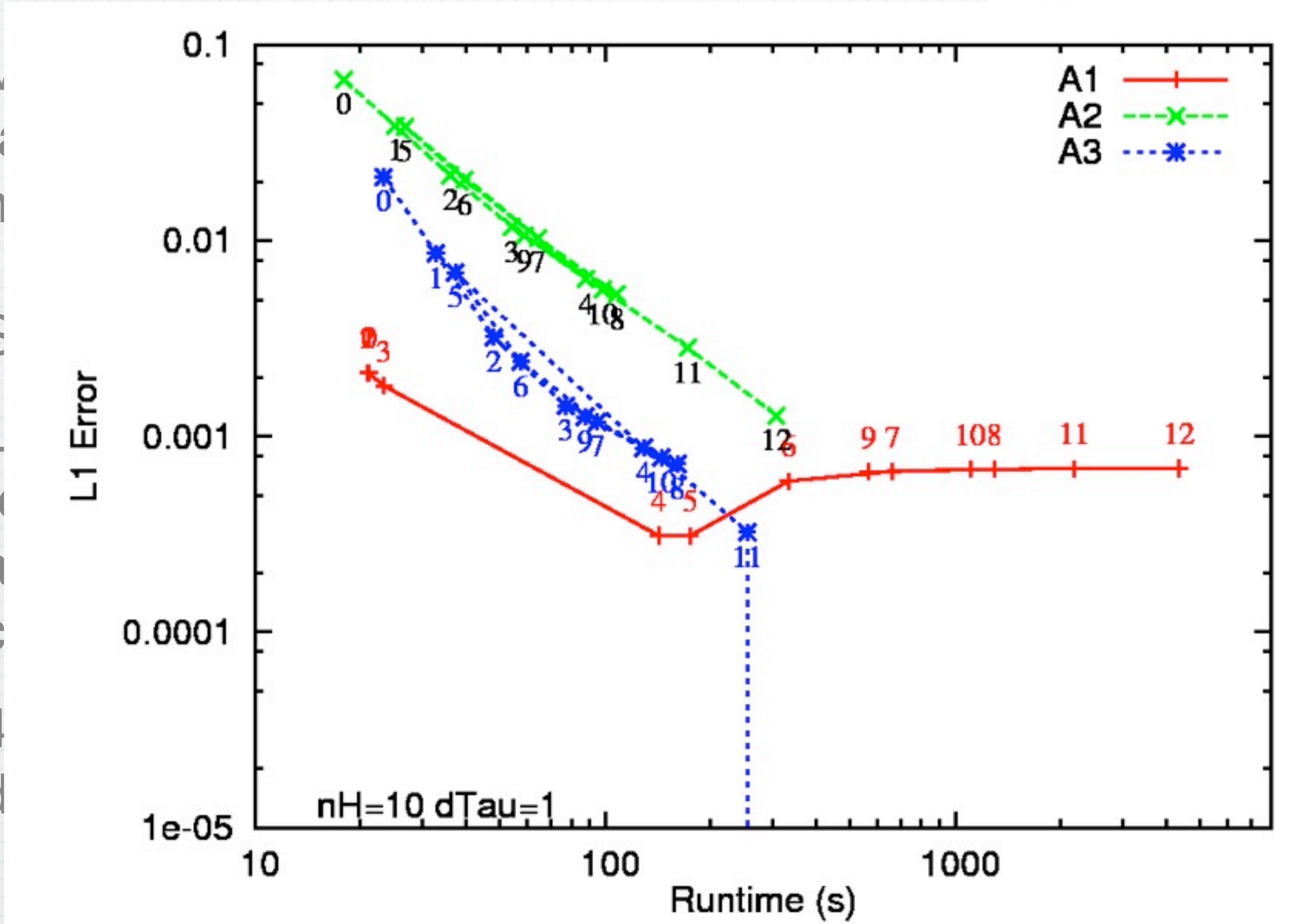

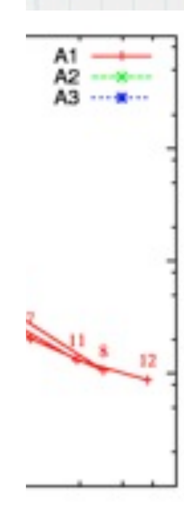

Accuracy vs. Runtime

* M ra n 1 S
* L r a c
* 4 d 1

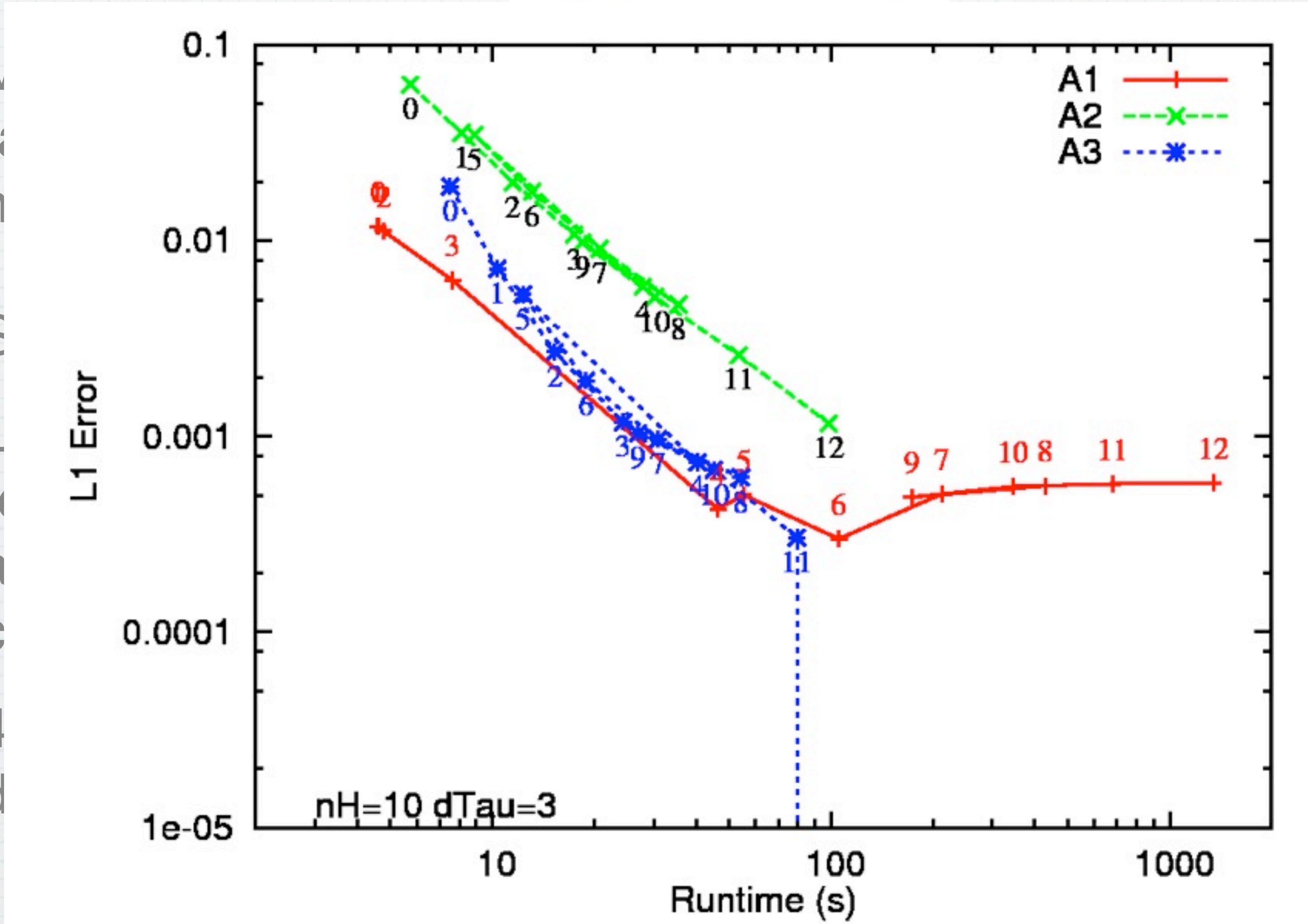

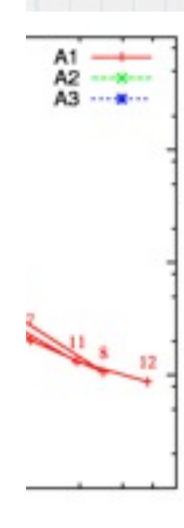

Accuracy vs. Runtime

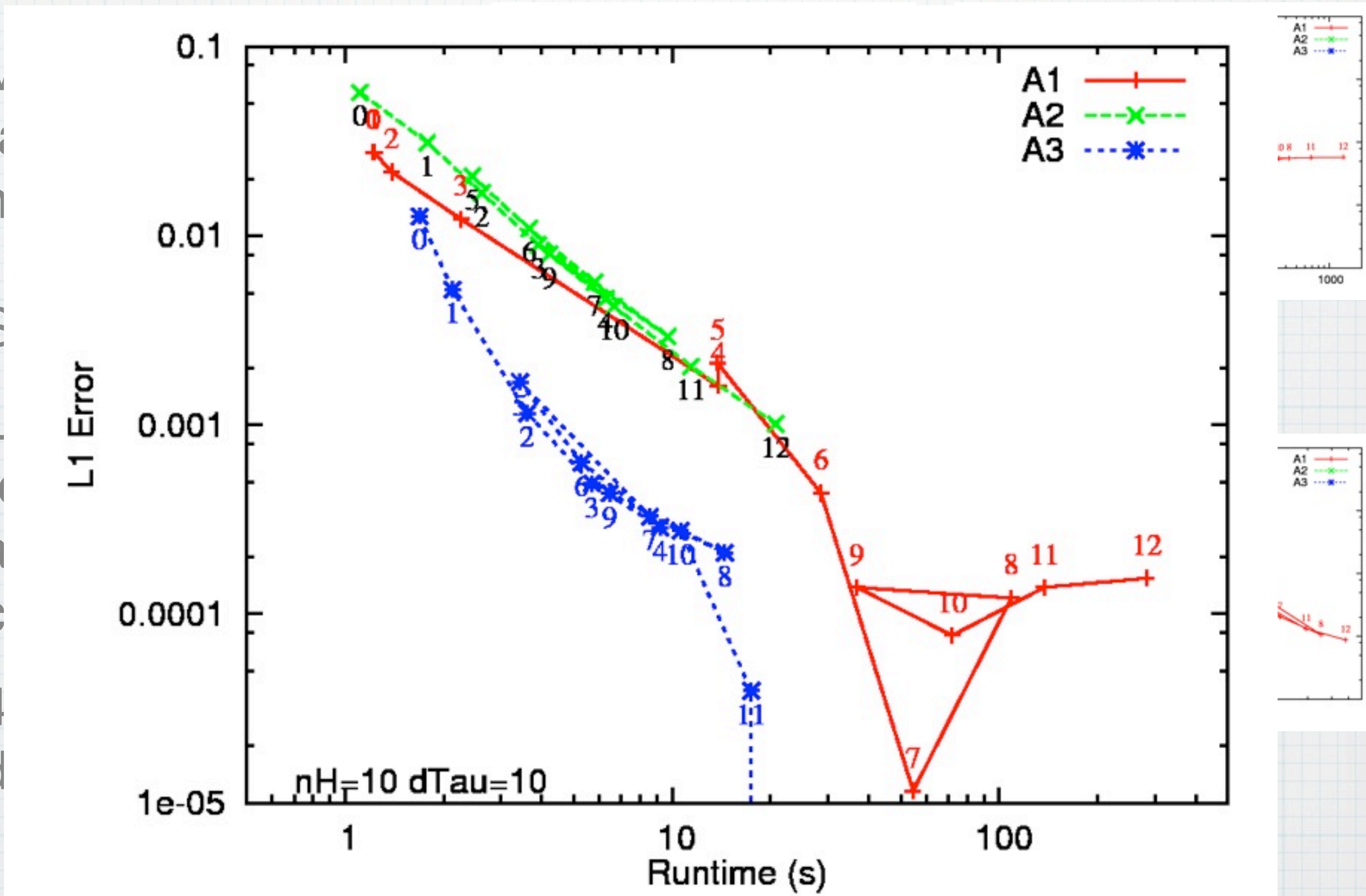

Accuracy vs. Runtime

* M
  ra
  n
  1
  S
* L
  r
  a
  c
* 4
  d
  1

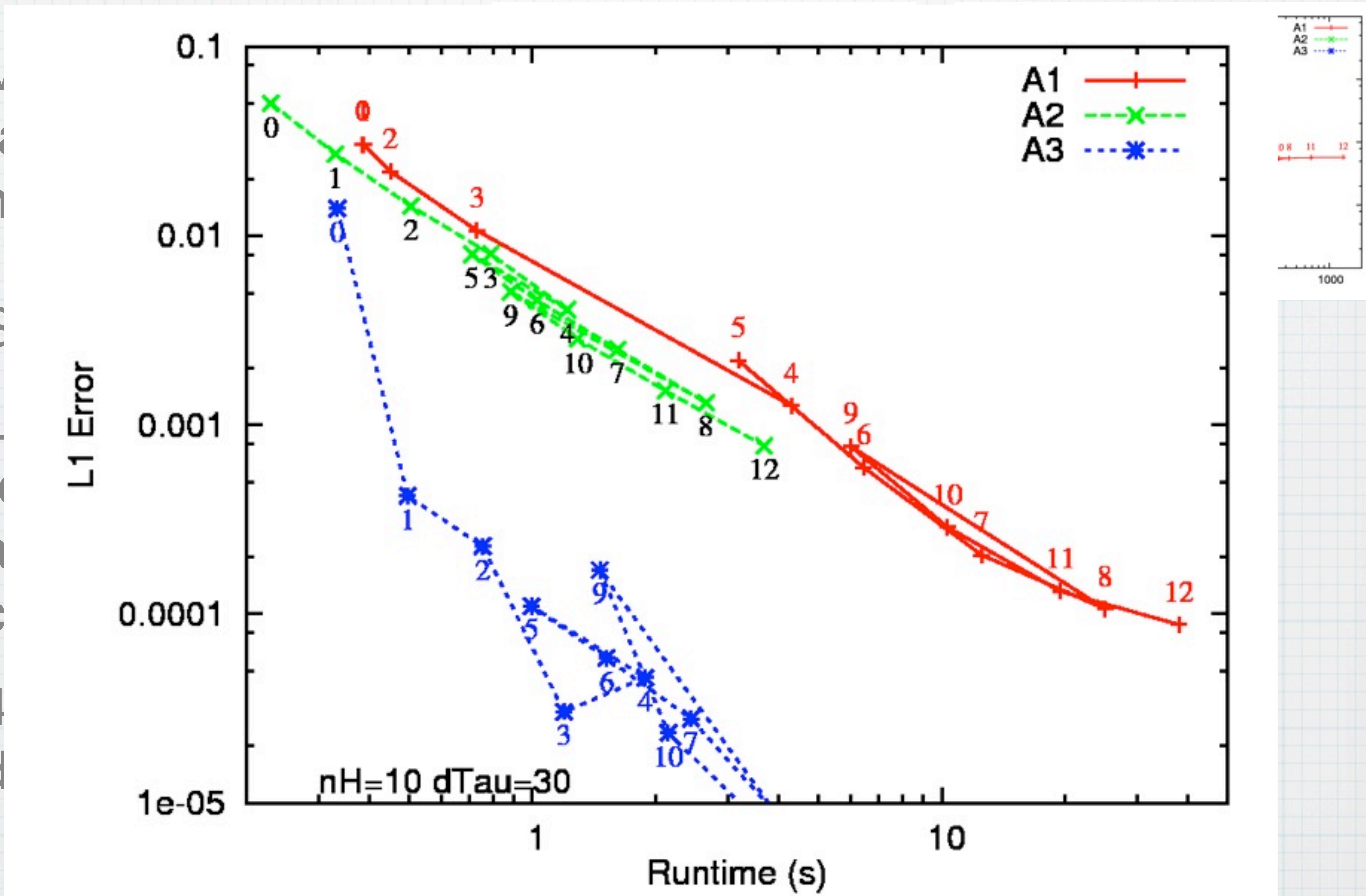

Parallel Scaling A1 vs. A3

- A2/A3 scale better than A1 because microphysics integration is not in the raytracing step.
- Scaling limited by causal raytracing.
- Runtime plotted vs. number of cores, N, using JUROPA at Juelich.
- Tests w/ SMT have 2 MPI processes per core.
- Ideal scaling t=c/N (c a constant)
- 2D RT has t=c.N^(-1/2)
  3D RT has t=c.N^(-2/3)

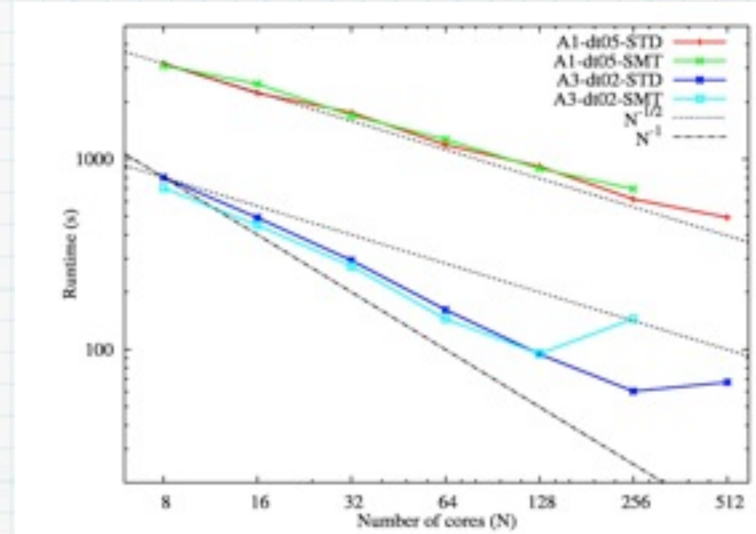

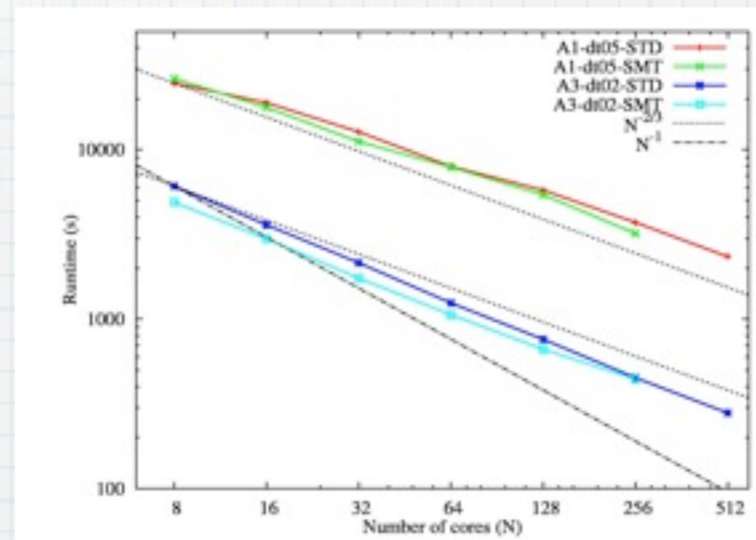

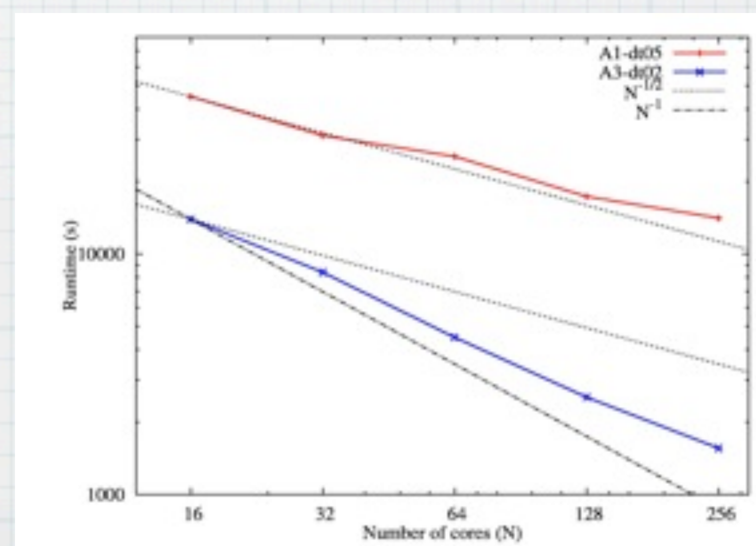

Parallel Scaling - 2D Static

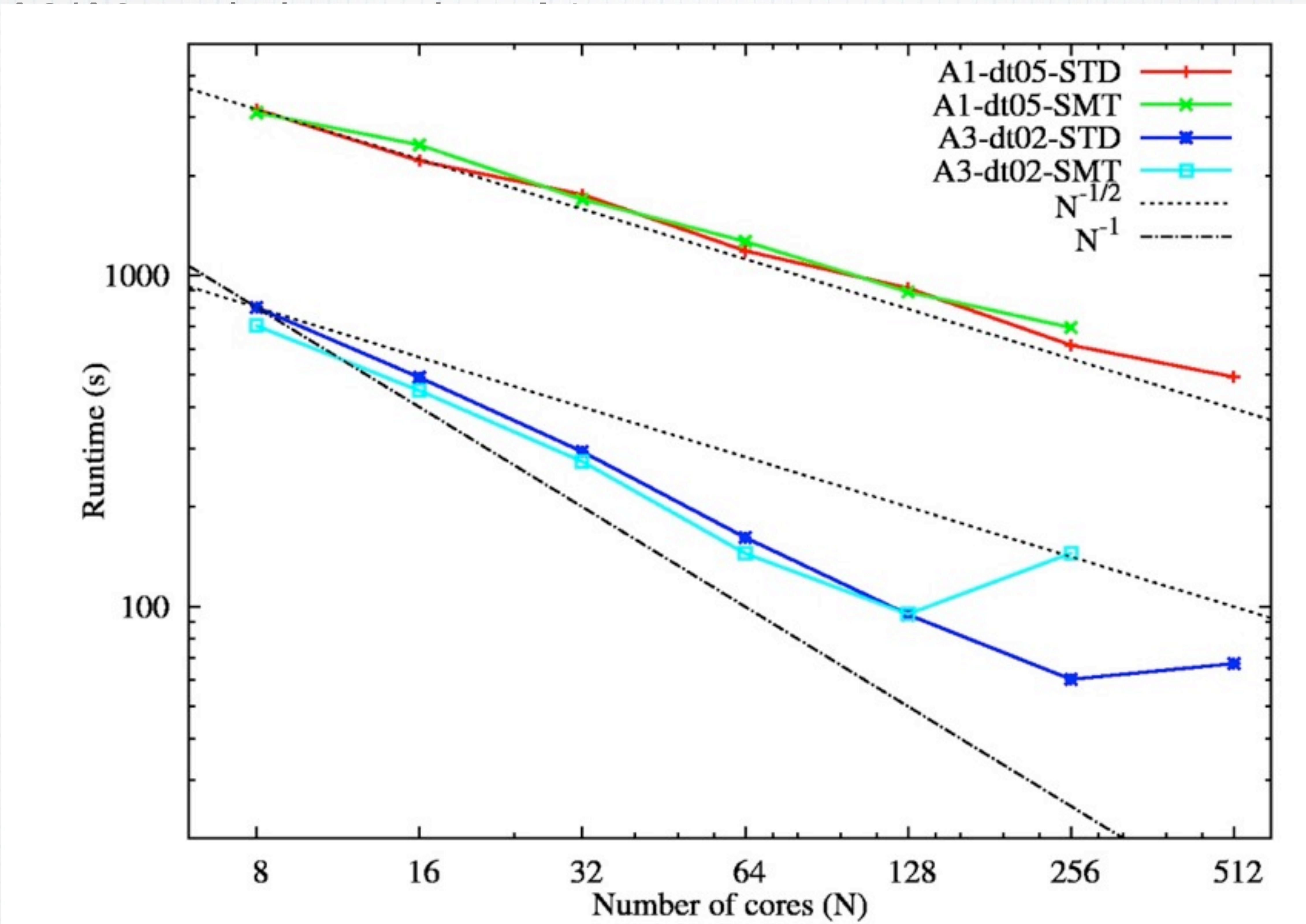

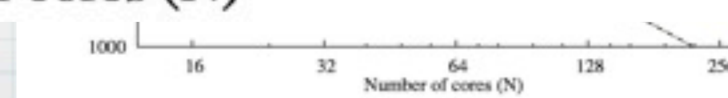

Parallel Scaling - 3D Static

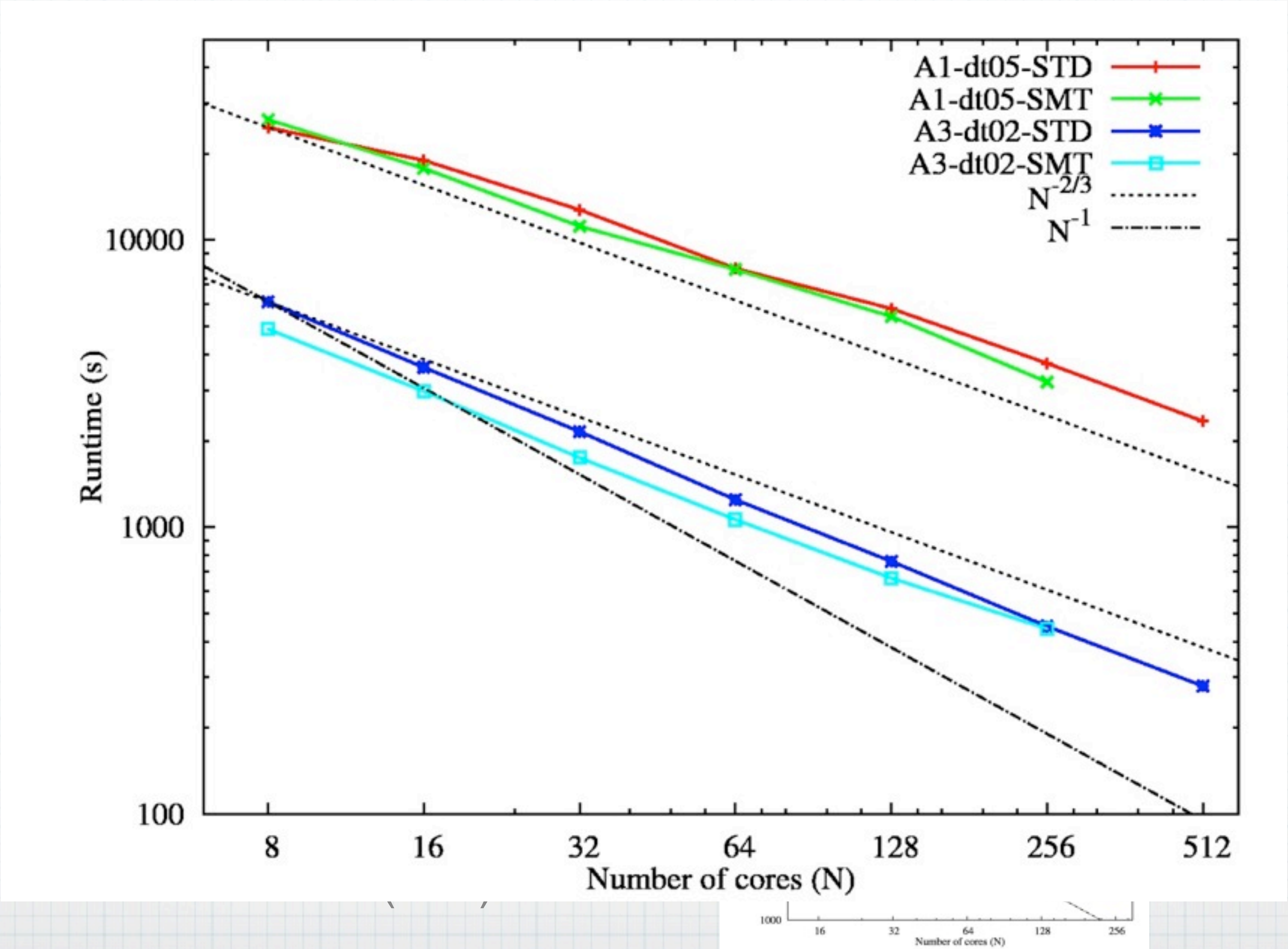

Parallel Scaling - 2D Dynamic

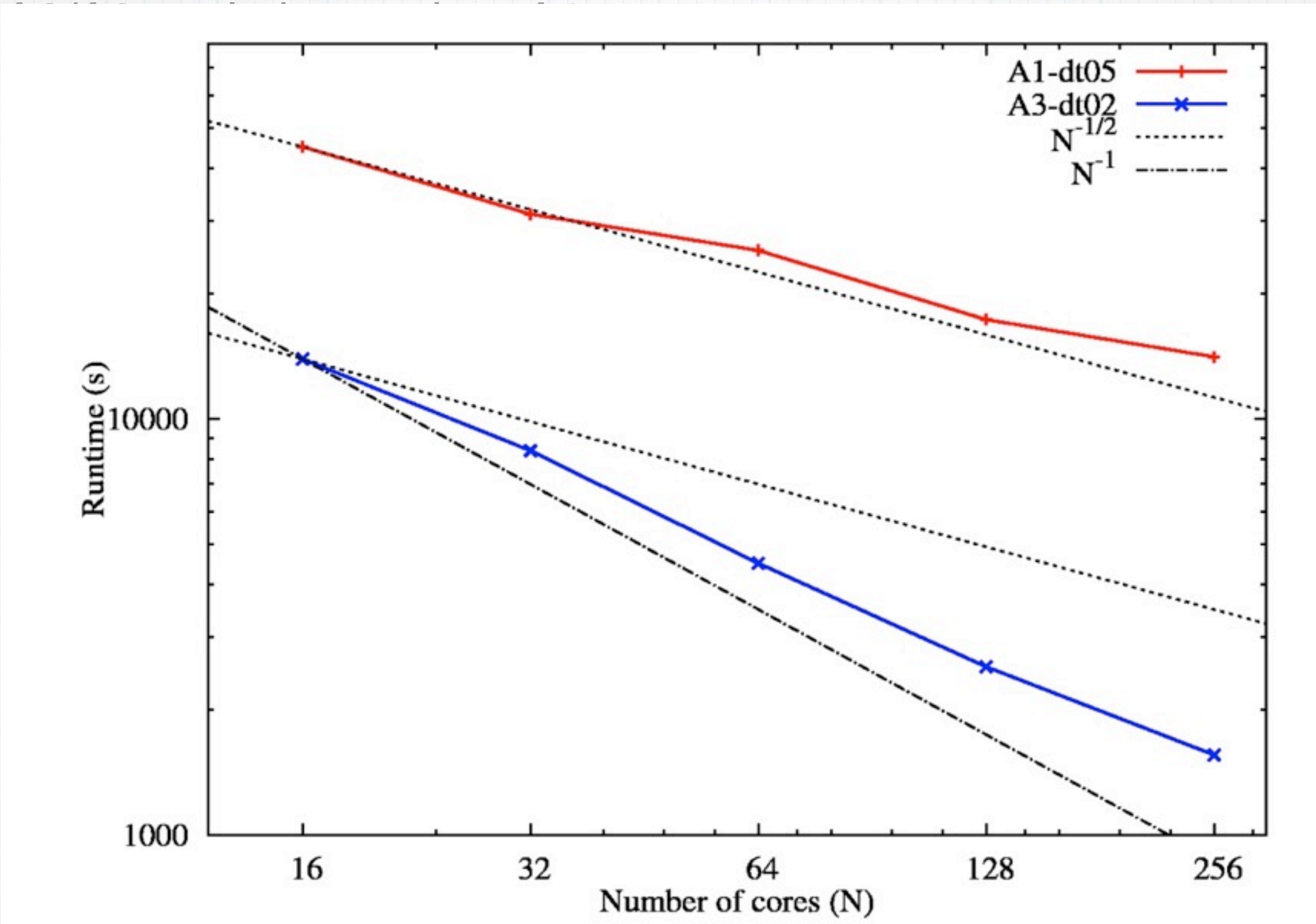

Conclusions

* 2nd order explicit algorithm (A3) is both more accurate and efficient than 1st order scheme (A2) commonly used.
* A3 is also more efficient than implicit method for this implementation,
  (but see Friedrich+(2012) for updated C2-ray algorithm).
* A3 allows full ionisation of grid-cell with 8 raytracings, with error <2% for all cases tested.
* This is a factor of 5-7x better than 1st order scheme.
* Upgrade from A2 to A3 should be straightforward, regardless of grid structure (also for diffuse radiation?).
* Parallel scaling is good - 50% efficiency on 256 cores, and continued speed-up to 1024 cores (for uniform grid).